Supporting Information

A Photoswitchable Heteroditopic Ion Pair Receptor

Zoran Kokan*,†,‡ and Michał J. Chmielewski*,†

†*Faculty of Chemistry, Biological and Chemical Research Centre, University of Warsaw*
Żwirki i Wigury 101, 02-089 Warszawa, Poland
‡ Division of Materials Chemistry, Ruđer Bošković Institute, Bijenička cesta 54, 10000 Zagreb, Croatia.

E-mail: zkokan@irb.hr, zoran.kokan@gmail.com
E-mail: mchmielewski@chem.uw.edu.pl

Contents

1 General Information

1.1 Materials

All reagents were purchased from Alfa Aesar or Sigma-Aldrich and used without further purification. Deuterated solvents were purchased from Euriso-top. Chloroform-d_1 was deacidified prior to use by passing through activated basic alumina (≈ 3 cm long pad in a Pasteur pipette). Acetonitrile-d_3 (Eurisotop catalogue number D021EAS, water content <0.05%) was purchased in septum-sealed 10 ml vials and used as received. TLC was carried out on Merck silica gel 60 F254 plates. Preparative chromatography was done using a Teledyne Isco CombiFlash system with RediSep Normal-phase Silica Flash Columns.

1.2 Instruments and Methods

The NMR spectra were measured on Agilent NMR (^{1}H: 400 MHz, ^{13}C: 100 MHz) spectrometer. Chemical shifts, δ, are reported in parts per million (ppm) and coupling constants, J, are given in hertz (Hz). The NMR spectra were referenced to the solvent residual signal[S1] (^{1}H: δ_{DMSO} = 2.50 ppm, $\delta_{chloroform}$ = 7.26 ppm, $\delta_{acetonitrile}$ = 1.94 ppm, $\delta_{dichloromethane}$ = 5.32 ppm, $\delta_{acetone}$ = 2.05 ppm; ^{13}C: δ_{DMSO} = 39.52 ppm). Data are reported as follows: chemical shift, multiplicity (s – singlet, d – doublet, t – triplet, dd- doublet of doublets, dt – doublet of triplets, td – triplet of doublets, ddd – doublet of doublet of doublets), coupling constant, and integration. The HR-ESI-MS spectra were obtained using a Quattro (ESI TOF) mass spectrometer with methanol as the spray solvent. Elemental analysis was performed using a CHN analyzer Vario EL III. UV-Vis spectra were obtained on Thermo Scientific Evolution 300 UV-Vis spectrometer. Hitachi F-7000 spectrophotometer was used as the source of monochromatic light for quantum yield measurements.

X-ray: X-ray quality single-crystals of complexes of *E*-**1**, *Z*-**1**, and *E*-**1** with various salts were subjected to the X-ray diffraction experiments at T = 100(2) K. They were mounted with paratone-N oil to the MiTeGen micro-mounts. Diffraction data were collected on the Agilent Technologies SuperNova Dual Source diffractometer with Mo$K\alpha$ radiation (λ = 0.71073 Å) using CrysAlis RED software.[S2] The analytical numeric absorption correction using a multifaceted crystal model based on expressions derived by R.C. Clark & J.S. Reid[S3] (*E*-**1**·NaI, *E*-**1**·KI, *E*-**1**·NH_4Br, and *E*-**1**·$LiClO_4$) and the numerical absorption correction based on gaussian integration over a multifaceted crystal model (*E*-**1**·NH_4I), implemented in SCALE3 ABSPACK scaling algorithm[S2] were applied. The structure determination procedure was carried out using the SHELX package.[S4] The structures were solved with direct methods and then successive least-square refinements were carried out based on full-matrix least-squares on F^2 using the XLMP program.[S4] All H-atoms bounded to the C-atoms were positioned geometrically, with C–H equal to 0.93 and 0.97 Å for the aromatic and methylene H-atoms, respectively, and constrained to ride on their parent atoms with U_{iso}(H) = 1.2U_{eq}(C). The H-atoms linked to the N-atoms were located on a Fourier difference map and constrained to ride on their parent atom with U_{iso}(H) = 1.2U_{eq}(N). In case of the N2−H2 / N2A−H2AA / N2B−H2BA bond in *E*-**1**·NaI, *E*-**1**·KI, *E*-**1**·NH_4Br, and *E*-**1**·$LiClO_4$, and the N3−H3A / N3A−H3AA / N3B−H3BA bond in *E*-**1**·NaI, *E*-**1**·$LiClO_4$, and *E*-**1**·NH_4Br, the DFIX 0.87 restraints were applied. Additionally, the atoms of the ammonium cations in the *E*-**1**·NH_4Br and *E*-**1**·NH_4I were a subject of numerous DANG 1.45 and/or DFIX 0.87 restraints. For *E*-**1**, few distinct peaks on the difference Fourier map were indicating the presence of a disordered solvent molecule. Unfortunately, all attempts to model this part of the structure failed. Therefore, the solvent contribution was removed by applying the appropriate MASK procedure in the Olex2 program.

2 Synthetic Procedures

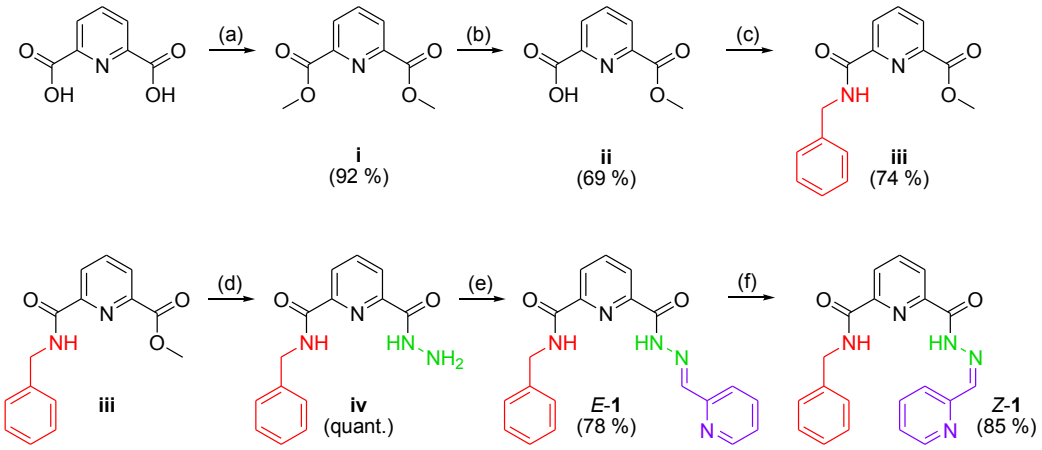

Scheme S 1. Synthetic pathway leading to the receptor **1**. Isolated yields are given in parentheses. (a) $MeOH/H_2SO_4$ (conc., cat.), reflux, overnight; (b) $NaOH/MeOH/H_2O$, MW (15 min, 50 °C, 150 W) followed by HCl_{aq}; (c) HBTU/DIPEA/benzylamine, DMF, RT, overnight; (d) hydrazine hydrate (98 %), EtOH, RT, overnight; (e) picolinaldehyde, TFA (cat.), EtOH, RT, overnight; (f) lithium iodide, 2% methanol/dichloromethane, irradiation at 365 nm, 32 °C, 1 h.

Preparation of **i**

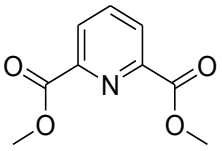

$C_9H_9NO_4$
Mol. Wt.: 195.17

Following the described procedure,[S5] pyridine-2,6-dicarboxylic acid (45.507 g, 272.46 mmol), methanol (325 mL), and sulphuric acid (96 %, 5.6 mL), were added to a 500 mL round bottom flask and refluxed overnight. After this time the reaction mixture was cooled down to room temperature and stirred for additional 3 h to allow the product to crystallize out. The precipitate was filtered off, washed with methanol (300 mL, 50 mL portions), and dried under vacuum to give pure product as white crystals (41.688 g). The filtrate and the washings were combined and reduced to ca. 100 mL volume on a rotary evaporator. After one week at room temperature, the crystalline precipitate was filtered off, washed with methanol and dried under vacuum to yield the second crop of the product (6.936 g). Combined yield: 48.624 g (92 %) of white crystalline solid. ^{1}H NMR in accordance with the previously published[S5] data: ^{1}H NMR (400 MHz, $CDCl_3$) δ 8.32 (d, J = 7.8 Hz, 2H), 8.03 (t, J = 7.8 Hz, 1H), 4.03 (s, 6H).

Preparation of **ii**

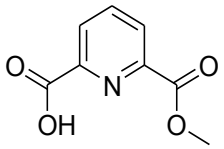

$C_8H_7NO_4$
Mol. Wt.: 181.15

In a 100 mL round bottom flask the diester **i** (536 mg, 2.74 mmol) was dissolved in methanol (30 mL), and to the resulting solution water (20 mL) was added. Some precipitate formed and the stirring mixture was heated to 50 °C in a CEM Discovery microwave reactor (150 W, "open vessel" method) to ensure complete dissolution of the material. $NaOH_{(aq)}$ (3.77 M, 692 µL, 0.95 eq) was added, and stirring was continued at 50 °C for 15 min. Upon cooling to RT, the volume was reduced under vacuum on a rotary evaporator to 10 mL (45 °C, water bath) and the mixture was transferred to a 100 mL separation funnel with 20 mL of water and extracted with dichloromethane (30 mL). To the aqueous layer HCl_{aq} (11.85 M, 220 µL, 0.95 eq) was added, and the precipitate extracted with ethyl-acetate (90 mL, 30 mL portions). The combined organic layers were dried over $MgSO_4$ (anhydr.) followed by solvent evaporation under vacuum. Yield: 327 mg (69 %), white powder. ^{1}H NMR in accordance with the previously published[S6] data: ^{1}H NMR (400 MHz, DMSO) δ 13.49 (s, 3H), 8.25 – 8.20 (m, 2H), 8.18 – 8.12 (m, 1H), 3.90 (s, 3H).

Preparation of **iii**

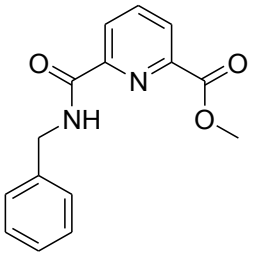

$C_{15}H_{14}N_2O_3$
Mol. Wt.: 270.28

In a 10 mL round bottom flask, **ii** (500 mg, 2.76 mmol, 1 eq) was dissolved in DMF (5 mL). To the clear solution HBTU (1053 mg, 2.777 mmol, 1 eq) was added and dissolved with the help of short ultra-sonication. DIPEA (500 µL, 3.03 mmol, 1.1 eq), was then added and the solution was stirred at room temperature for 5 min. To the resulting dark red solution, benzylamine (600 µL, 5.49 mmol, 2 eq), was added and stirring was continued at RT for 2 days. The clear orange solution was transferred to a 250 mL separating funnel with ethyl acetate (100 mL) and washed with aqueous $NaHCO_3$ (sat., 100 mL). The aqueous layer was extracted with ethyl acetate (100 mL). The combined organic layers were dried over Na_2SO_4 and the solvent was evaporated on a rotary evaporator. The crude residue was purified by automated flash chromatography on a prepacked silica gel column (EtOAc/hexane, R_f = 0.40 in 1:1 hexane:ethyl-acetate; gradient elution from 10 % to 50 % of EtOAc). Yield: 553 mg (74 %), yellowish viscous liquid. Analytical sample was recrystallized from CH_2Cl_2/pentane to yield white crystals.

^{1}H NMR (400 MHz, DMSO) δ 9.08 (t, J = 6.3 Hz, 1H), 8.26 (dd, J = 7.1, 1.9 Hz, 1H), 8.23 – 8.15 (m, 2H), 7.41 – 7.27 (m, 4H), 7.26 – 7.13 (m, 1H), 4.53 (d, J = 6.4 Hz, 2H), 3.90 (s, 3H).

^{13}C NMR (101 MHz, DMSO) δ 164.63, 163.28, 150.28, 146.58, 139.41, 139.34, 128.30, 127.48, 127.26, 126.86, 125.36, 52.70, 42.55.

TOF HRMS ESI+ (*m/z*): $C_{15}H_{14}N_2O_3Na^+$ ([M+Na]$^+$), calcd 293.0902; found 293.0894.

Elemental CHN analysis (%):$C_{15}H_{14}N_2O_3$, calcd C 66.66, H 5.22, N 10.36; found C 66.68, H 5.36, N 10.34.

Preparation of **iv**

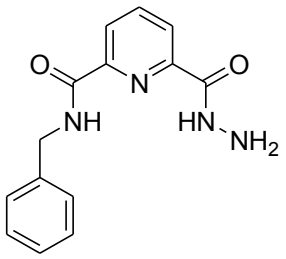

$C_{14}H_{14}N_4O_2$
Mol. Wt.: 270.29

In a 25 mL round bottom flask, **iii** (553 mg, 2.05 mmol, 1 eq) was dissolved in absolute ethanol (12.5 mL). Hydrazine monohydrate (400 µL, 8.25 mmol, 4 eq) was added, and the solution was stirred at room temperature overnight. The volatiles were evaporated under reduced pressure, and the crude product was used in the next reaction step without any further purification. Yield: nearly quantitative with minor impurities (by ^{1}H NMR), yellow solid.

^{1}H NMR (400 MHz, DMSO) δ 10.57 (t, *J* = 3.1 Hz, 1H), 9.99 (t, *J* = 6.4 Hz, 1H), 8.23 – 8.14 (m, 3H), 7.36 – 7.32 (m, 4H), 7.29 – 7.22 (m, 1H), 4.64 (d, *J* = 4.0 Hz, 2H), 4.57 (d, *J* = 6.4 Hz, 2H).

Preparation of *E*-**1**

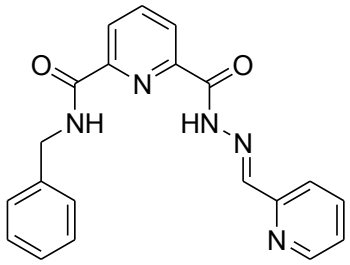

$C_{20}H_{17}N_5O_2$
Mol. Wt.: 359.38

In a 15 mL round bottom flask, **iv** (550 mg, 2.03 mmol, 1 eq) was dissolved in absolute ethanol (12 mL). Picolinaldehyde (230 µL, 2.42 mmol, 1.2 eq) and a drop of TFA were added and the yellow solution was stirred at room temperature overnight. The solvent was removed under reduced pressure. The residue was dissolved in dichloromethane (15 mL), pre-loaded on silica by evaporation with 1 g of silica-gel, and purified by automated flash chromatography on a prepacked silica column (methanol/dichloromethane, gradient from 0 % to 5 % of methanol, R_f = 0.27 in 7 % methanol/dichloromethane). Yield: 568 mg (78 %), white powder.

^{1}H NMR (400 MHz, $CDCl_3$) δ 11.10 (s, 1H), 8.50 (ddd, *J* = 4.9, 1.7, 0.9 Hz, 1H), 8.46 – 8.37 (m, 3H), 8.06 (t, *J* = 7.8 Hz, 2H), 7.68 (td, *J* = 7.7, 1.6 Hz, 1H), 7.36 – 7.20 (m, 6H), 4.69 (d, *J* = 6.2 Hz, 2H).

^{1}H NMR (400 MHz, CD_2Cl_2) δ 10.98 (s, 1H), 8.54 (ddd, *J* = 4.9, 1.7, 1.0 Hz, 1H), 8.45 – 8.29 (m, 4H), 8.10 (t, *J* = 7.8 Hz, 1H), 8.03 (dt, *J* = 8.0, 0.9 Hz, 1H), 7.75 – 7.69 (m, 1H), 7.39 – 7.21 (m, 6H), 4.68 (d, *J* = 6.3 Hz, 2H).

^{1}H NMR (400 MHz, CD_3CN) δ 11.30 (s, 1H), 8.90 (t, *J* = 5.0 Hz, 1H), 8.63 (ddd, *J* = 4.9, 1.7, 1.0 Hz, 1H), 8.56 (s, 1H), 8.36 (d, *J* = 7.8 Hz, 1H), 8.17 (dd, *J* = 8.2, 7.4 Hz, 1H), 8.05 (dt, *J* = 8.0, 1.0 Hz, 1H), 7.84 (td, *J* = 7.6, 1.5 Hz, 1H), 7.45 – 7.33 (m, 5H), 7.32 – 7.24 (m, 1H), 4.69 (d, *J* = 6.5 Hz, 2H).

^{1}H NMR (400 MHz, DMSO) δ 12.33 (s, 1H), 9.89 (t, *J* = 6.4 Hz, 1H), 8.37 – 8.24 (m, 3H), 8.04 (dt, *J* = 8.0, 1.1 Hz, 1H), 7.92 (td, *J* = 7.8, 1.6 Hz, 1H), 7.46 (ddd, *J* = 7.4, 4.9, 1.2 Hz, 1H), 7.41 – 7.33 (m, 4H), 7.29 – 7.24 (m, 1H), 4.66 (d, *J* = 6.4 Hz, 2H).

^{13}C NMR (101 MHz, DMSO) δ 163.25, 159.75, 153.04, 150.14, 149.69, 148.86, 147.89, 139.87, 139.22, 137.02, 128.42, 127.13, 126.92, 125.27, 125.18, 124.71, 120.10, 42.38.

^{1}H NMR (400 MHz, 10% $CD_3CN/CDCl_3$) δ 11.16 (s, 1H), 8.73 (t, *J* = 4.8 Hz, 1H), 8.50 (ddd, *J* = 4.8, 1.6, 0.9 Hz, 1H), 8.44 (s, 1H), 8.32 (ddd, *J* = 7.9, 2.1, 1.1 Hz, 2H), 8.08 (dt, *J* = 8.1, 0.9 Hz, 1H), 8.01 (t, *J* = 7.8 Hz, 1H), 7.67 (td, *J* = 7.8, 1.2 Hz, 1H), 7.39 – 7.08 (m, 6H), 4.62 (d, *J* = 6.5 Hz, 2H).

TOF HRMS ESI+ (*m*/*z*): $C_{20}H_{17}N_5O_2Na^+$ ([M+Na]$^+$), calcd 382.1280; found 382.1268.

Elemental CHN analysis (%): $C_{20}H_{17}N_5O_2$, calcd C 66.84, H 4.77, N 19.49; found C 66.69, H 4.71, N 19.44.

Preparation of *Z*-**1**

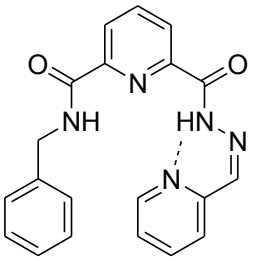

$C_{20}H_{17}N_5O_2$
Mol. Wt.: 359.38

In a 40 mL screw capped vial (9.5×2.75 cm, clear glass) with a stir bar, *E*-**1** (100 mg, 0.278 mmol, 1 eq) and lithium iodide (43 mg, 0.32 mmol, 1.1 eq) were dissolved in 2% methanol/chloroform mixture (v/v). The solution was irradiated at 365 nm (bandwidth ≈ 20 nm) for 1 h in a photo-reactor equipped with 8 UV bulbs (Philips PL-S 9W/2P BLB) and a ventilator for air cooling (temperature inside the reactor was 32 °C). After this time the reaction mixture was pre-loaded on silica by evaporation with 1 g of silica-gel using rotary evaporator (40 °C, water bath). The solid sample was purified by automated flash chromatography on a 12 g prepacked silica column (methanol/dichloromethane gradient from 0 % to 5 % of methanol, R_f = 0.35 in 3 % methanol/dichloromethane). Yield: 85 mg (85 %), white powder.

^{1}H NMR (400 MHz, CD_3CN) δ 15.67 (s, 1H), 8.54 (s, 1H), 8.40 (dd, *J* = 7.7, 1.2 Hz, 1H), 8.39 (dd, *J* = 7.9, 1.2 Hz, 1H), 8.21 (t, *J* = 7.8 Hz, 1H), 8.15 (ddd, *J* = 4.9, 1.6, 0.7 Hz, 1H), 7.94 (td, *J* = 7.8, 1.8 Hz, 1H),

7.63 (s, 1H), 7.62 (dt, *J* = 7.7, 1.0 Hz, 1H), 7.46 – 7.41 (m, 2H), 7.41 – 7.35 (m, 2H), 7.35 – 7.29 (m, 1H), 7.21 (ddd, *J* = 7.7, 4.9, 1.2 Hz, 1H), 4.78 (d, *J* = 6.4 Hz, 2H).

^{1}H NMR (400 MHz, $CDCl_3$) δ 15.58 (s, 1H), 8.50 (ddd, *J* = 7.9, 3.6, 1.2 Hz, 1H), 8.43 (t, *J* = 6.2 Hz, 1H), 8.11 (t, *J* = 7.8 Hz, 1H), 7.85 (ddd, *J* = 4.8, 1.4, 0.6 Hz, 1H), 7.80 (td, *J* = 7.8, 1.8 Hz, 1H), 7.58 (s, 1H), 7.46 (dt, *J* = 7.9, 1.0 Hz, 1H), 7.44 – 7.32 (m, 5H), 6.98 (ddd, *J* = 7.7, 4.9, 1.2 Hz, 1H), 4.83 (d, *J* = 6.3 Hz, 2H).

^{13}C NMR (101 MHz, DMSO) δ 163.71, 160.71, 151.57, 149.55, 148.52, 148.10, 140.33, 139.91, 139.05, 138.32, 128.57, 127.74, 127.26, 126.69, 125.42, 125.37, 124.60, 42.78.

3 NMR Spectra

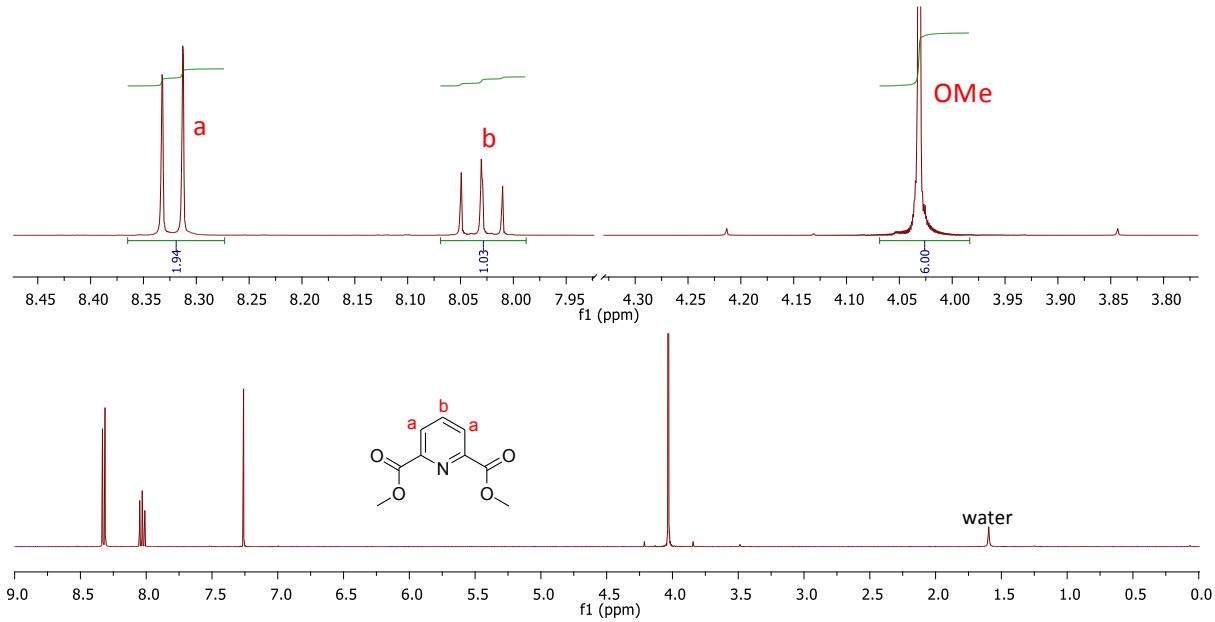

Figure S 1. ^{1}H NMR spectrum of **i** in chloroform-d_1.

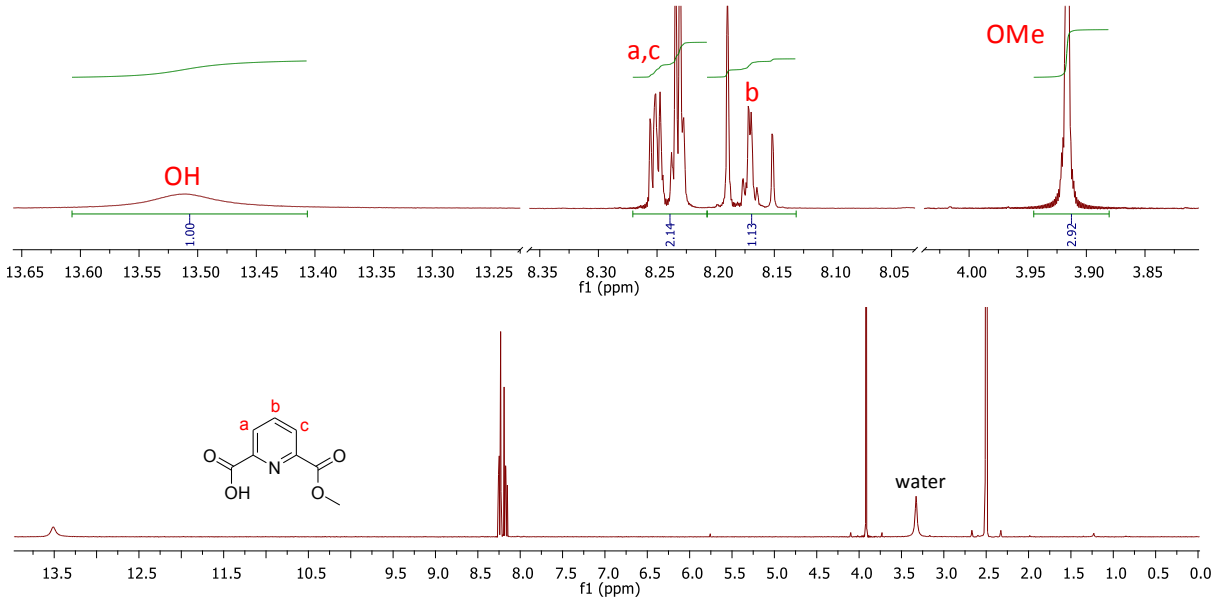

Figure S 2. ^{1}H NMR spectrum of **ii** in DMSO-d_6.

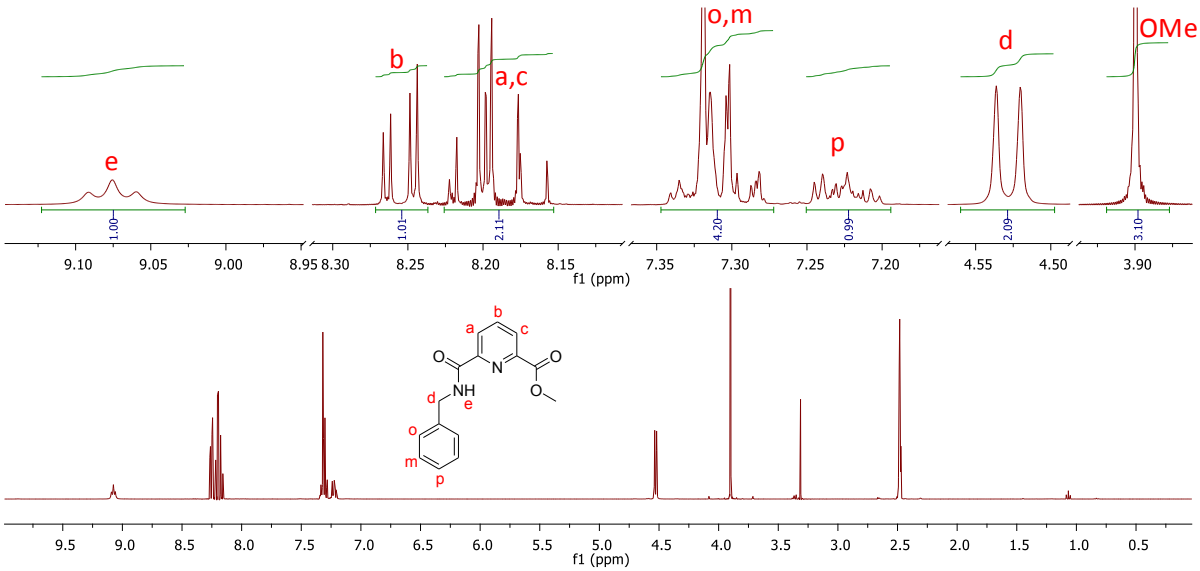

Figure S 3. ^{1}H NMR spectrum of **iii** in DMSO-d_6.

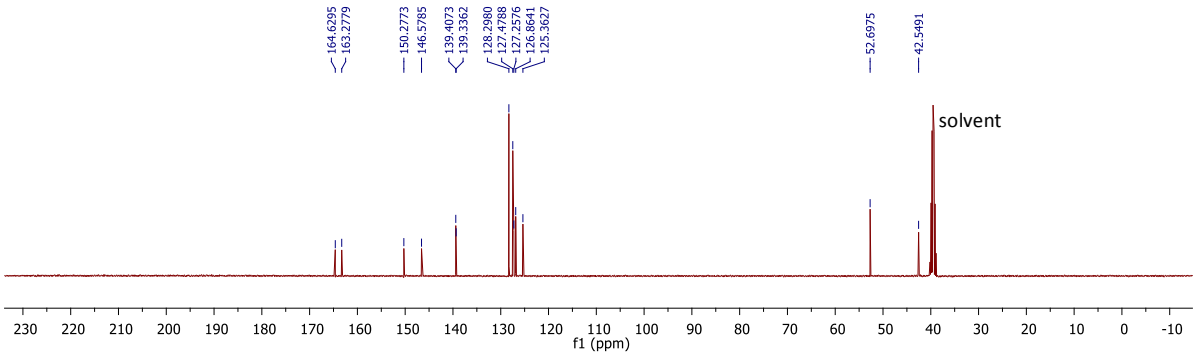

Figure S 4. ^{13}C NMR spectrum of **iii** in DMSO-d_6.

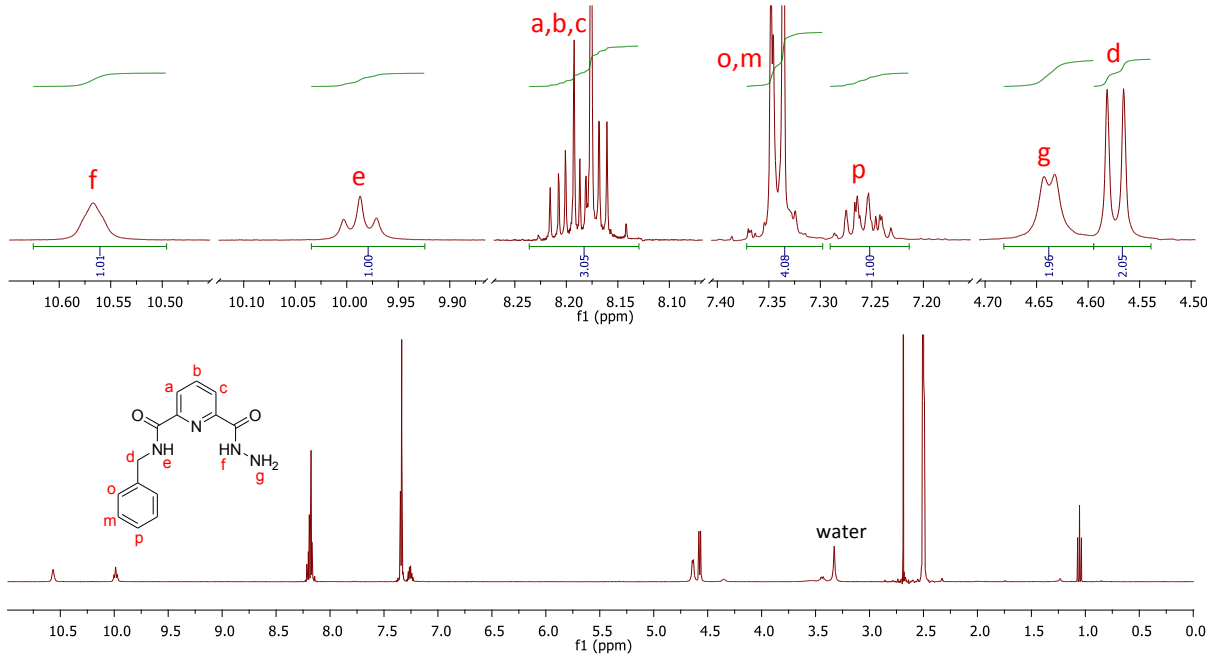

Figure S 5. ^{1}H NMR spectrum of **iv** in DMSO-d_6.

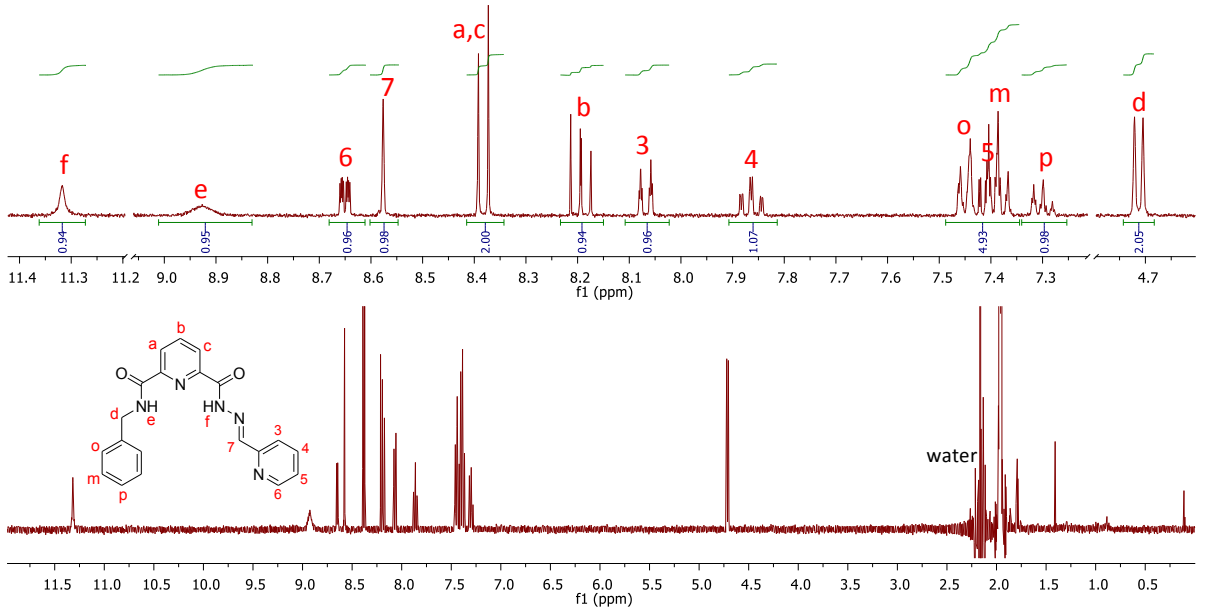

Figure S 6. ^{1}H NMR spectrum of *E*-**1** in acetonitrile-d_3.

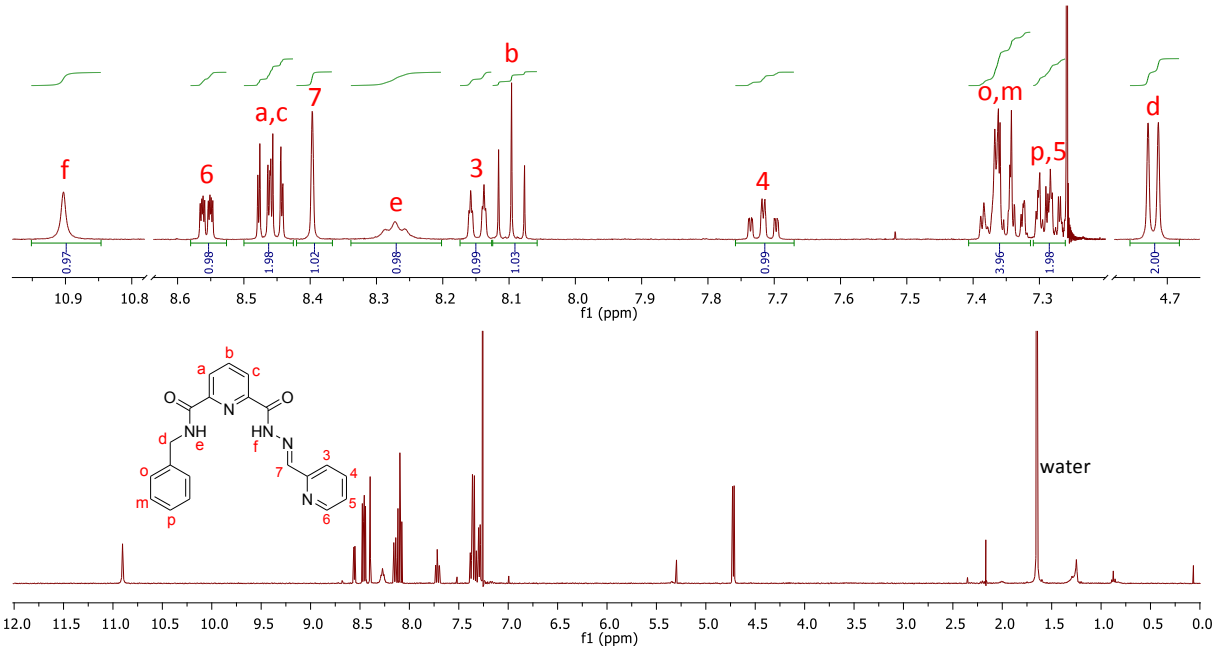

Figure S 7. ^{1}H NMR spectrum of *E*-**1** in chloroform-d_1.

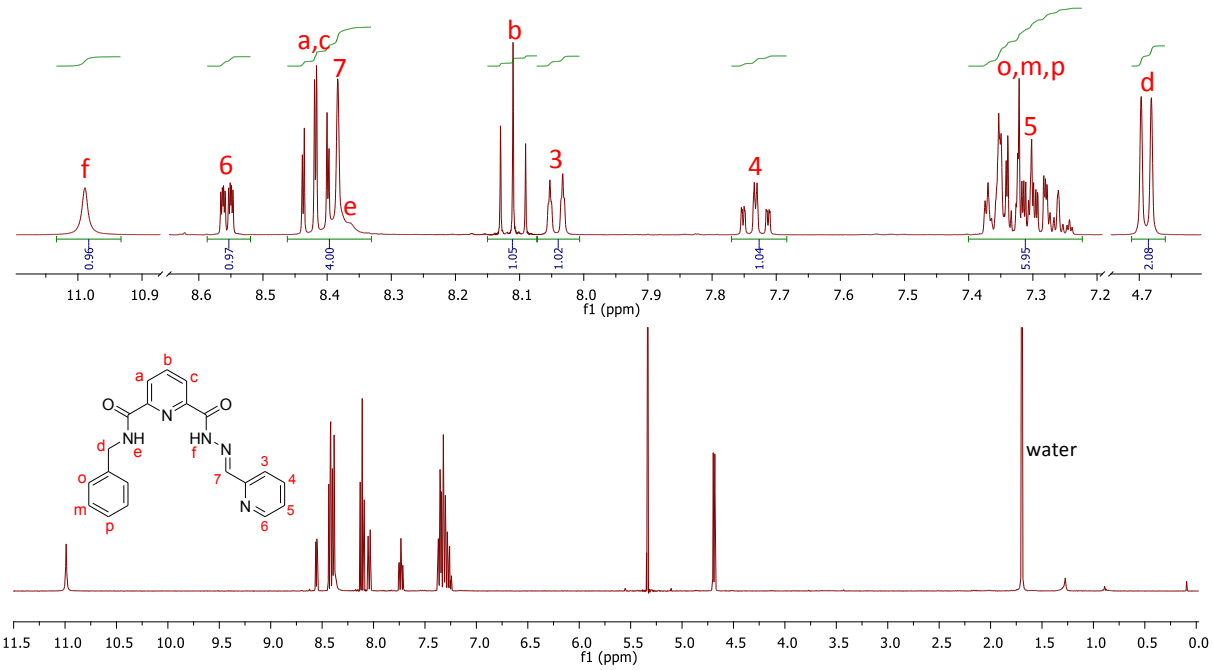

Figure S 8. ^{1}H NMR spectrum of *E*-**1** in dichloromethane-d_2.

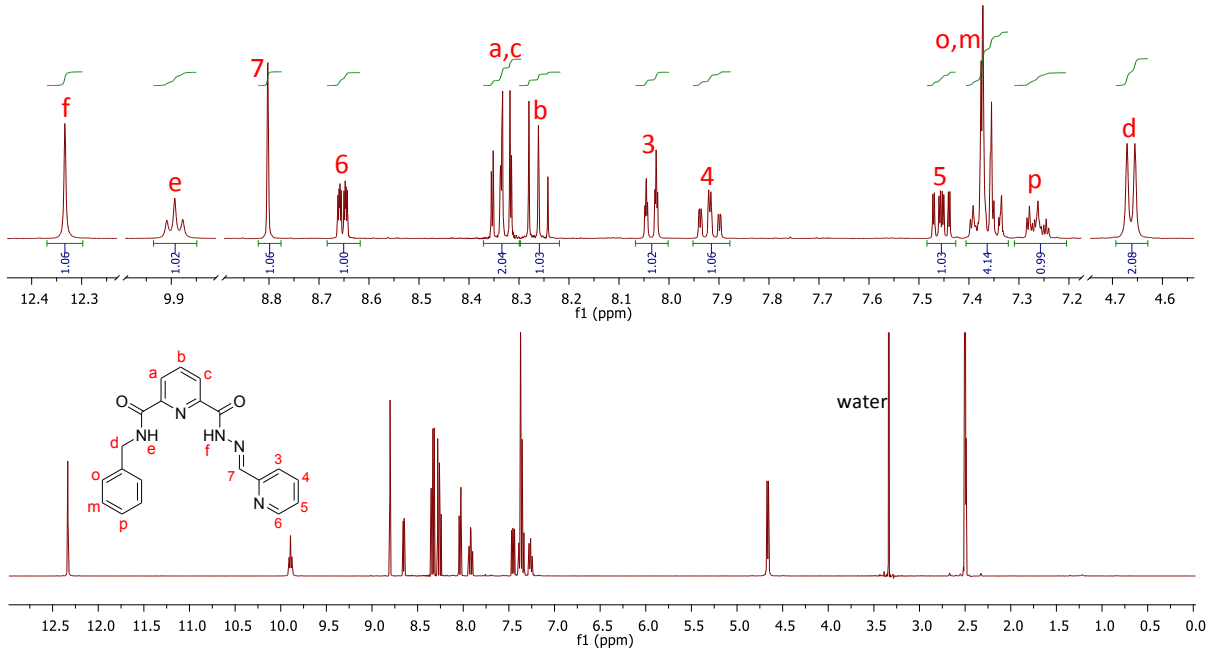

Figure S 9. ^{1}H NMR spectrum of *E*-**1** in DMSO-d_6.

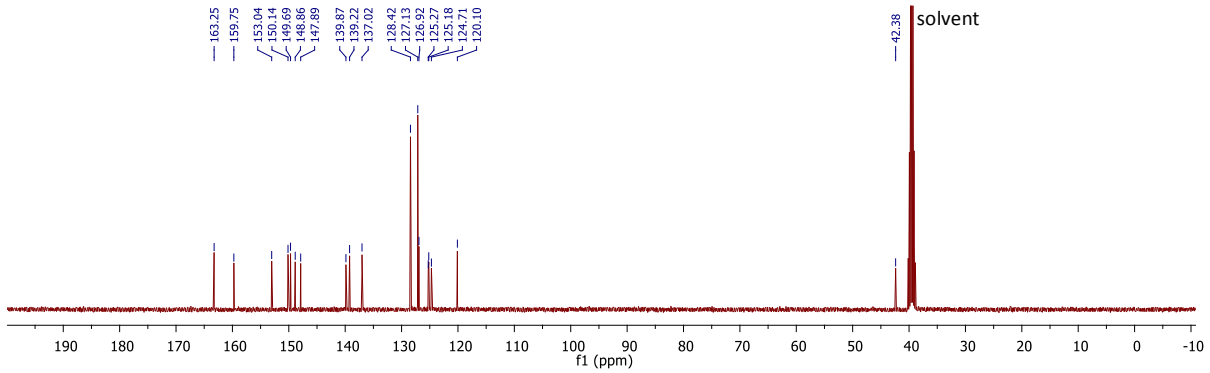

Figure S 10. ^{13}C NMR spectrum of *E*-**1** in DMSO-d_6.

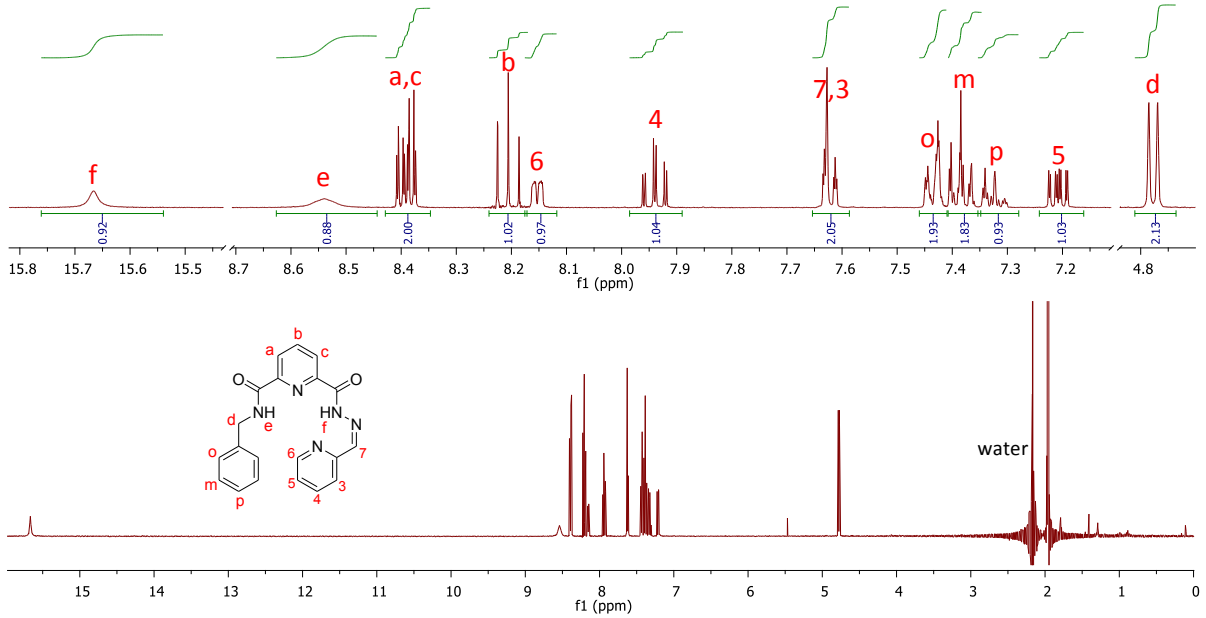

Figure S 11. ^{1}H NMR spectrum of *Z*-**1** in acetonitrile-d_3.

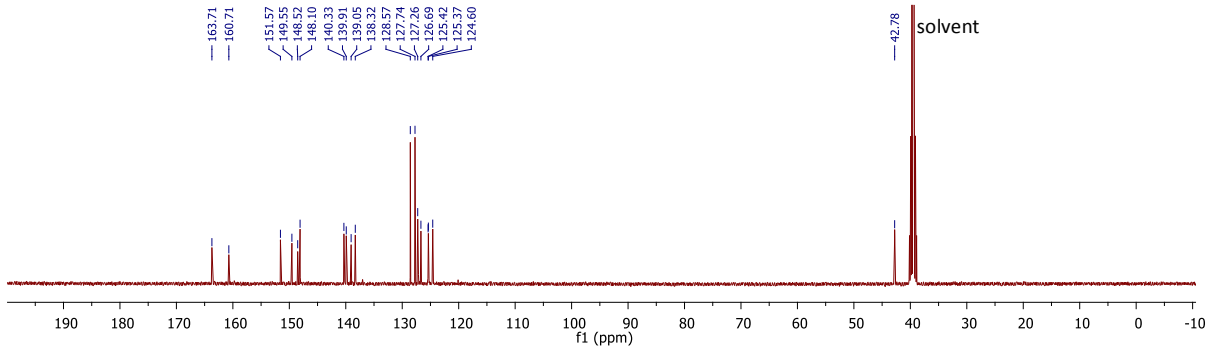

Figure S 12. ^{13}C NMR spectrum of *Z*-**1** in DMSO-d_6.

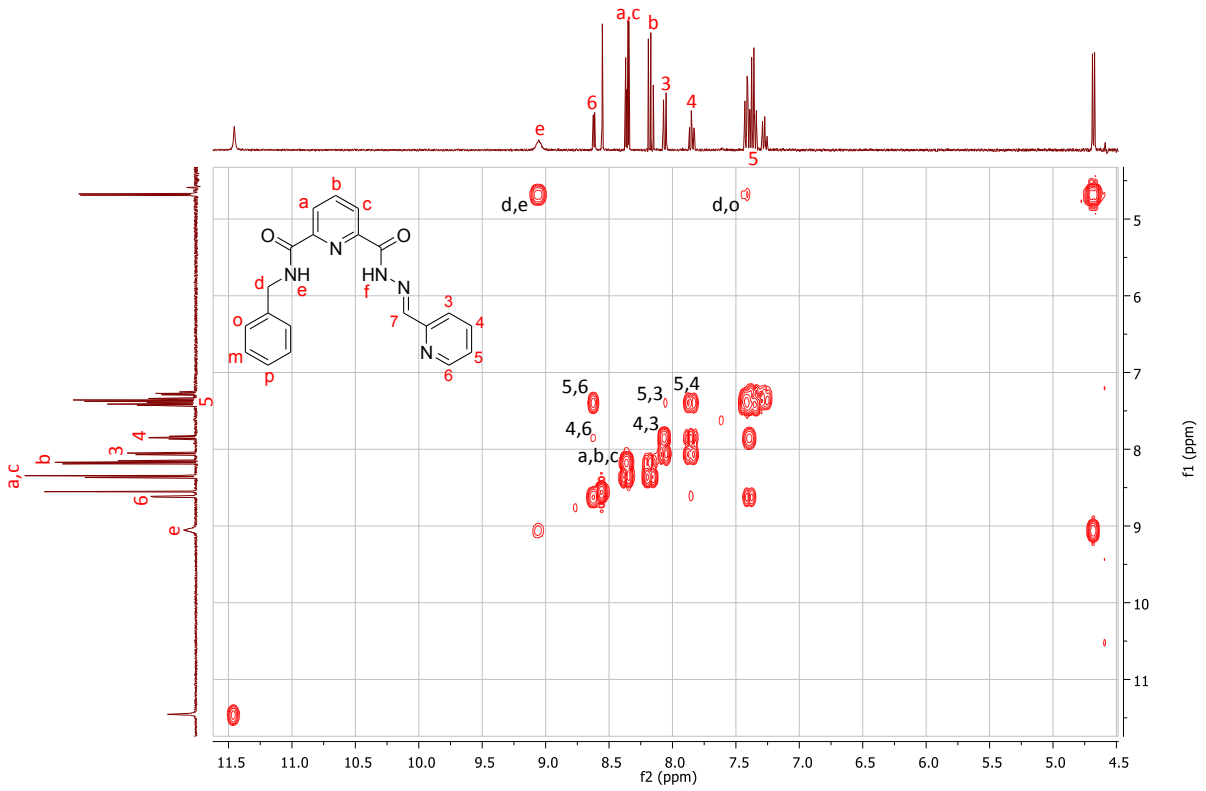

Figure S 13. ^{1}H gCOSY (acetonitrile-d_3) spectrum of *E*-**1** (4 mM).

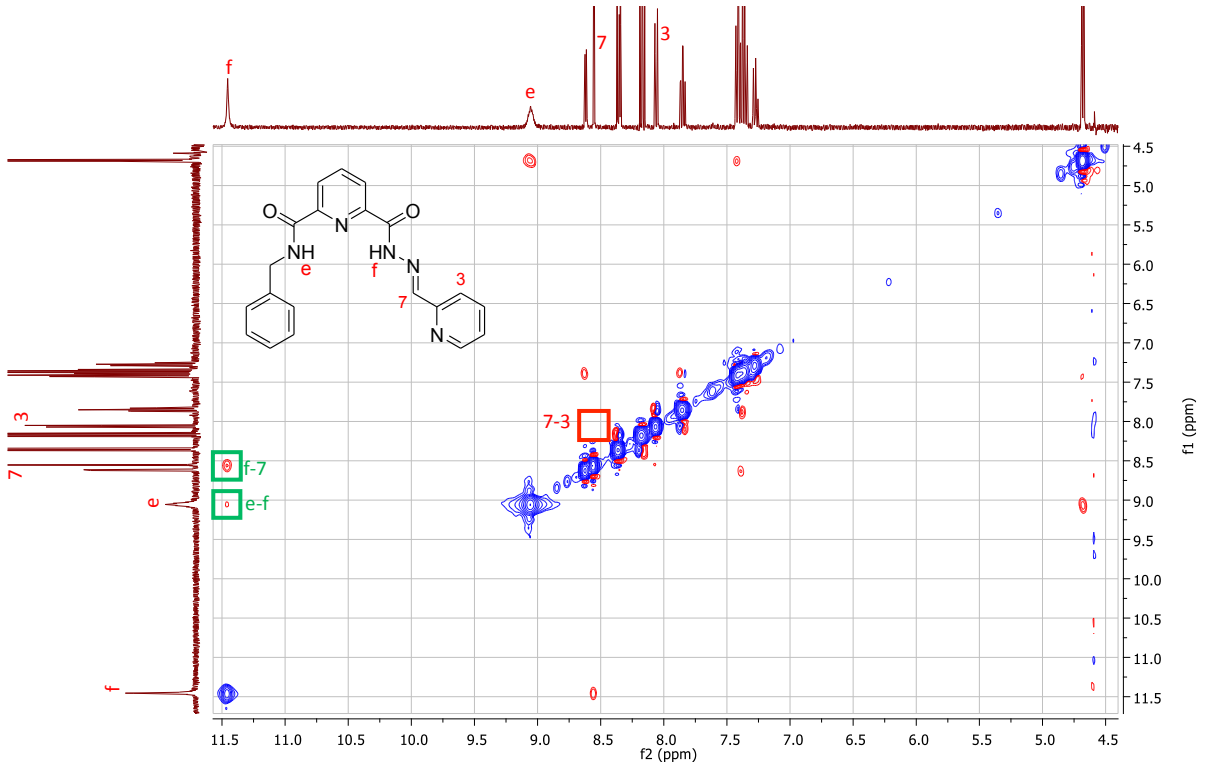

Figure S 14. ^{1}H ROESY (acetonitrile-d_3) spectrum of *E*-**1** (4 mM), supporting *syn*-conformation of the central pyridine carbonyls in solution. The absence of contact (red square) between the 3H of the terminal pyridine and the imine CH suggests that the free receptor exists predominately in the depicted conformation, as opposed to the bound receptor (see Figure S 15).

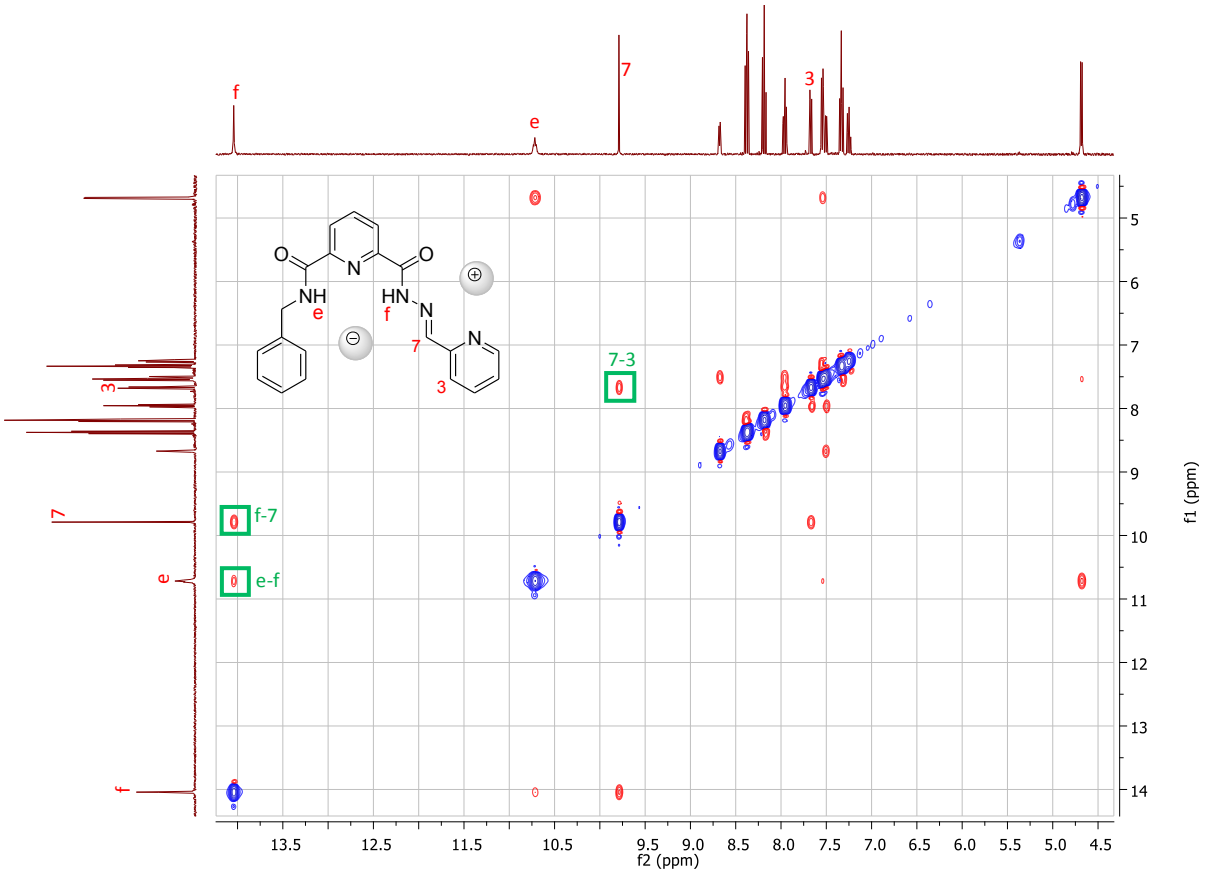

Figure S 15. ^{1}H ROESY (acetonitrile-d_3) spectrum of *E*-**1** (4 mM) with LiBr (5 eq). The assigned peaks indicate that the conformation of the bound receptor in acetonitrile solution is retained with respect to X-ray single crystal structures.

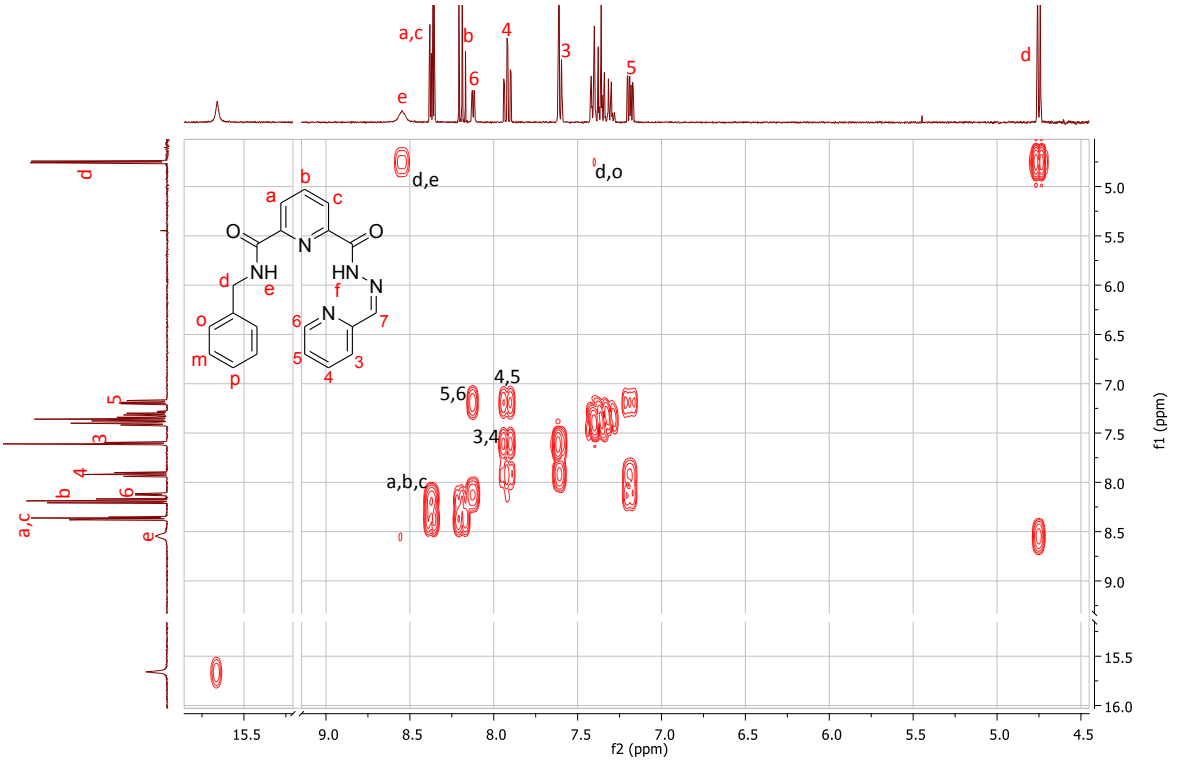

Figure S 16. ^{1}H gCOSY (acetonitrile-d_3) spectrum of *Z*-**1** (4 mM).

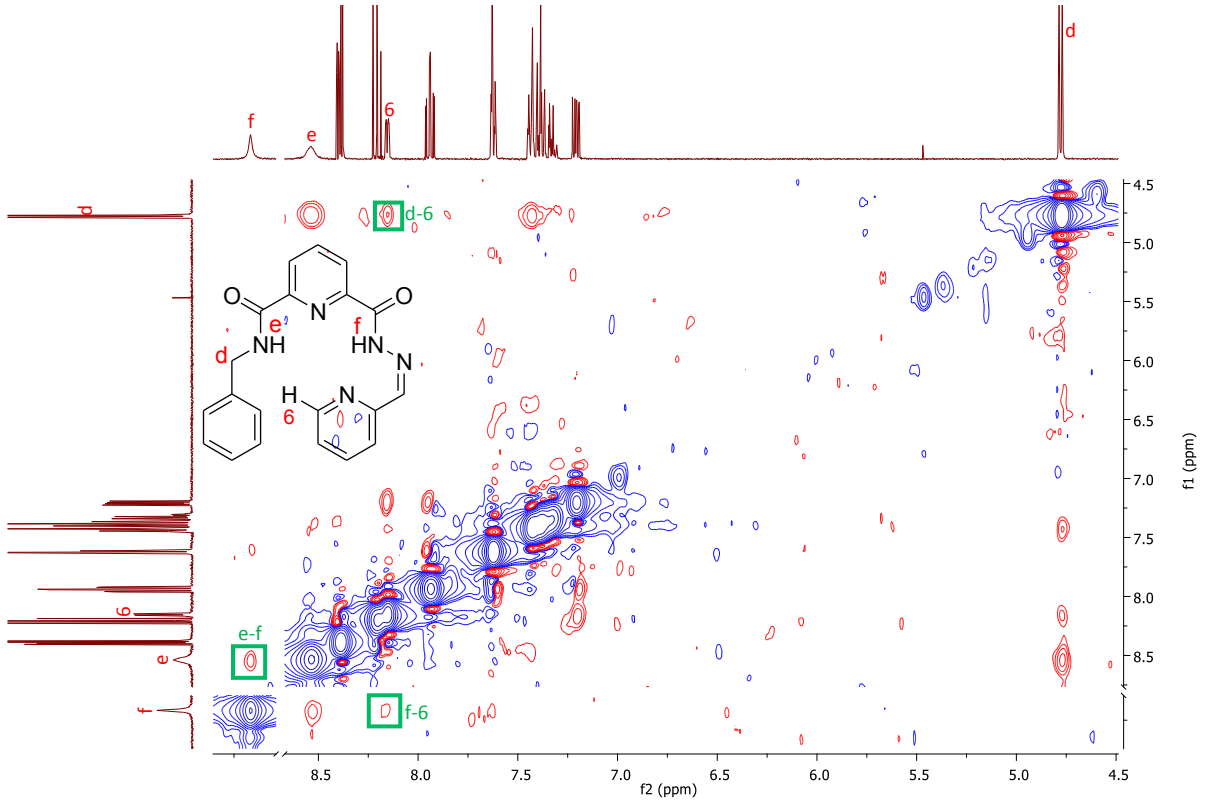

Figure S 17. ^{1}H NOESY (acetonitrile-d_3) of *Z*-**1**, supporting the depicted conformation in solution.

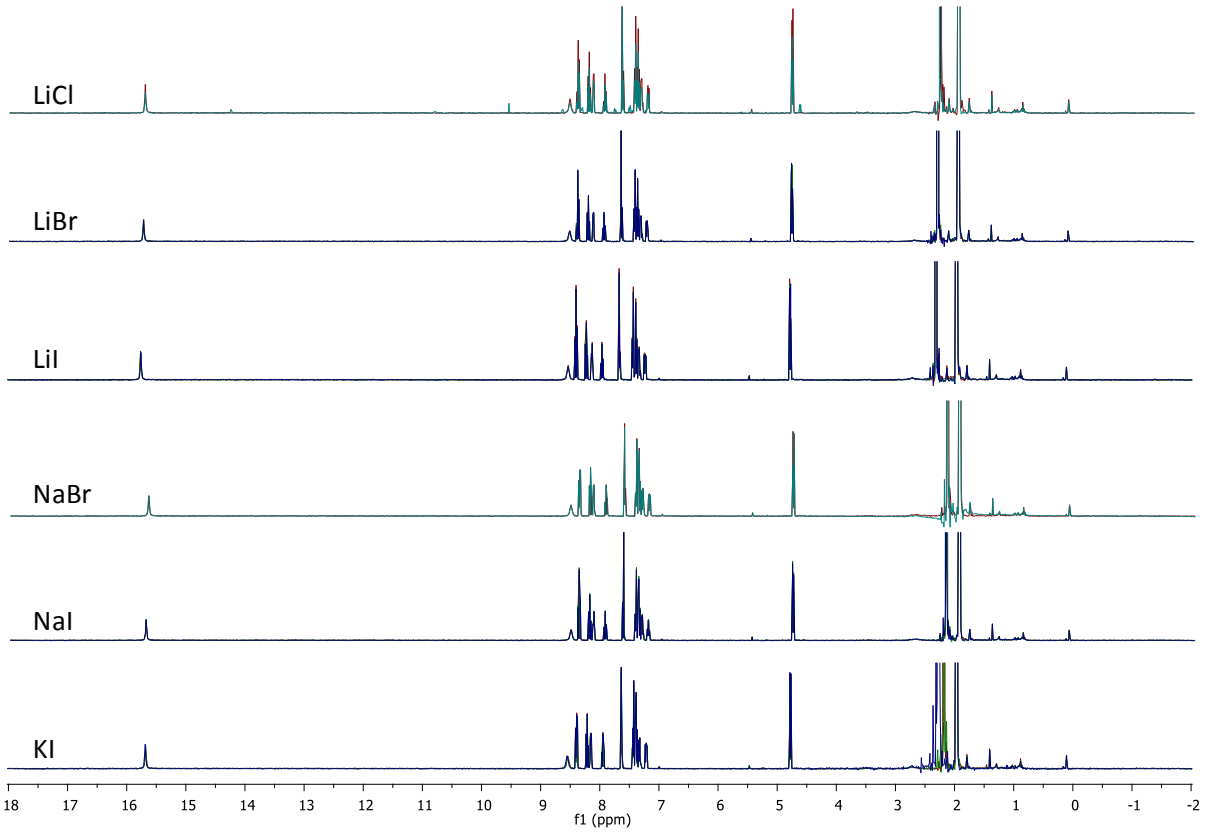

Figure S 18. Overlapped ^{1}H NMR spectra of *Z*-**1** in acetonitrile-d_3 with 5 eq. of the salt, after 1 and 7 days of standing in the dark. No significant changes were observed in the spectra within the investigated time period. In the case of LiCl, less than 10% of isomerization to *E*-**1** was observed only after 7 days. Due to the limited solubility of NaBr, only 1 eq. was used.

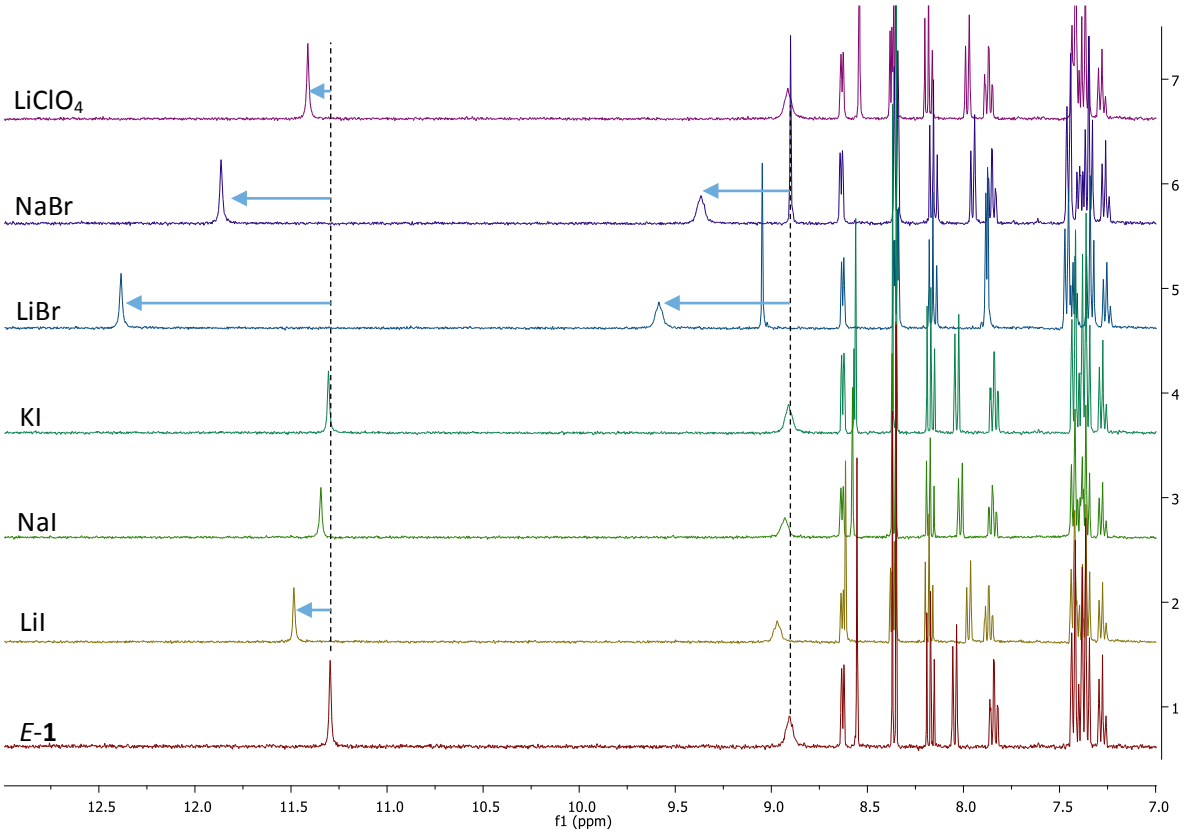

Figure S 19. Stack of ^{1}H NMR spectra of *E*-**1** in acetonitrile-d_3 (2 mM) with 1 equivalent of the corresponding salt. The indicated chemical shift changes of NH protons suggest only weak binding of iodide and perchlorate salts, and stronger binding of bromide salts (vide infra).

4 NMR Titrations

4.1 General Procedure for ^{1}H NMR Titrations

All the reagents were weighted separately on a Mettler Toledo Excellence XA105DU analytical balance (readability 0.01 mg) in screw-capped vials sealed with Teflon-covered septa. All the solvent/solution manipulations were done using gas-tight Hamilton glass syringes. Titrants were prepared by dissolving appropriate salts in the solution of the receptor (unless specified otherwise), in order to avoid dilution of the receptor during titration. Titrations were performed in screw-capped NMR tubes sealed with Teflon-covered septa, by adding aliquots of the titrant solution to the receptor solution (0.600 mL, 2 mM) and recording ^{1}H NMR spectra after each addition. The NMR spectra were measured on Agilent 400 MHz spectrometer. Salts with evident solubility issues were not investigated.

Methods used for NMR titrations of **1**:

- Method A; titration with single salt (avoided when solubility issues were evident)
- Method B; titration with TBA halogenide in the presence of 1 equivalent of alkali tetraphenylborate salt.

4.2 Data Fitting and Model Equilibria

The ^{1}H NMR titration data were fitted with HypNMR software, which allows simultaneous fitting of multiple titration curves. Simple 1:1 binding model was used for tetrabutylammonium and tetraphenylborate salts. For ion pair binding, a more complex model was used as shown on Scheme S 2 and in Table S 1. In this model, the binding constants and chemical shifts for simple 1:1 anion binding and 1:1 cation binding were fixed at the average values obtained from two separate titration experiments with tetrabutylammonium and tetraphenylborate salts.

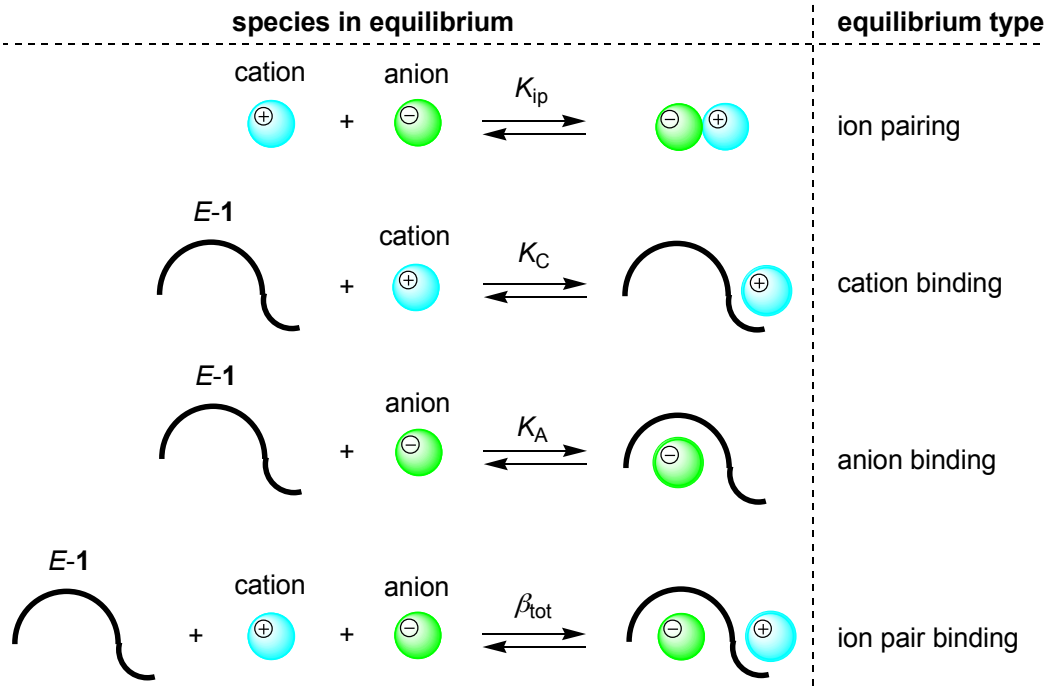

Scheme S 2. Different equilibria considered for the fitting of ^{1}H NMR titration data.

Table S 1. The model applied and the equilibrium constants obtained from fitting the ^{1}H NMR titration data for receptor **1** and various salts in acetonitrile-d_3. In the cases of individual anion and cation titrations, and in titration Method B, the counter ions were tetrabutylammonium cation and tetraphenylborate anion. Ion pairing with these counter ions was not included in the model since they are known to associate only very weakly in acetonitrile solutions.[S7]

Complexed Species	Titration Method	Model Equilibria	log(equilibrium constant)[(a)]	Cooperativity Factor, α[(b)]
titrations of *E*-**1**				
Cl^-	A	1:1 anion binding	2.81, 2.78; refined	
Br^-	A	1:1 anion binding	1.95, 1.95; refined	
I^-	A	1:1 anion binding	0.59, 0.81 refined	
Li^+	A	1:1 cation binding	2.11, 2.05; refined	
Na^+	A	1:1 cation binding	1.56, 1.51; refined	
K^+	A	1:1 cation binding	1.25, 1.30; refined	
Li^+Cl^-	B	**ion pair binding**	**6.32, 6.16**; refined	23
		1:1 anion binding	2.80; fixed	
		1:1 cation binding	2.08; fixed	
		ion pairing	3.20, 3.11; refined[(c)]	
Li^+Br^-	A and B	**ion pair binding**	**5.40, 5.59**; refined	29
		1:1 anion binding	1.95; fixed	
		1:1 cation binding	2.08; fixed	
		ion pairing	2.21; fixed[(d)]	
Li^+I^-	A and B	**ion pair binding**	**4.21, 4.26**; refined	15
		1:1 anion binding	0.70; fixed	
		1:1 cation binding	2.08; fixed	
		ion pairing	1.37; fixed[(d)]	
Na^+Br^-	B	**ion pair binding**	**4.89, 4.83**; refined	26
		1:1 anion binding	1.96; fixed	
		1:1 cation binding	1.54; fixed	
		ion pairing	2.87; 2.59 refined	
Na^+I^-	A and B	**ion pair binding**	**3.39, 3.47**; refined	8
		1:1 anion binding	0.70; fixed	
		1:1 cation binding	1.54; fixed	
		ion pairing	1.44; fixed[(d)]	
K^+I^-	B	**ion pair binding**	**3.15**; **3.25**; refined	9
		1:1 anion binding	0.70; fixed	
		1:1 cation binding	1.28; fixed	
		ion pairing	1.4; fixed	
titrations of *Z*-**1**[(e)]				
Li^+I^-	A	1:1 cation binding	< 1; refined	
		ion pairing	1.37; fixed[(d)]	
Li^+Br^-	A	1:1 cation binding	< 1; refined	
		ion pairing	2.21; fixed[(d)]	
Na^+I^-	A	1:1 cation binding	< 1; refined	
		ion pairing	1.44; fixed[(d)]	

[(a)] values of two independent experiments are shown.

[(b)] calculated as $\alpha = \beta_{tot}/(K_A \times K_C)$ where β_{tot}, K_A, and K_C represent average values of cumulative ion pair, anion, and cation binding constants, respectively. For iodide, K_A was taken as 1, even though experiments indicate $K_A < 1$.

[(c)] in good agreement with the literature value[S8] of 3.5, although the authors stated large uncertainty of the measurement

[(d)] literature value[S9]

[(e)] Since anion binding site in *Z*-**1** is inaccessible, only cation binding was considered. However, data could not be fitted satisfactorily and indicate only very weak interactions with the investigated salts.

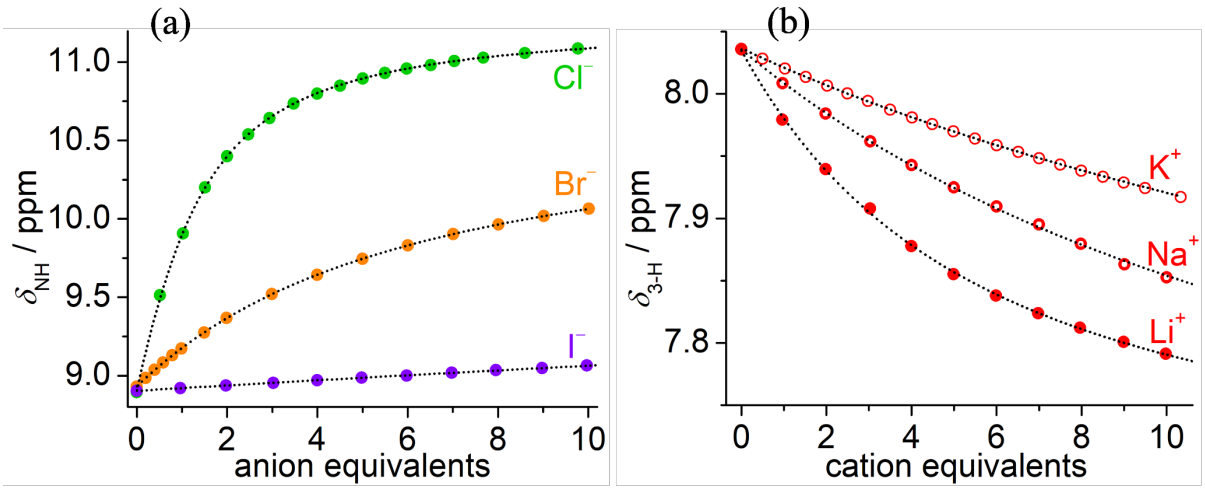

Figure S 20. The results of ^{1}H NMR spectroscopic titrations of *E*-**1** (2 mM, acetonitrile-d_3) with individual (a) anions and (b) cations as their TBA^+/Ph_4B^- salts, respectively. Panel (a) shows chemical shift changes of the amide NH proton, which is the most sensitive to anion binding whereas panel (b) shows chemical shift changes of the 3-H proton of the 2-pyridyl moiety, which is indicative of cation binding. Dotted lines represent the results of data fitting to a simple 1:1 binding model.

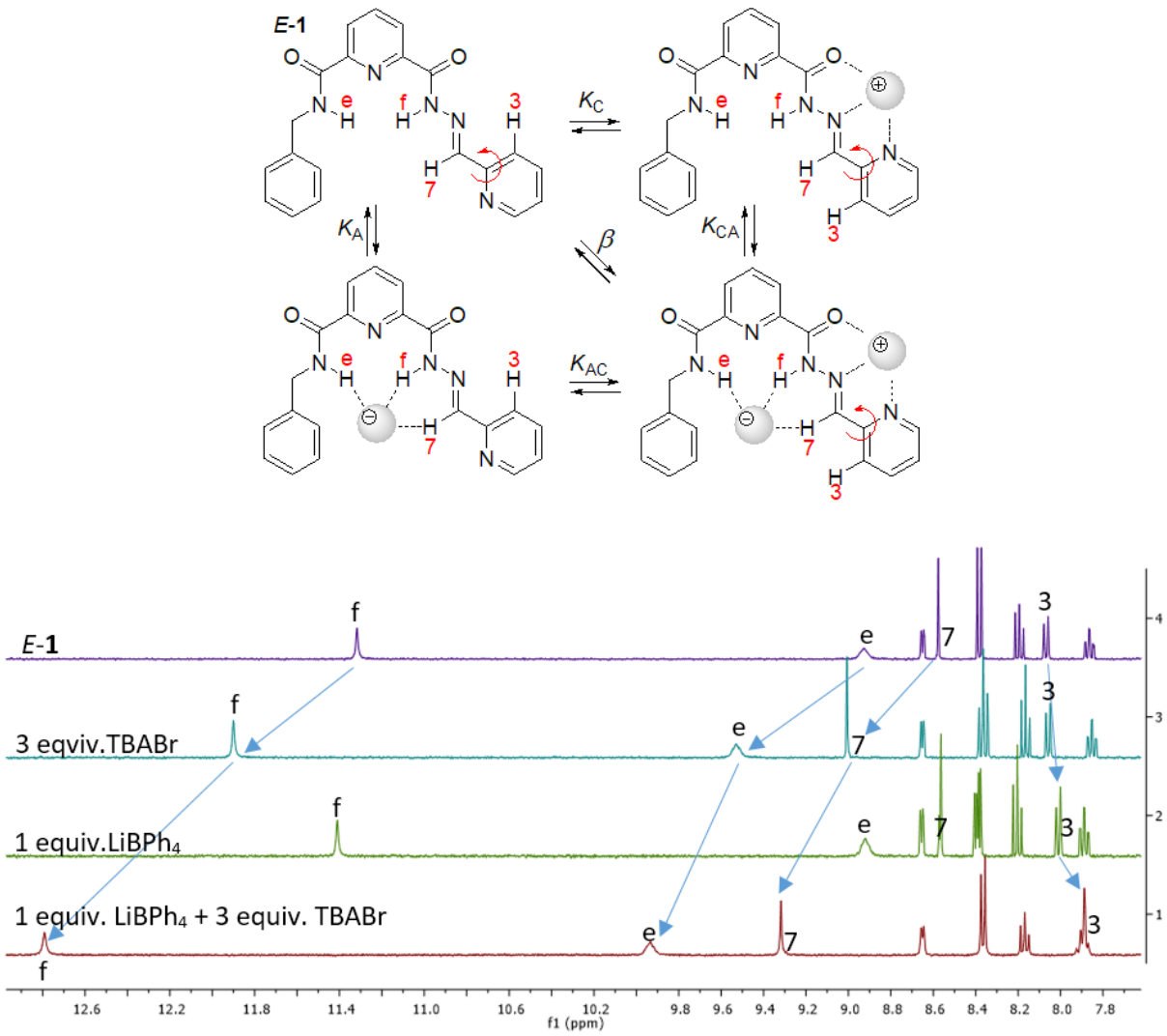

Figure S 21. ^{1}H NMR spectra of *E*-**1** (2 mM, acetonitrile-d_3) in the absence (top) and in the presence of various salts. The chemical shift changes marked with arrows suggest strong cooperative binding of Li^+Br^- ion pair to the receptor.

4.3 Anion Binding

4.3.1 Titration of *E*-**1** with Cl^- in acetonitrile-d_3

Titration of *E*-**1** with TBACl showed significant changes in the ^{1}H NMR chemical shifts of protons e, f, and 7, characteristic of anion binding. These data were simultaneously fitted to the model shown in Scheme S 3, using HypNMR software.

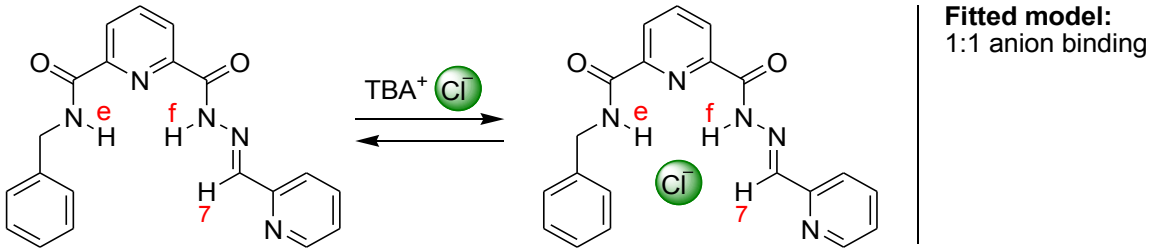

Scheme S 3. Chloride binding to *E*-**1**. Chemical shifts of the indicated protons were used for fitting.

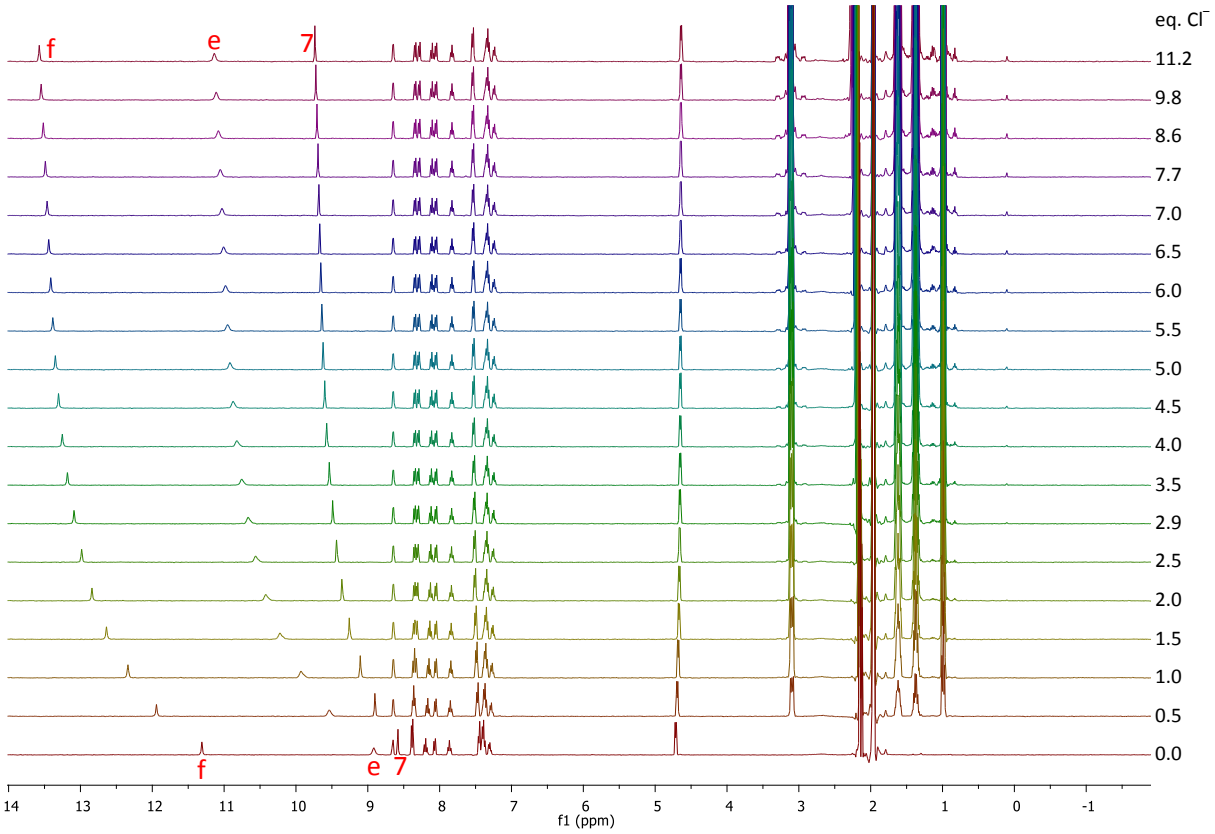

Figure S 22. ^{1}H NMR titration (acetonitrile-d_3) of *E*-**1** (2 mM) with TBACl. The assigned peaks were used for fitting.

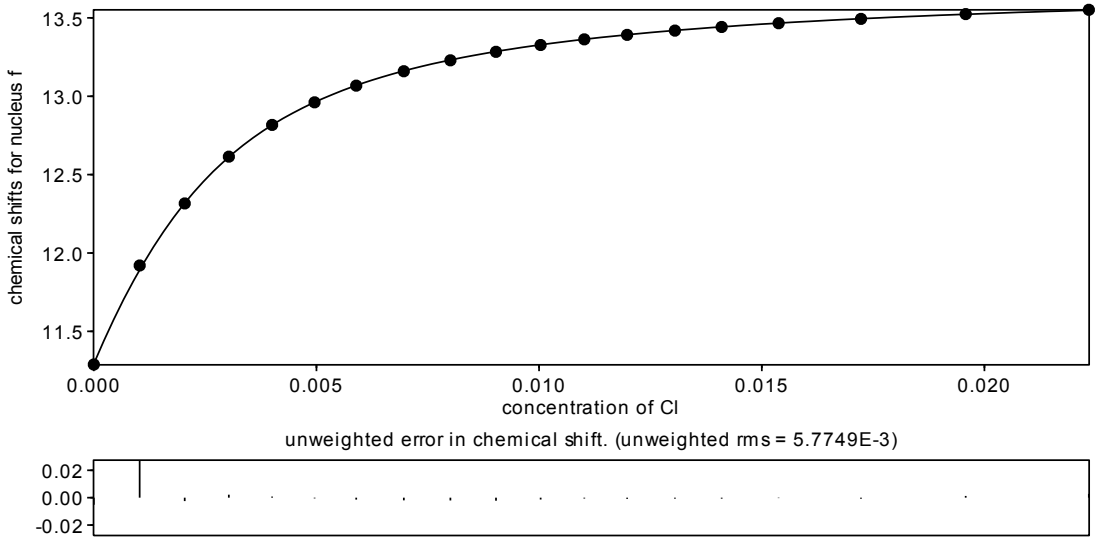

Figure S 23. Data points and fitting curve for ^{1}H NMR titration (acetonitrile-d_3) of *E*-**1** (2 mM) with TBACl.

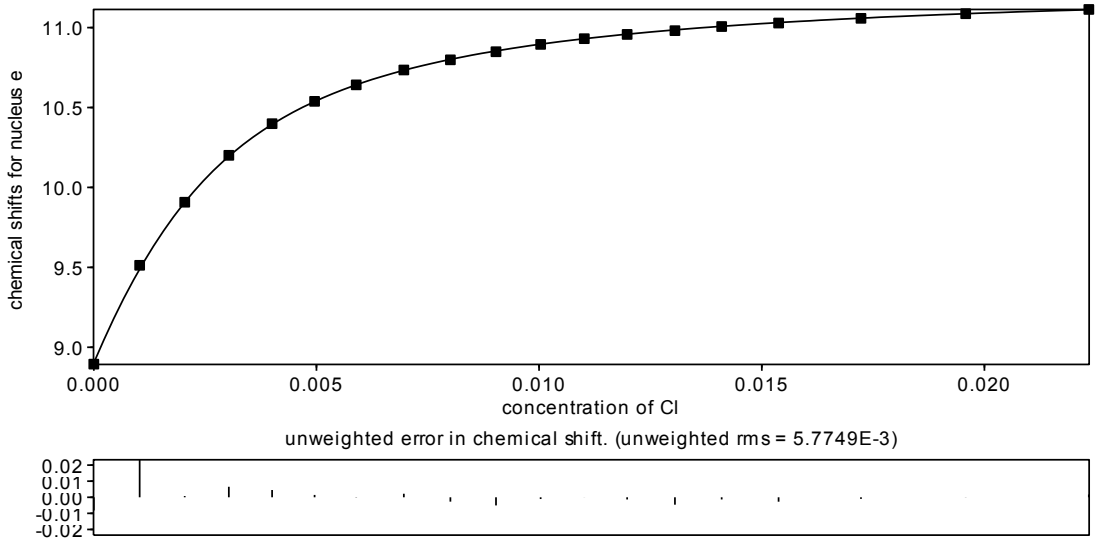

Figure S 24. Data points and fitting curve for ^{1}H NMR titration (acetonitrile-d_3) of *E*-**1** (2 mM) with TBACl.

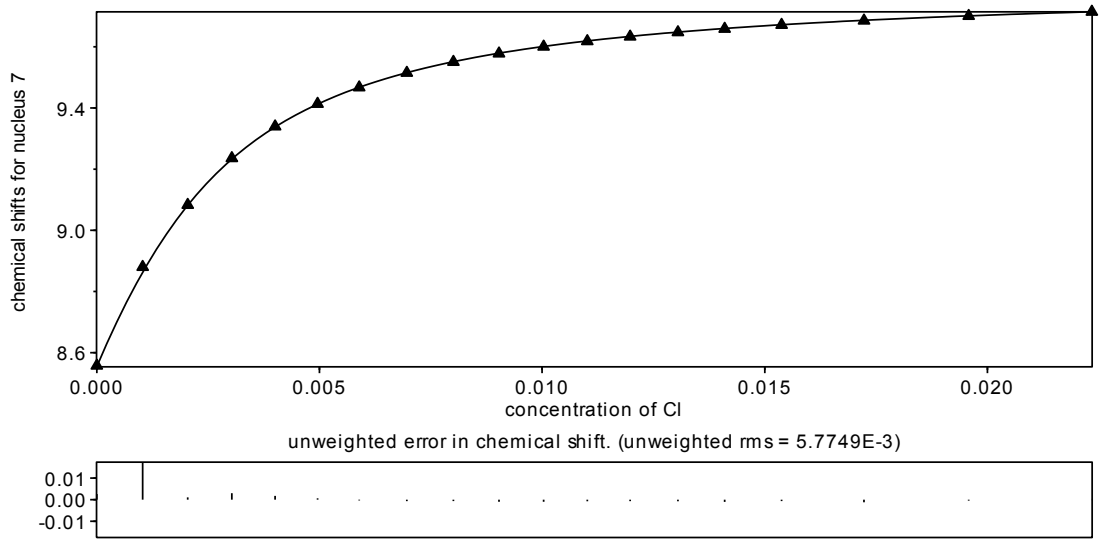

Figure S 25. Data points and fitting curve for ^{1}H NMR titration (acetonitrile-d_3) of *E*-**1** (2 mM) with TBACl.

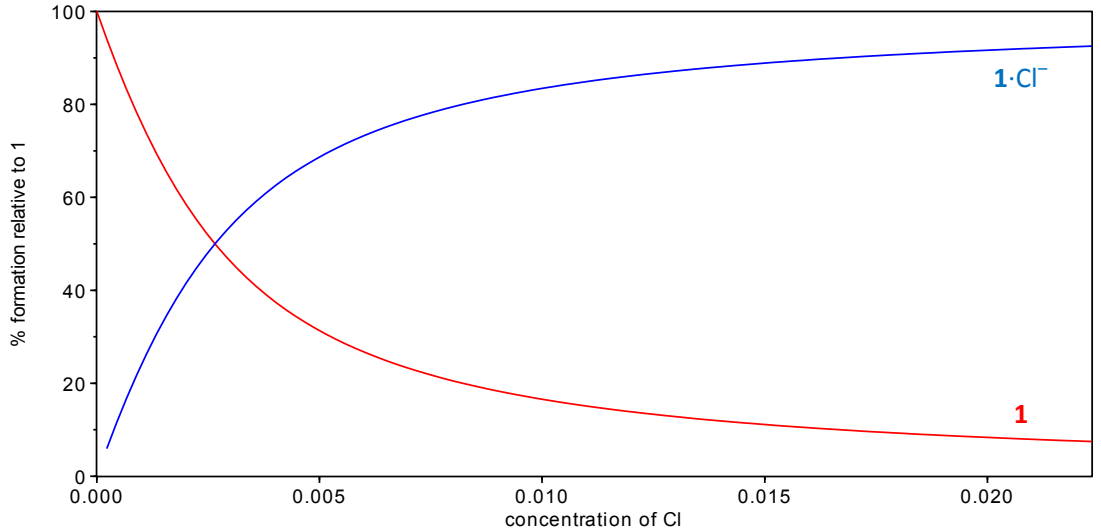

Figure S 26. Speciation diagram for the ^{1}H NMR titration of *E*-**1** (2 mM in acetonitrile-d_3) with TBACl.

4.3.2 Titration of *E*-**1** with Br^- in acetonitrile-d_3

Titration of *E*-**1** with TBABr showed significant changes in the ^{1}H NMR chemical shifts of protons e, f, and 7, characteristic of anion binding. These data were simultaneously fitted to the model shown in Scheme S 4, using HypNMR software.

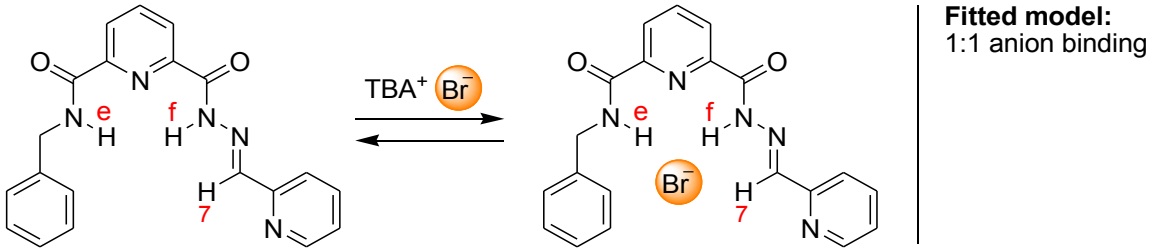

Scheme S 4. Bromide binding to *E*-**1**. Chemical shifts of the indicated protons were used for fitting.

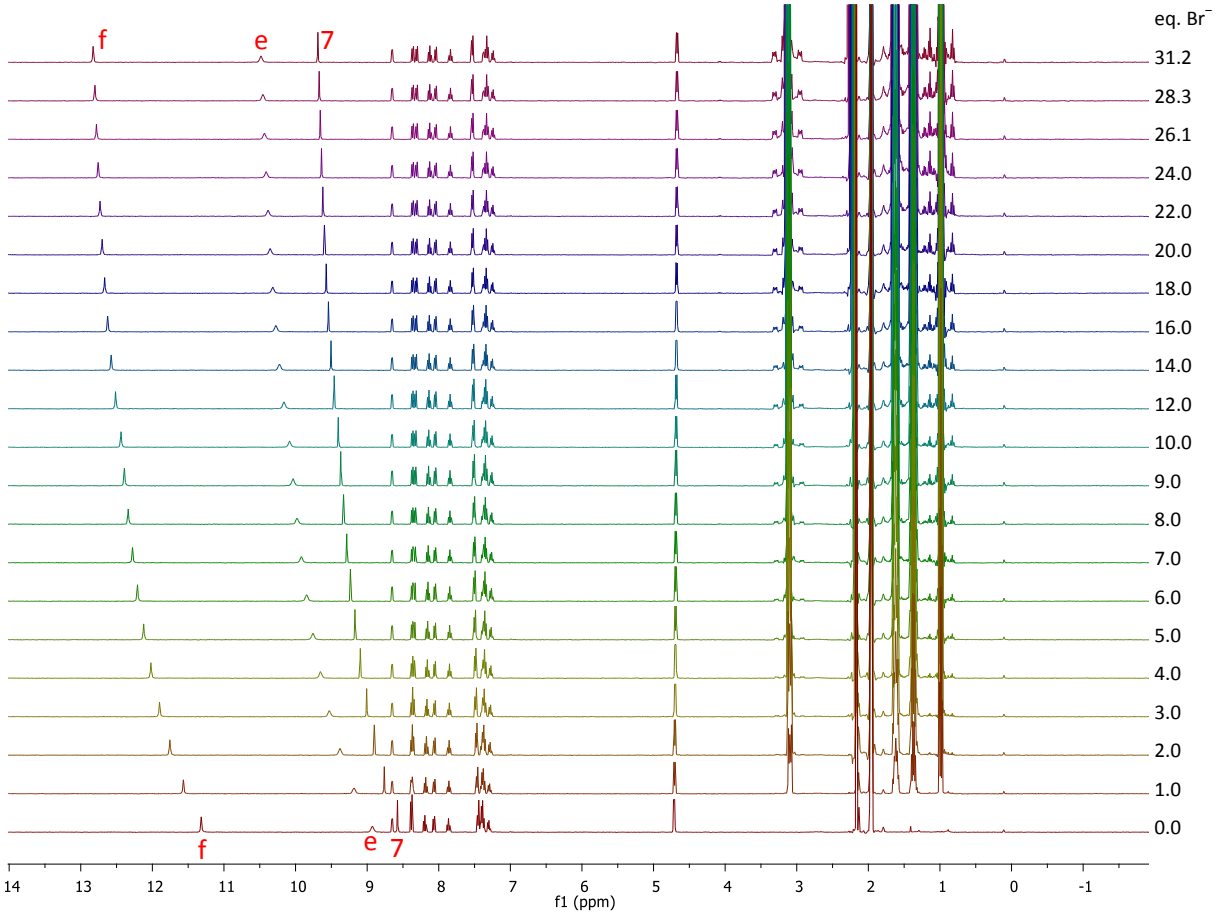

Figure S 27. ^{1}H NMR titration (acetonitrile-d_3) of *E*-**1** (2 mM) with TBABr. The assigned peaks were used for fitting.

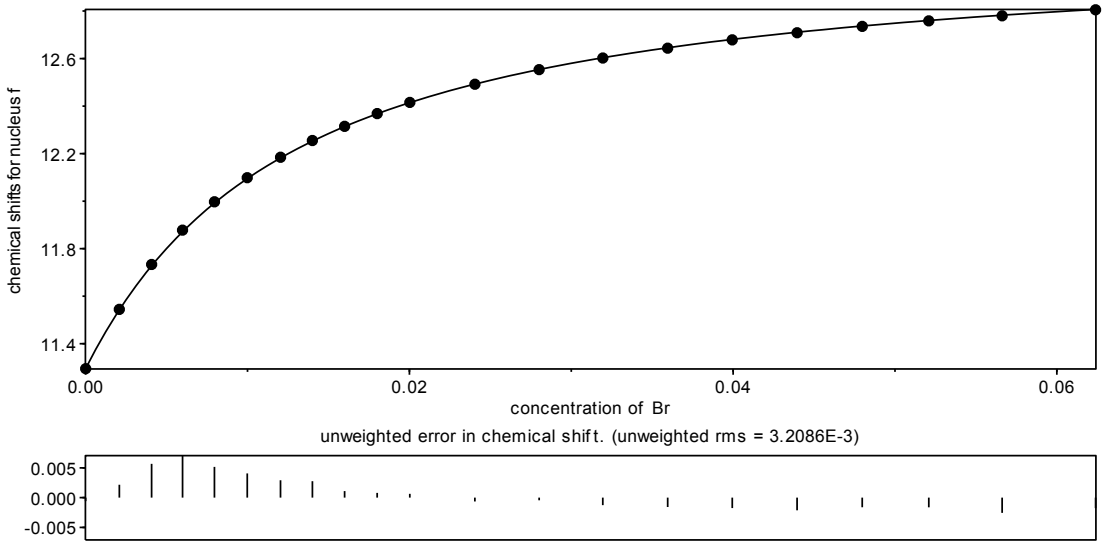

Figure S 28. Data points and fitting curve for ^{1}H NMR titration (acetonitrile-d_3) of *E*-**1** (2 mM) with TBABr.

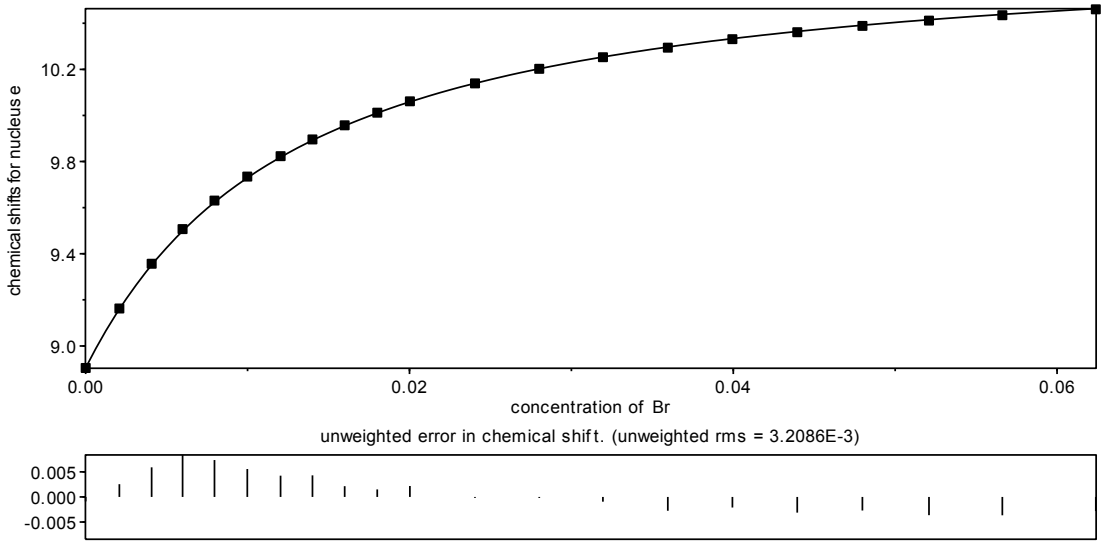

Figure S 29. Data points and fitting curve for ^{1}H NMR titration (acetonitrile-d_3) of *E*-**1** (2 mM) with TBABr.

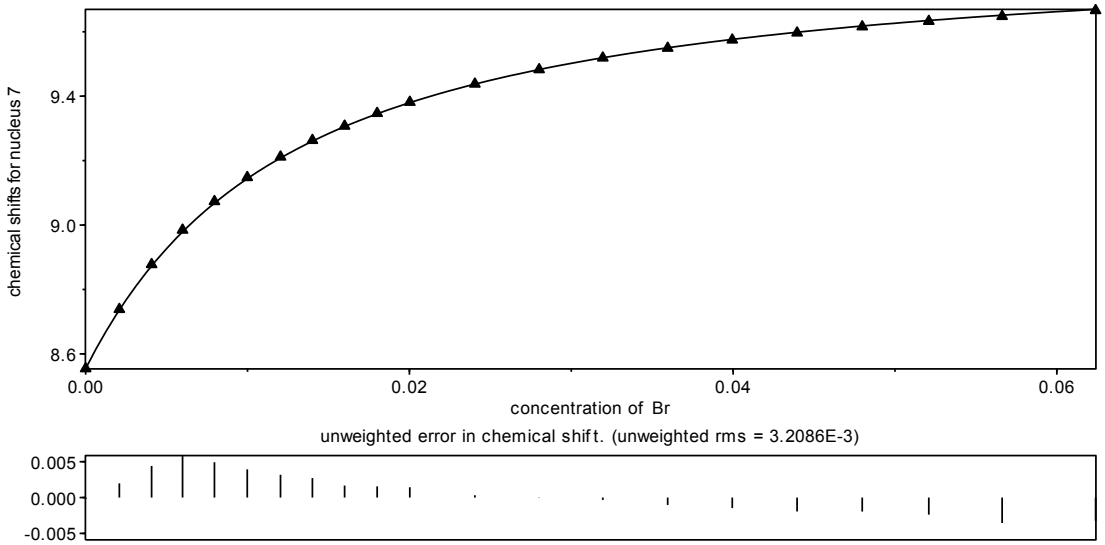

Figure S 30. Data points and fitting curve for ^{1}H NMR titration (acetonitrile-d_3) of *E*-**1** (2 mM) with TBABr.

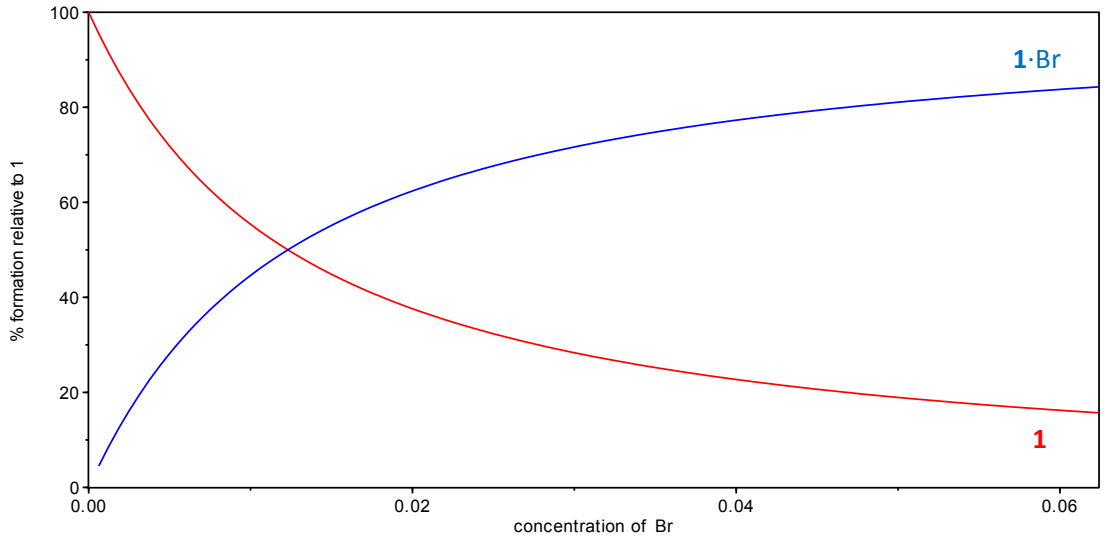

Figure S 31. Speciation diagram for the ^{1}H NMR titration of *E*-**1** (2 mM in acetonitrile-d_3) with TBABr.

4.3.3 Titration of *E*-**1** with I^- in acetonitrile-d_3

Titration of *E*-**1** with TBAI showed significant changes in the ^{1}H NMR chemical shifts of protons e, f, and 7, characteristic of anion binding. These data were simultaneously fitted to the model shown in Scheme S 5, using HypNMR software.

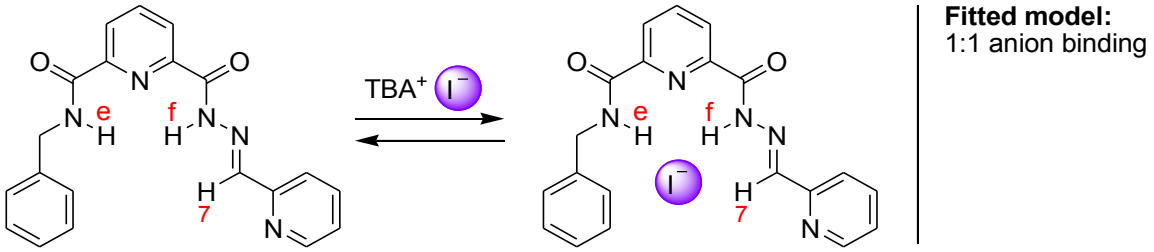

Scheme S 5. Iodide binding to *E*-**1**. Chemical shifts of the indicated protons were used for fitting.

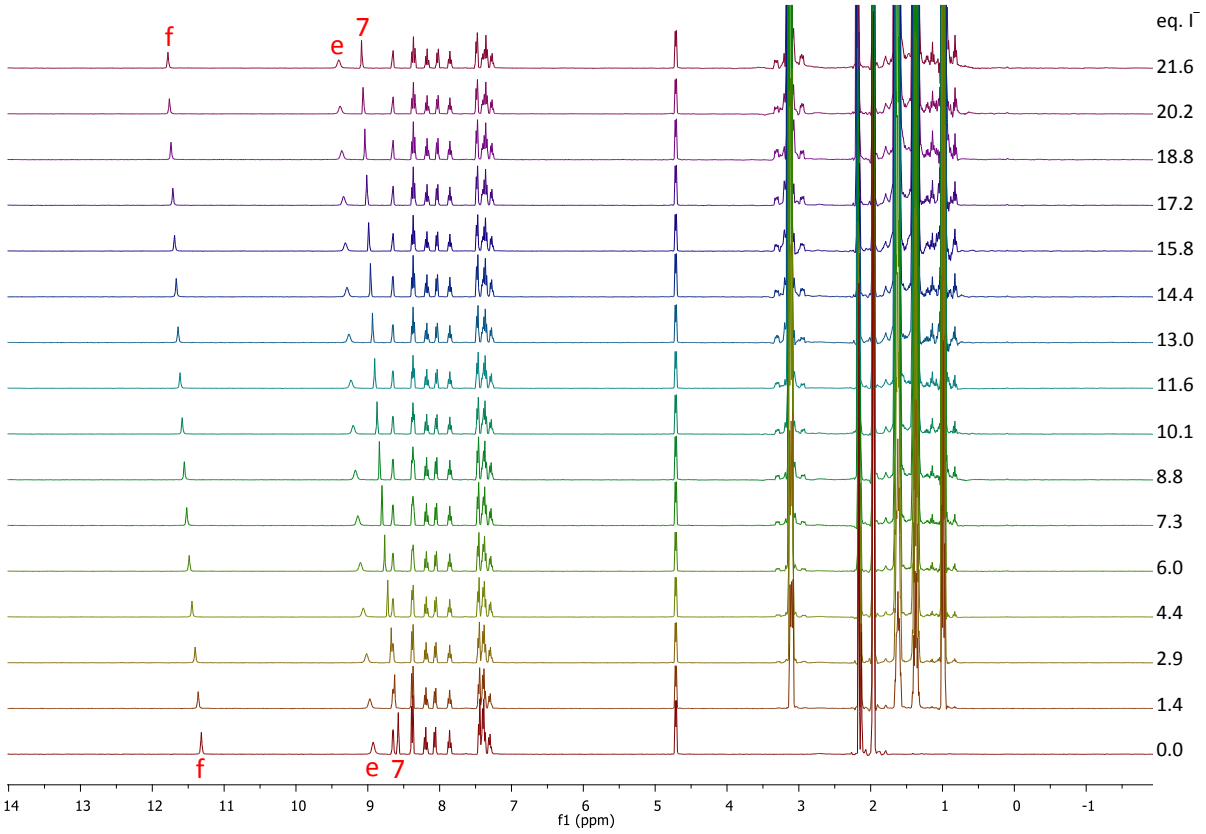

Figure S 32. ^{1}H NMR titration (acetonitrile-d_3) of *E*-**1** (4 mM) with TBAI. The assigned peaks were used for fitting. Due to weak binding, best fit was obtained by manual fitting.

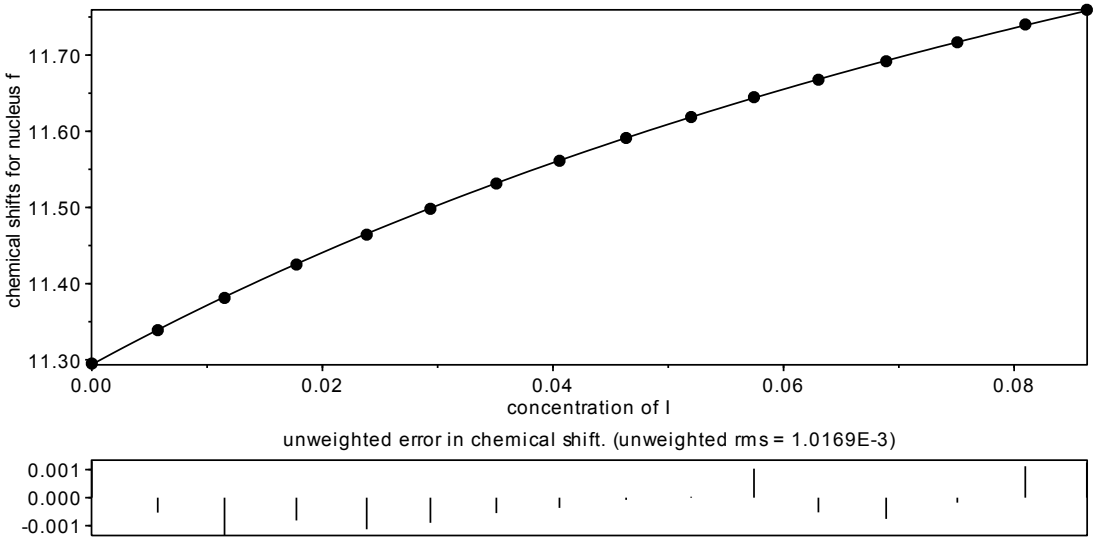

Figure S 33. Data points and fitting curve for ^{1}H NMR titration (acetonitrile-d_3) of *E*-**1** (4 mM) with TBAI.

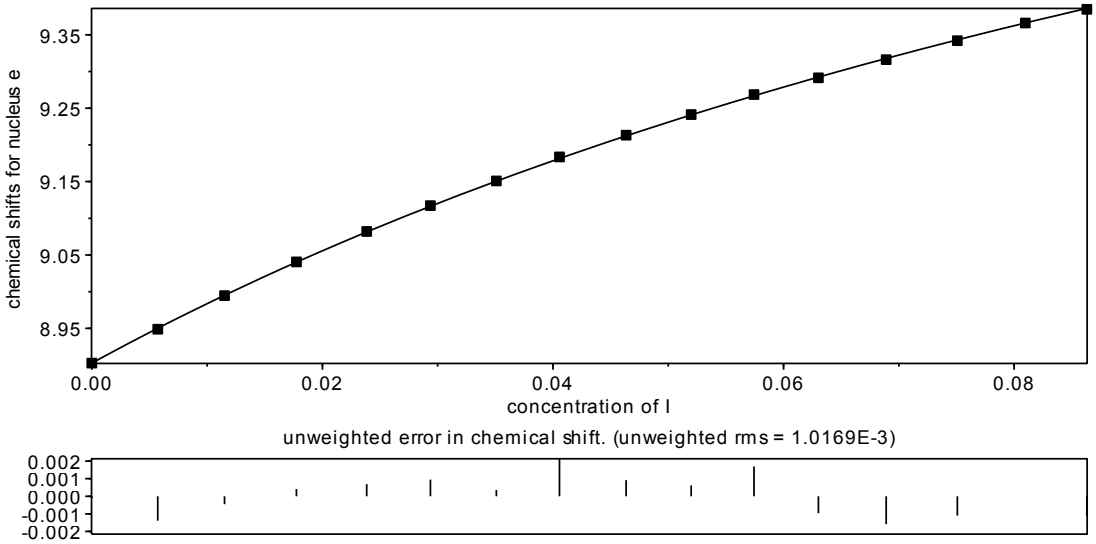

Figure S 34. Data points and fitting curve for ^{1}H NMR titration (acetonitrile-d_3) of *E*-**1** (4 mM) with TBAI.

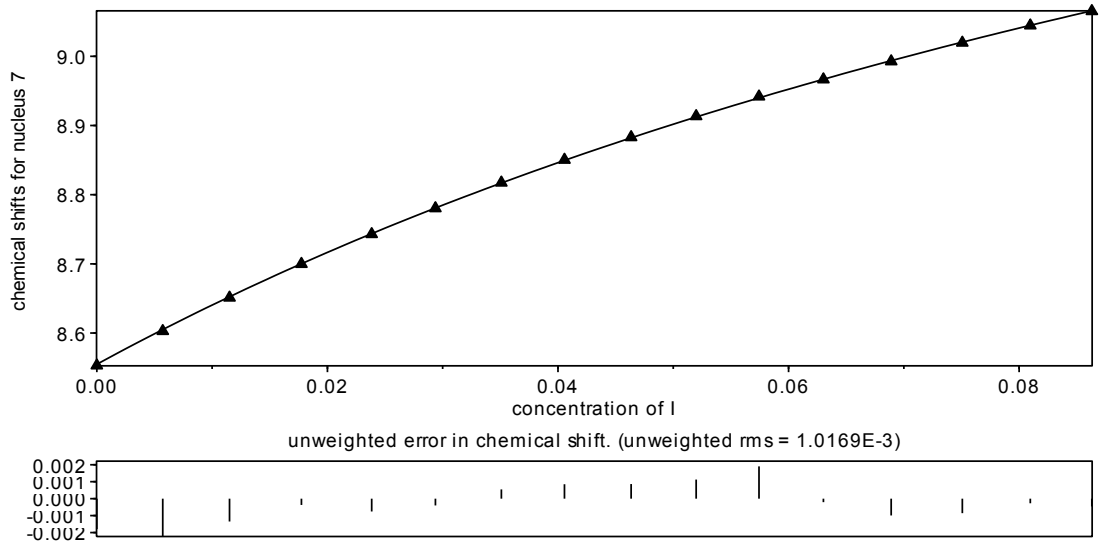

Figure S 35. Data points and fitting curve for ^{1}H NMR titration (acetonitrile-d_3) of *E*-**1** (4 mM) with TBAI.

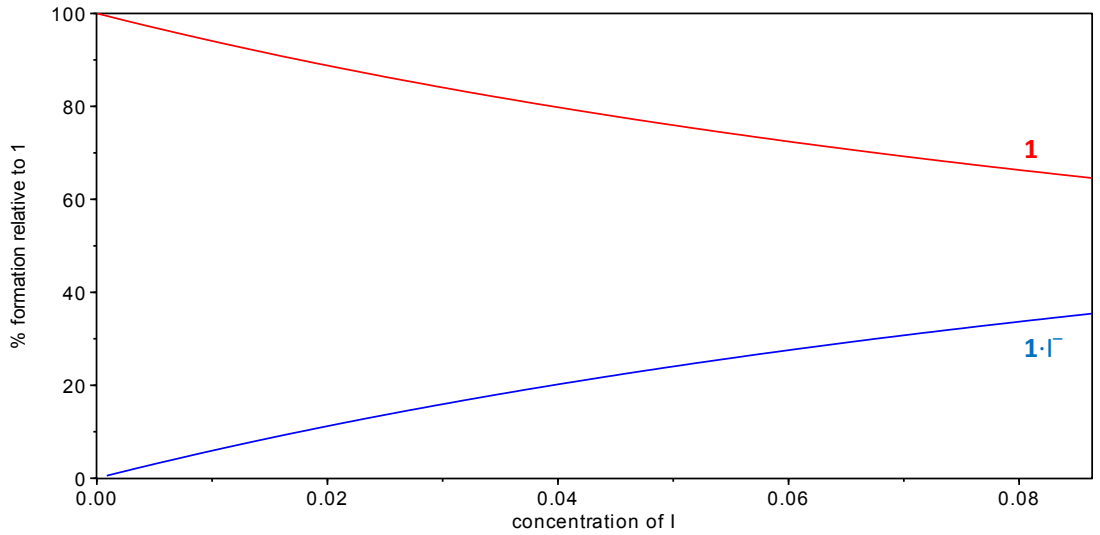

Figure S 36. Speciation diagram for the ^{1}H NMR titration of *E*-**1** (4 mM in acetonitrile-d_3) with TBAI.

4.4 Cation Binding

4.4.1 Titration of *E*-**1** with Li^+ in acetonitrile-d_3

Titration of *E*-**1** with $Li(CH_3OCH_2CH_2OCH_3)_3BPh_4$ showed significant changes in the ^1H NMR chemical shifts of proton 3, characteristic of cation binding, which were fitted to the model shown in Scheme S 6, using HypNMR software.

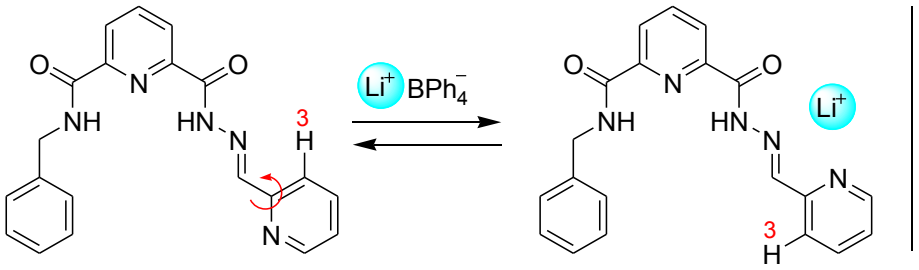

Scheme S 6. Lithium cation binding to *E*-**1**. Chemical shift of the indicated proton was used for fitting.

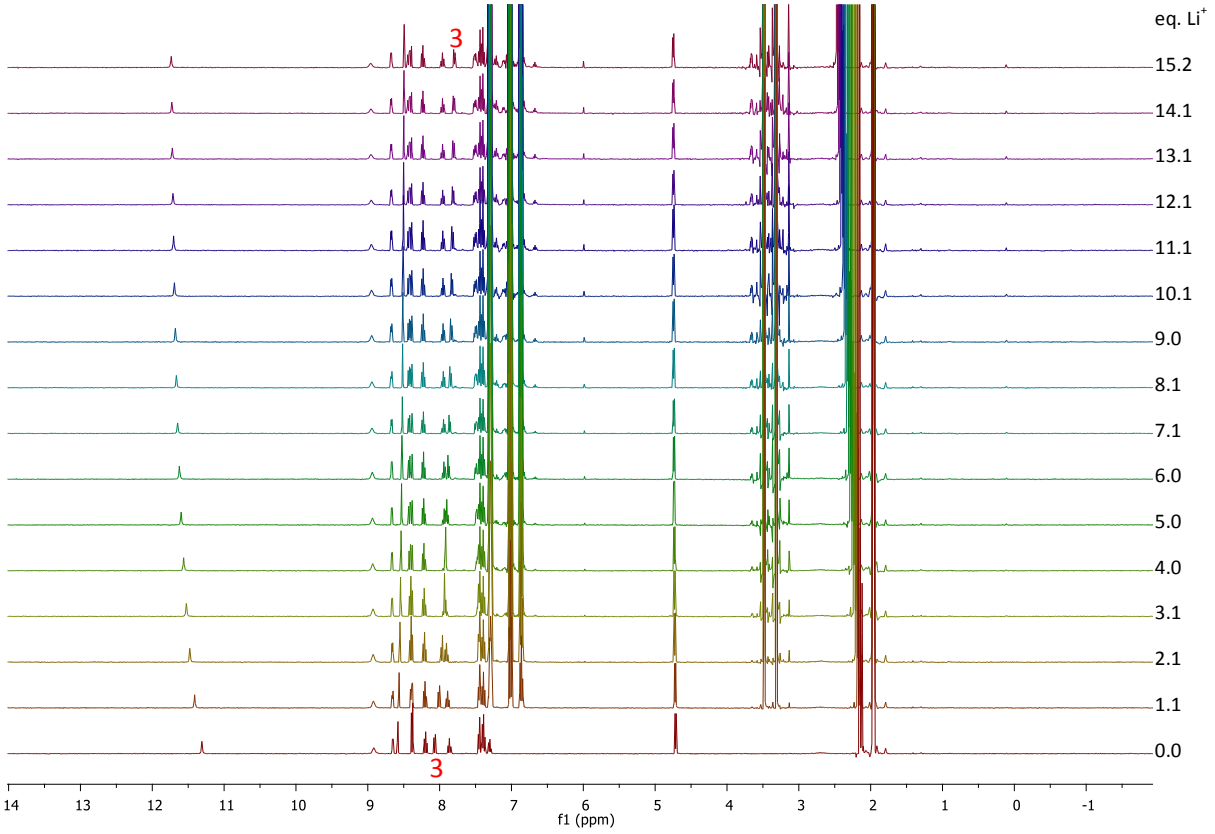

Figure S 37. ^1H NMR titration (acetonitrile-d_3) of *E*-**1** (2 mM) with $Li(CH_3OCH_2CH_2OCH_3)_3BPh_4$. Nucleus "3" was used for fitting.

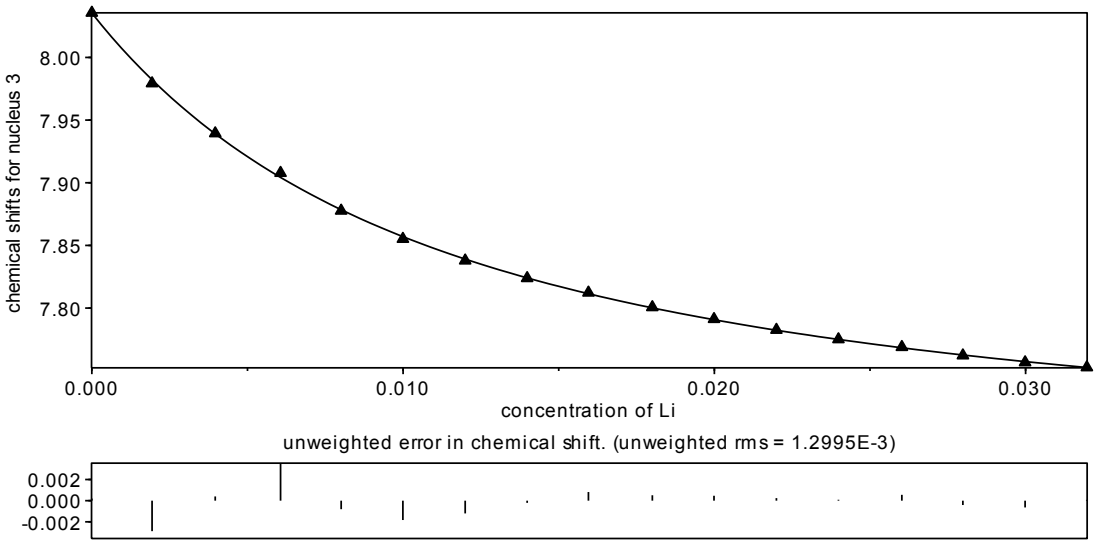

Figure S 38. Data points and fitting curve for ^{1}H NMR titration (acetonitrile-d_3) of *E*-**1** (2 mM) with $Li(CH_3OCH_2CH_2OCH_3)_3BPh_4$.

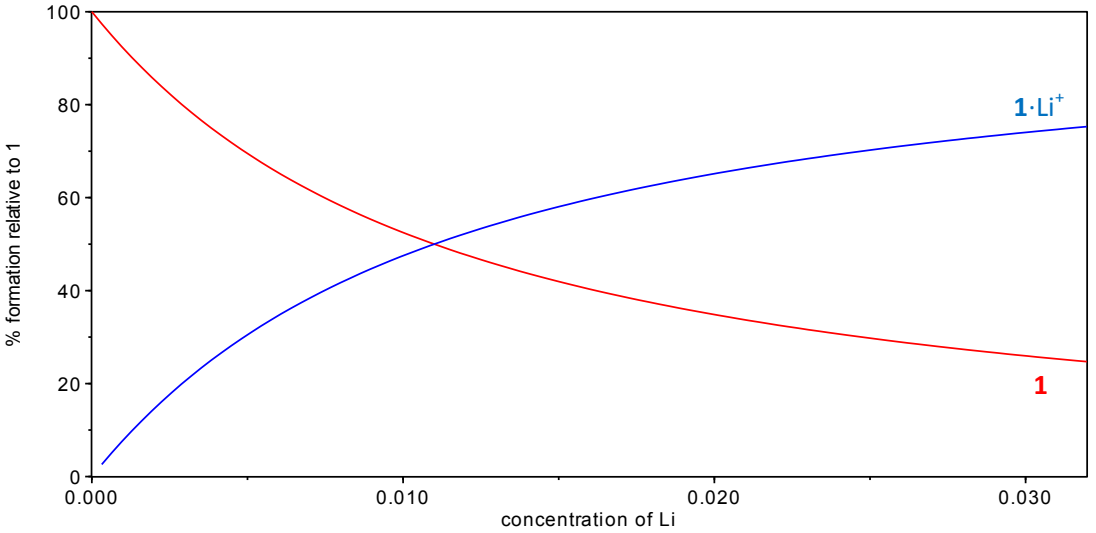

Figure S 39. Speciation diagram for the ^{1}H NMR titration of *E*-**1** (2 mM in acetonitrile-d_3) with $Li(CH_3OCH_2CH_2OCH_3)_3BPh_4$.

4.4.2 Titration of *E*-**1** with Na^+ in acetonitrile-d_3

Titration of *E*-**1** with $NaBPh_4$ showed significant changes in the ^1H NMR chemical shifts of proton 3, characteristic of cation binding, which were fitted to the model shown in Scheme S 7, using HypNMR software.

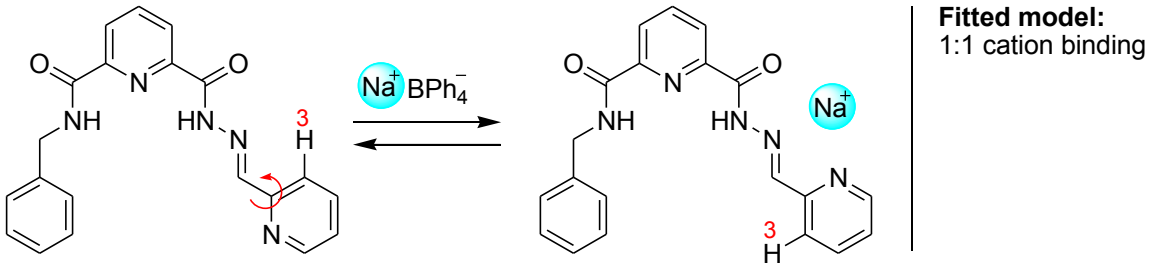

Scheme S 7. Sodium cation binding to *E*-**1**. Chemical shift of the indicated proton was used for fitting.

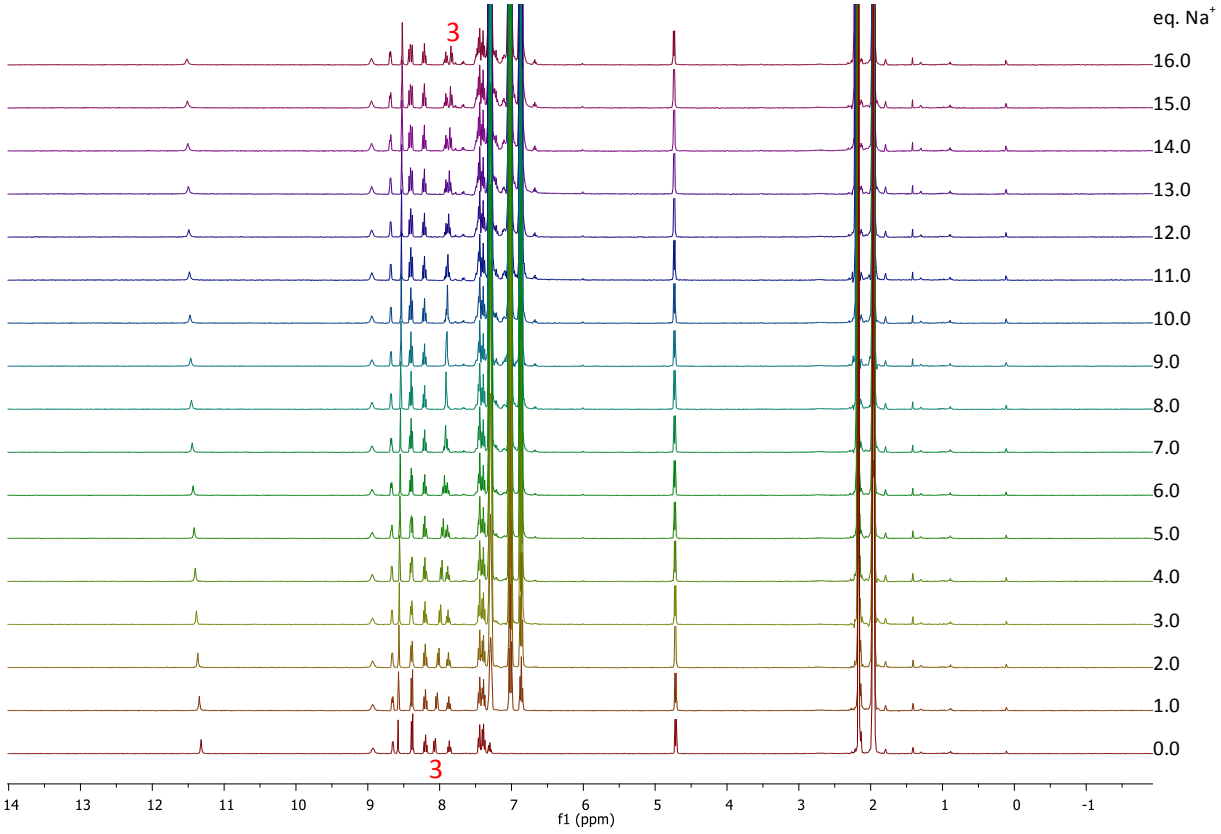

Figure S 40. ^1H NMR titration (acetonitrile-d_3) of *E*-**1** (2 mM) with $NaBPh_4$. Nucleus "3" was used for fitting.

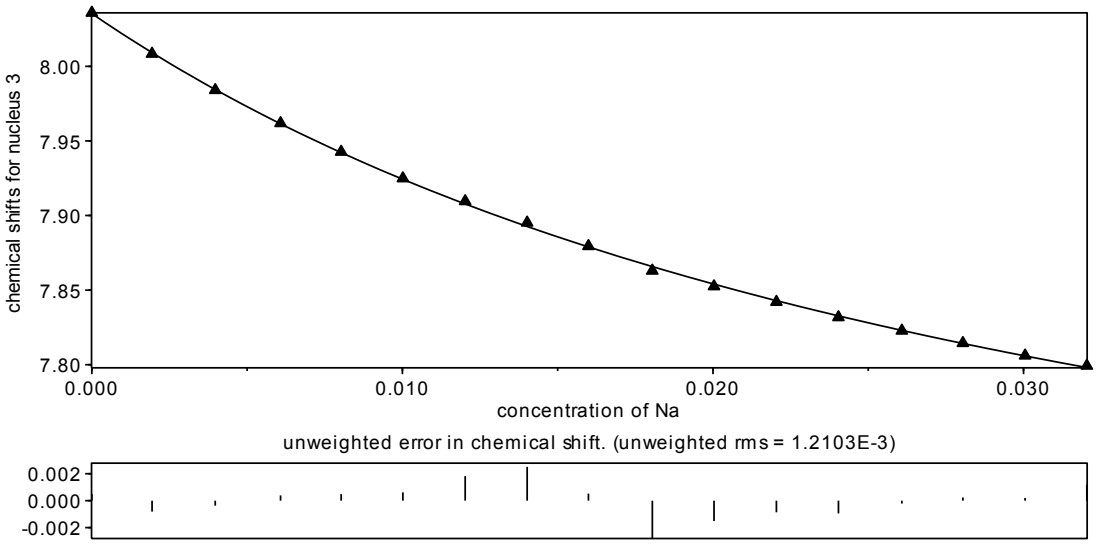

Figure S 41. Data points and fitting curve for ^{1}H NMR titration (acetonitrile-d_3) of *E*-**1** (2 mM) with $NaBPh_4$.

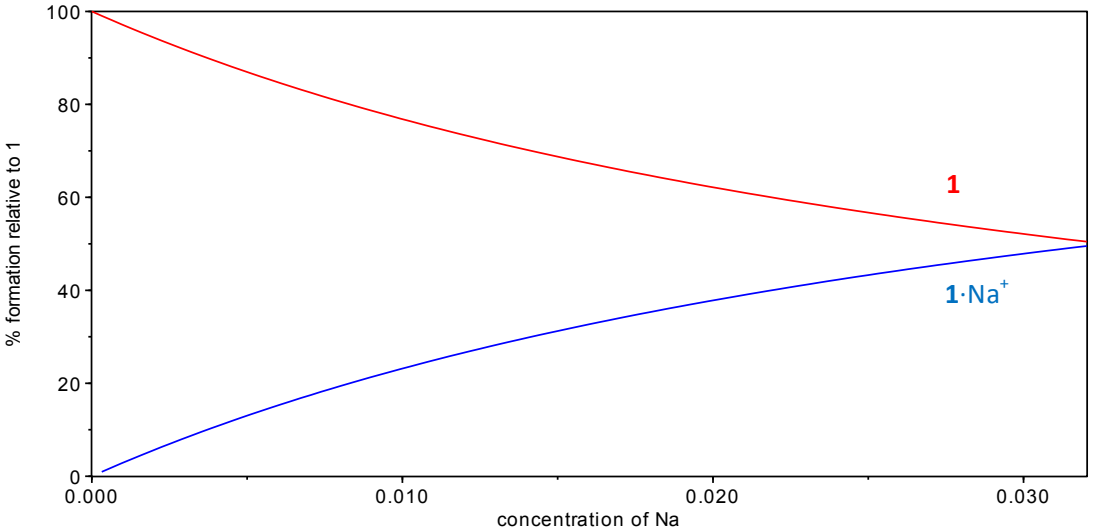

Figure S 42. Speciation diagram for the ^{1}H NMR titration of *E*-**1** (2 mM in acetonitrile-d_3) with $NaBPh_4$.

4.4.3 Titration of *E*-**1** with K^+ in acetonitrile-d_3

Titration of *E*-**1** with $KBPh_4$ showed significant changes in the ^1H NMR chemical shifts of proton 3, characteristic of cation binding, which were fitted to the model shown in Scheme S 8, using HypNMR software.

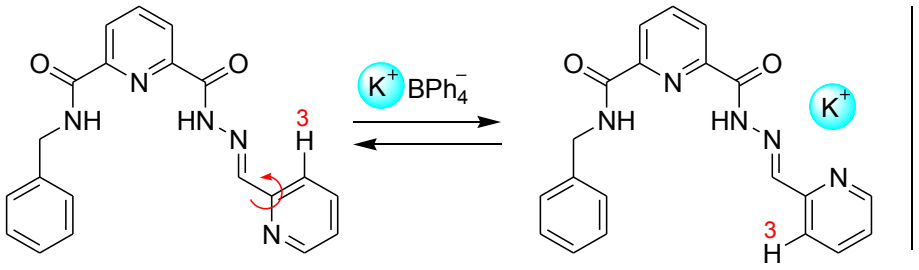

Scheme S 8. Potassium cation binding to *E*-**1**. Chemical shift of the indicated proton was used for fitting.

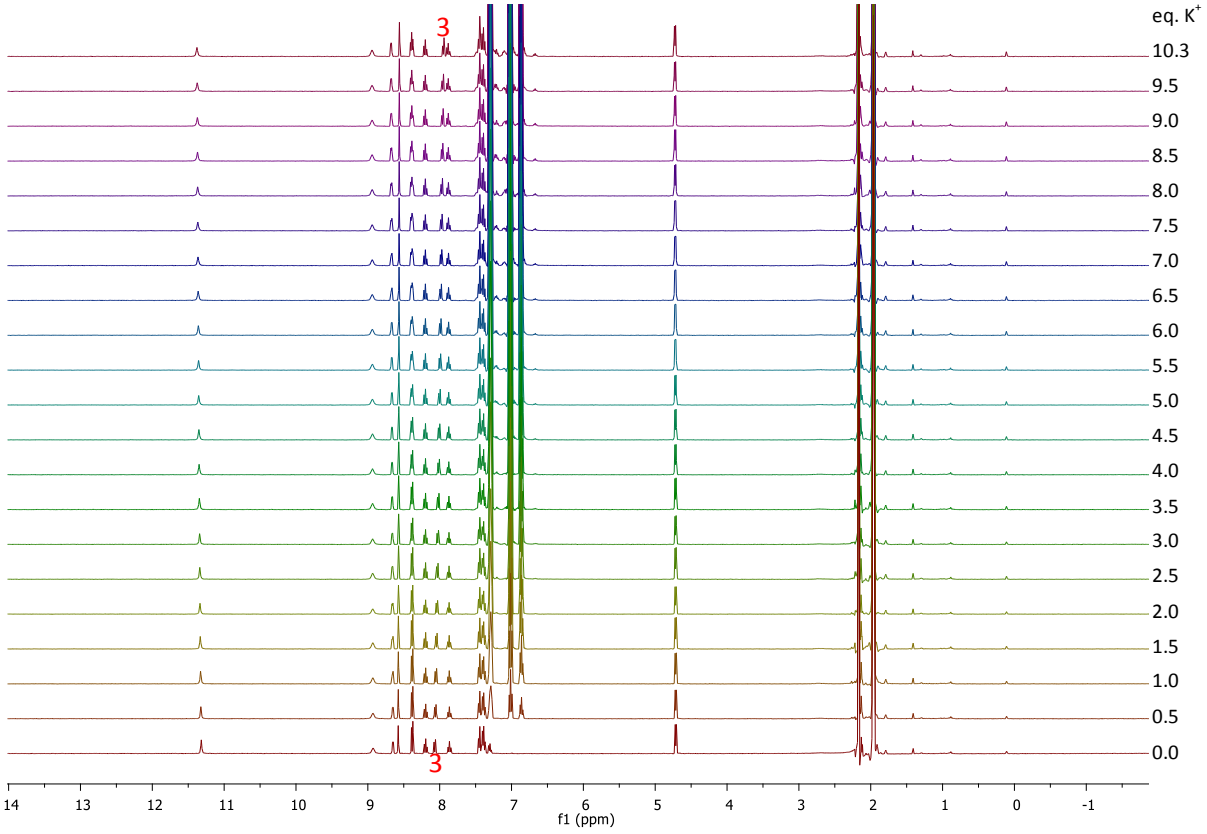

Figure S 43. ^1H NMR titration (acetonitrile-d_3) of *E*-**1** (2 mM) with $KBPh_4$. Nucleus "3" was used for fitting.

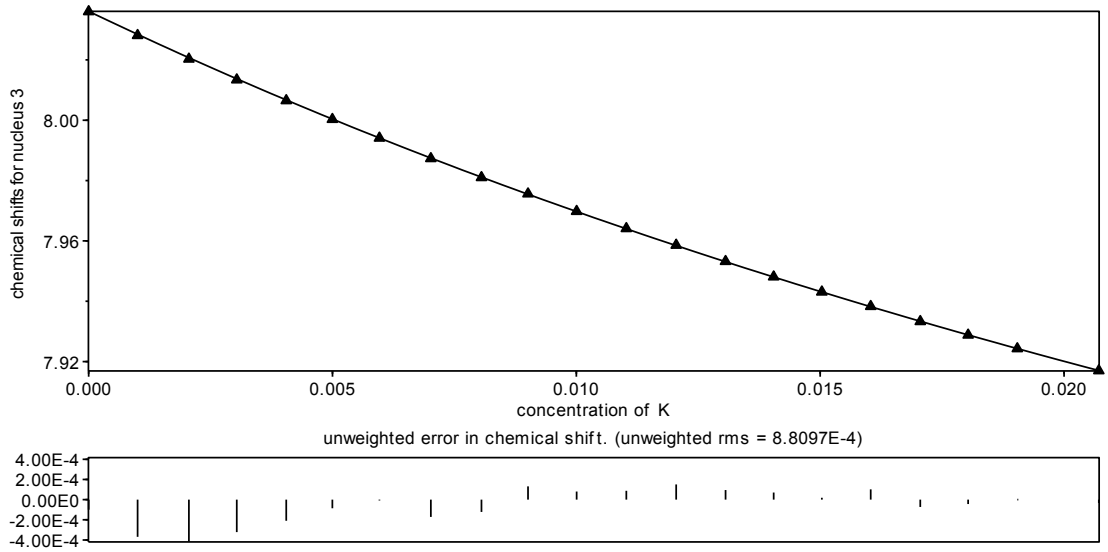

Figure S 44. Data points and fitting curve for ^{1}H NMR titration (acetonitrile-d_3) of *E*-**1** (2 mM) with $KBPh_4$.

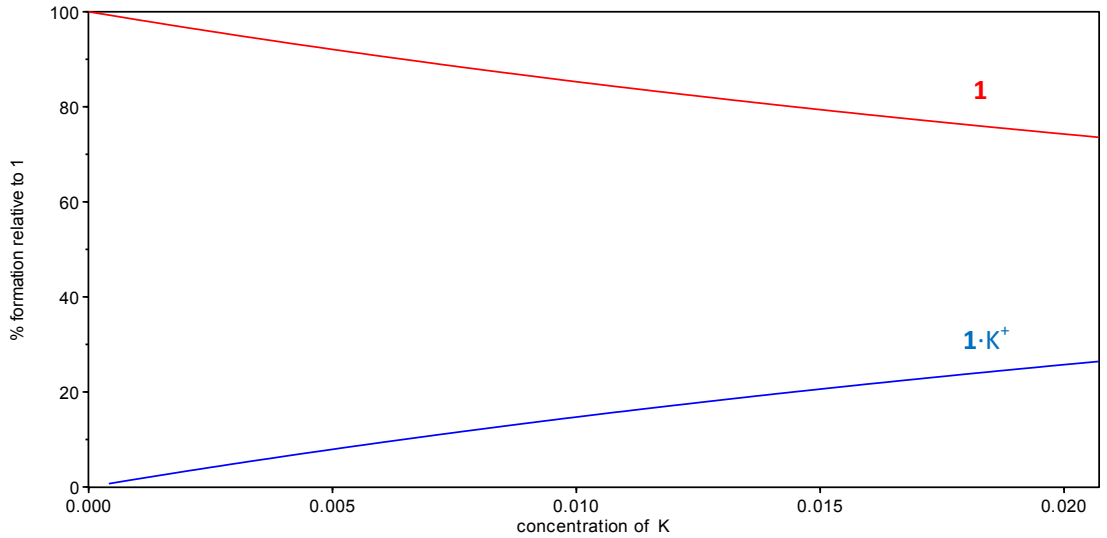

Figure S 45. Speciation diagram for the ^{1}H NMR titration of *E*-**1** (2 mM in acetonitrile-d_3) with $KBPh_4$.

4.5 Ion Pairs Binding

4.5.1 Titration of *E*-**1** with Cl^- in the presence of 1 equiv. of Li^+ in acetonitrile-d_3

Titration of *E*-**1** with TBACl in the presence of 1 equiv. of $Li(CH_3OCH_2CH_2OCH_3)_3BPh_4$ showed significant changes in the ^1H NMR chemical shifts of protons f, e, and 7. These data were simultaneously fitted to the model shown in Scheme S 9, using HypNMR software.

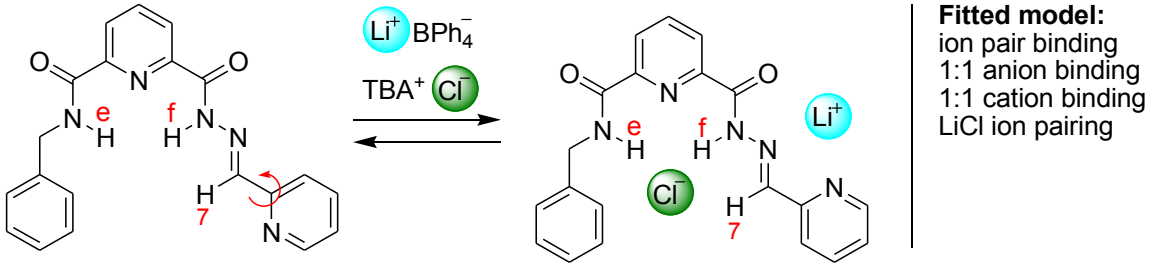

Scheme S 9. LiCl binding to *E*-**1**. Chemical shifts of the indicated protons were used for fitting.

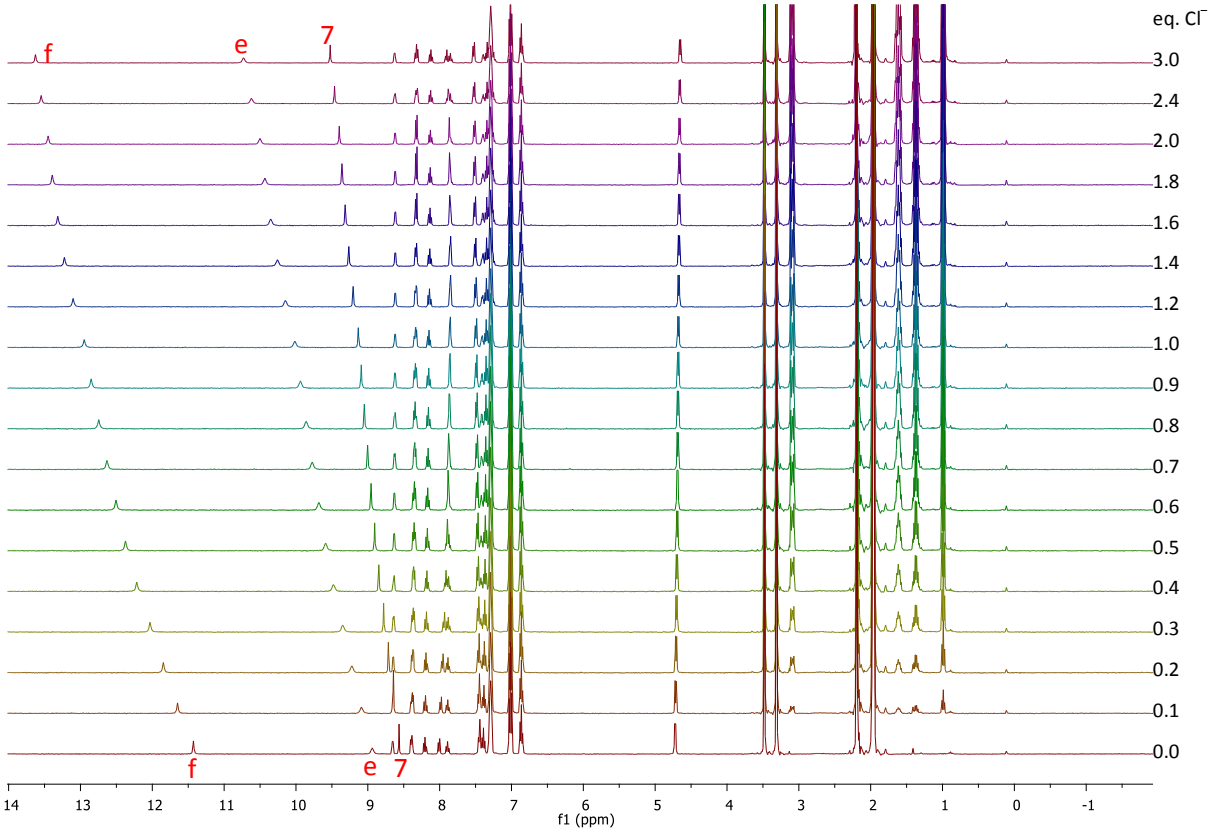

Figure S 46. ^1H NMR titration (acetonitrile-d_3) of *E*-**1** (2 mM) with TBACl (0–3 eq, bottom to top) in the presence of 1 equiv. of $Li(CH_3OCH_2CH_2OCH_3)_3BPh_4$. The assigned peaks were used for fitting.

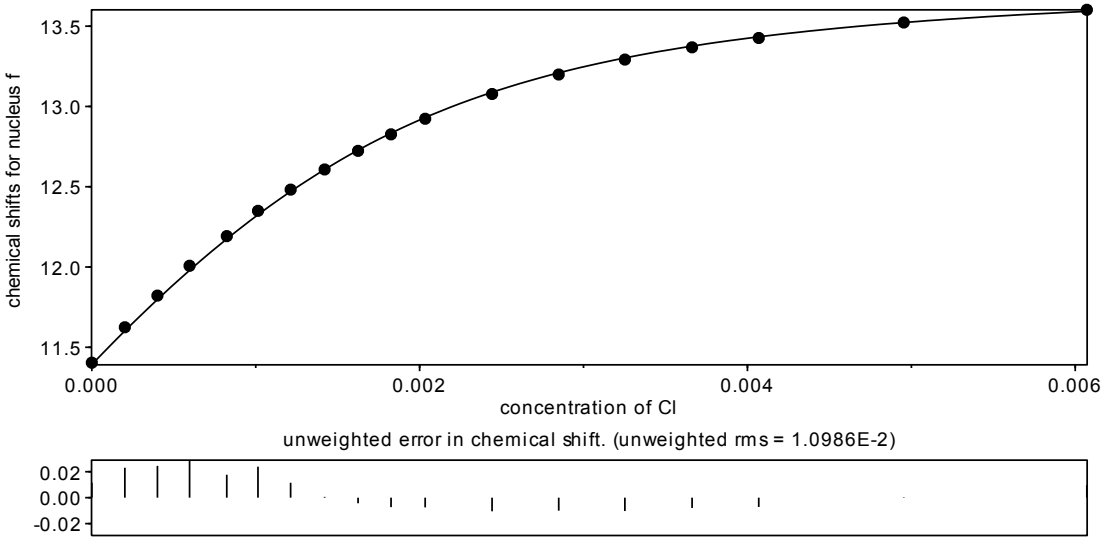

Figure S 47. Data points and fitting curve for ^{1}H NMR titration (acetonitrile-d_3) of *E*-**1** (2 mM) with TBACl in the presence of 1 equiv. of $Li(CH_3OCH_2CH_2OCH_3)_3BPh_4$.

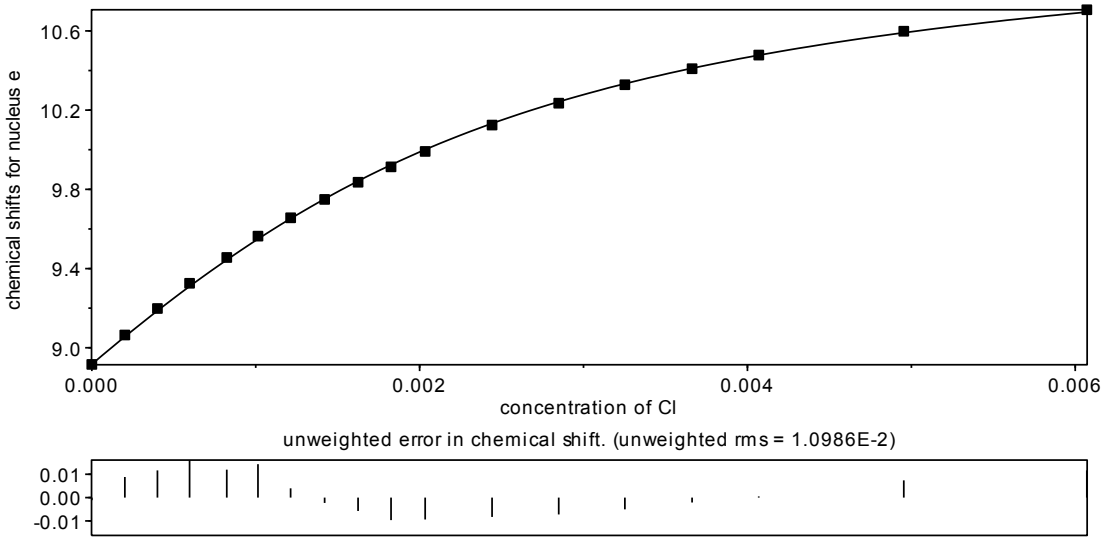

Figure S 48. Data points and fitting curve for ^{1}H NMR titration (acetonitrile-d_3) of *E*-**1** (2 mM) with TBACl in the presence of 1 equiv. of $Li(CH_3OCH_2CH_2OCH_3)_3BPh_4$.

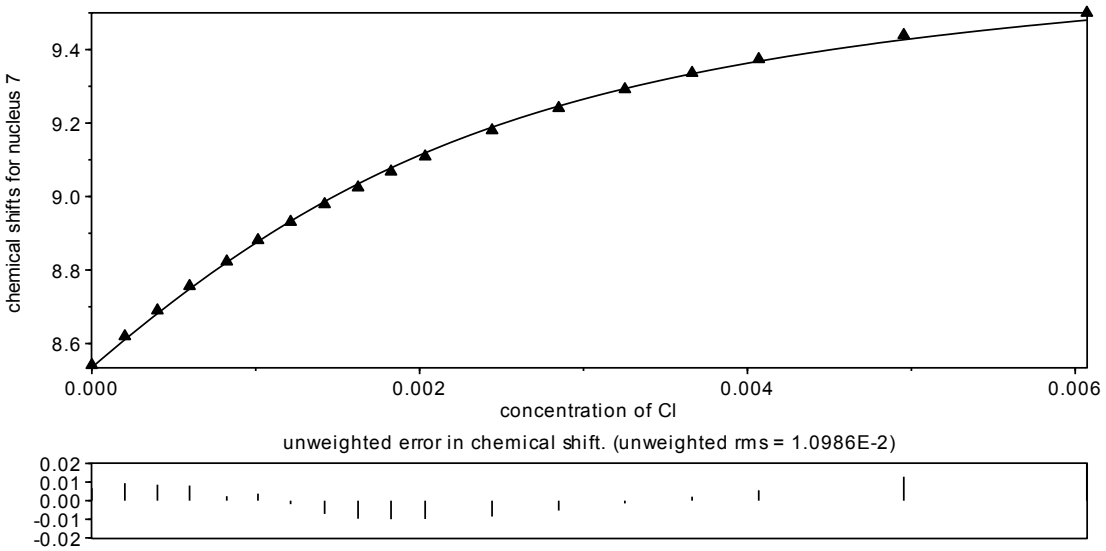

Figure S 49. Data points and fitting curve for ^{1}H NMR titration (acetonitrile-d_3) of *E*-**1** (2 mM) with TBACl in the presence of 1 equiv. of $Li(CH_3OCH_2CH_2OCH_3)_3BPh_4$.

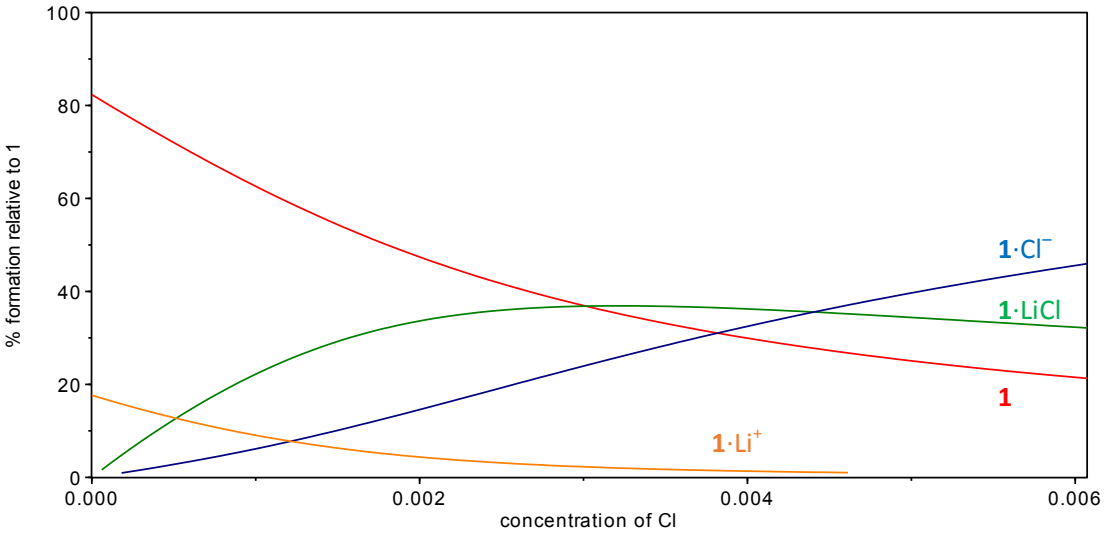

Figure S 50. Speciation diagram for the ^{1}H NMR titration of *E*-**1** (2 mM in acetonitrile-d_3) with TBACl in the presence of 1 equiv. of $Li(CH_3OCH_2CH_2OCH_3)_3BPh_4$.

4.5.2 Titration of *E*-**1** with Br^- in the presence of 1 eq. of Li^+ in acetonitrile-d_3

Titration of *E*-**1** with TBABr in the presence of 1 equiv. of $Li(CH_3OCH_2CH_2OCH_3)_3BPh_4$ showed significant changes in the ^1H NMR chemical shifts of protons f, e, and 7. These data were simultaneously fitted to the model shown in Scheme S 10, using HypNMR software.

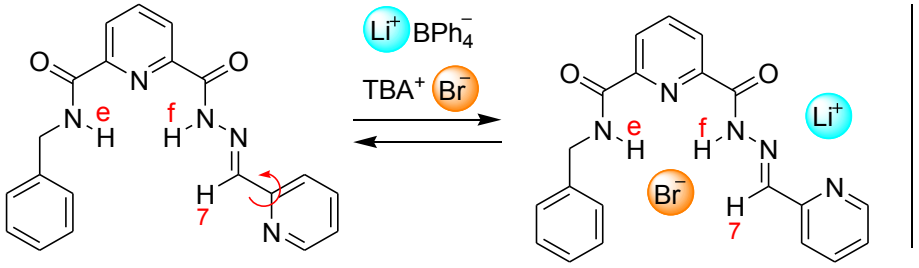

Scheme S 10. LiBr binding to *E*-**1**. Chemical shifts of the indicated protons were used for fitting.

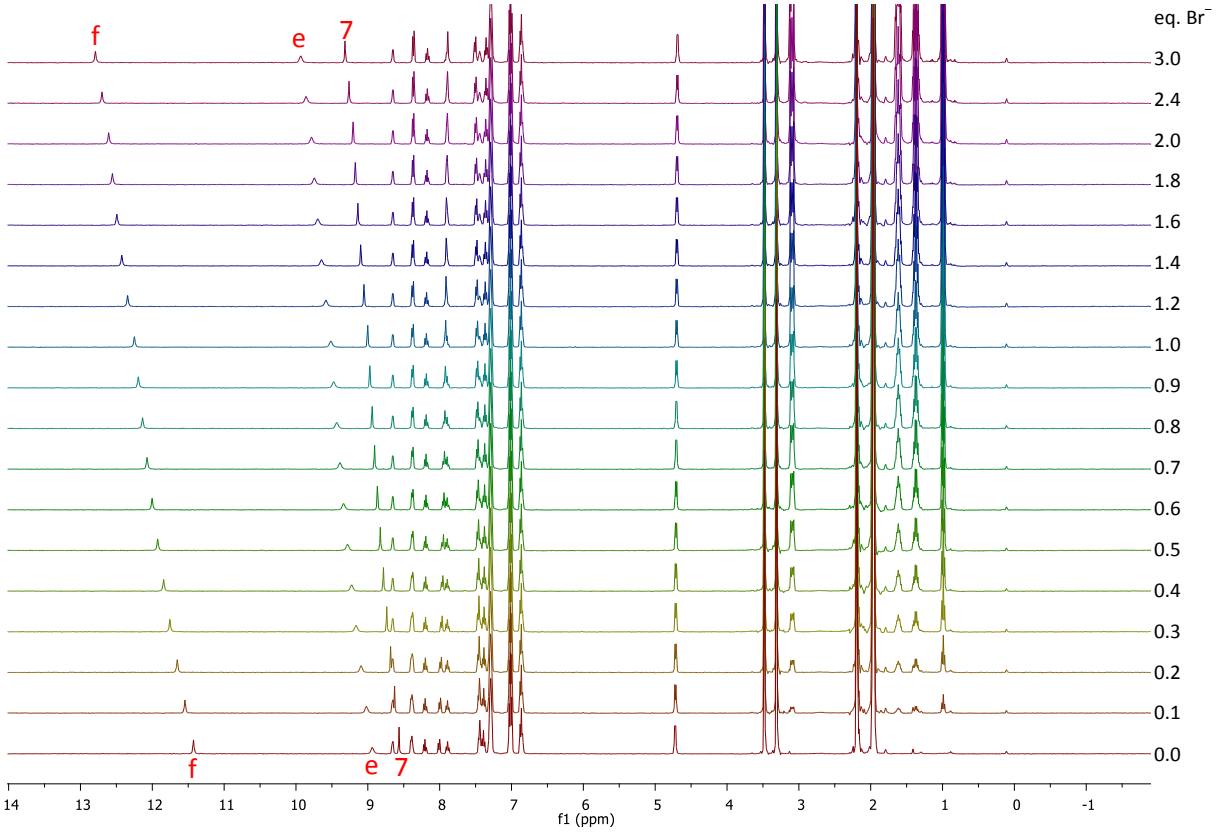

Figure S 51. ^1H NMR titration (acetonitrile-d_3) of *E*-**1** (2 mM) with TBABr in the presence of 1 equiv. of $Li(CH_3OCH_2CH_2OCH_3)_3$-BPh_4. The assigned peaks were used for fitting.

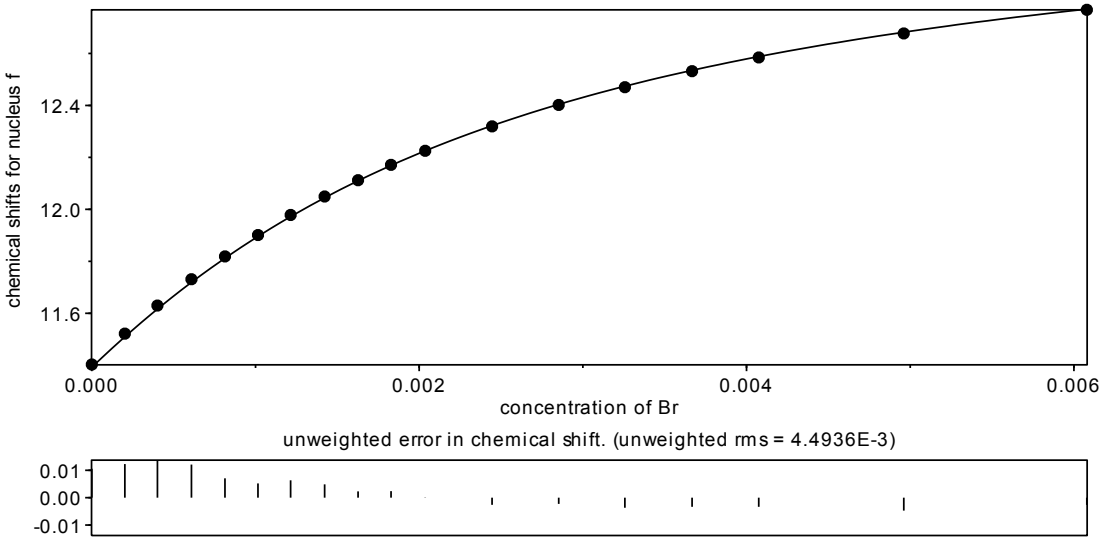

Figure S 52. Data points and fitting curve for ^{1}H NMR titration (acetonitrile-d_3) of *E*-**1** (2 mM) with TBABr in the presence of 1 equiv. of $Li(CH_3OCH_2CH_2OCH_3)_3BPh_4$.

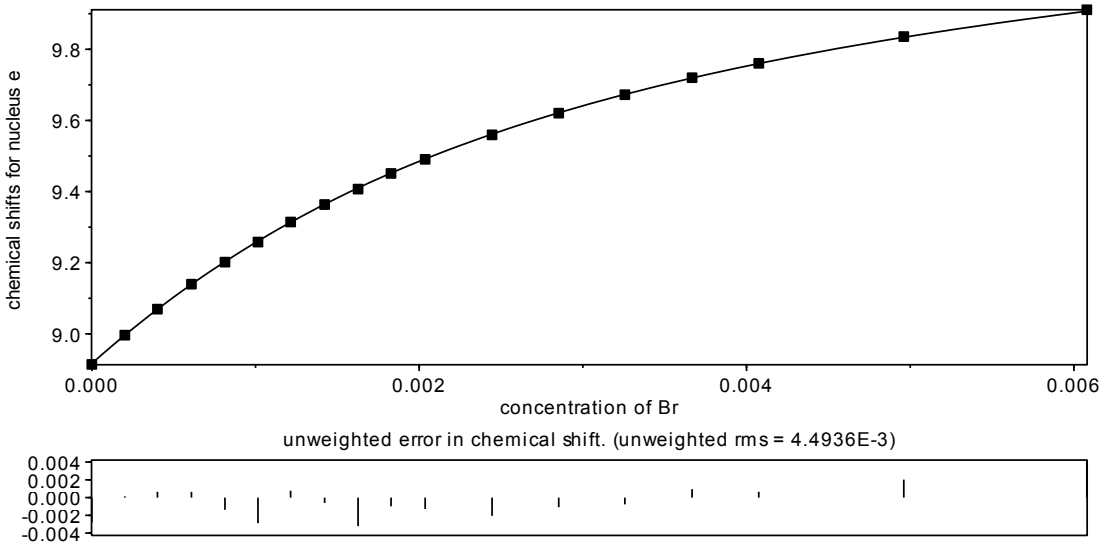

Figure S 53. Data points and fitting curve for ^{1}H NMR titration (acetonitrile-d_3) of *E*-**1** (2 mM) with TBABr in the presence of 1 equiv. of $Li(CH_3OCH_2CH_2OCH_3)_3BPh_4$.

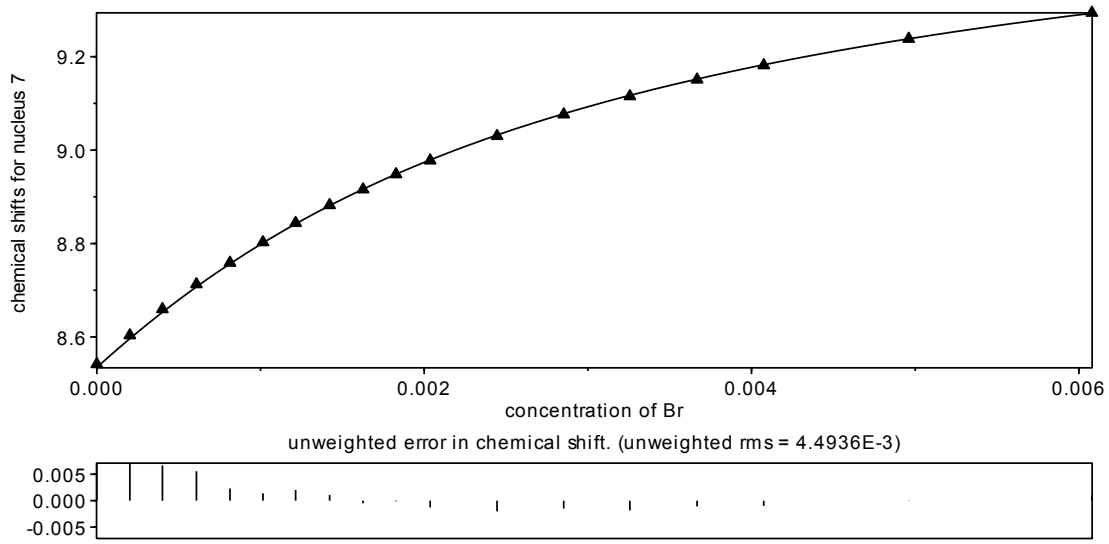

Figure S 54. Data points and fitting curve for ^{1}H NMR titration (acetonitrile-d_3) of *E*-**1** (2 mM) with TBABr in the presence of 1 equiv. of $Li(CH_3OCH_2CH_2OCH_3)_3BPh_4$.

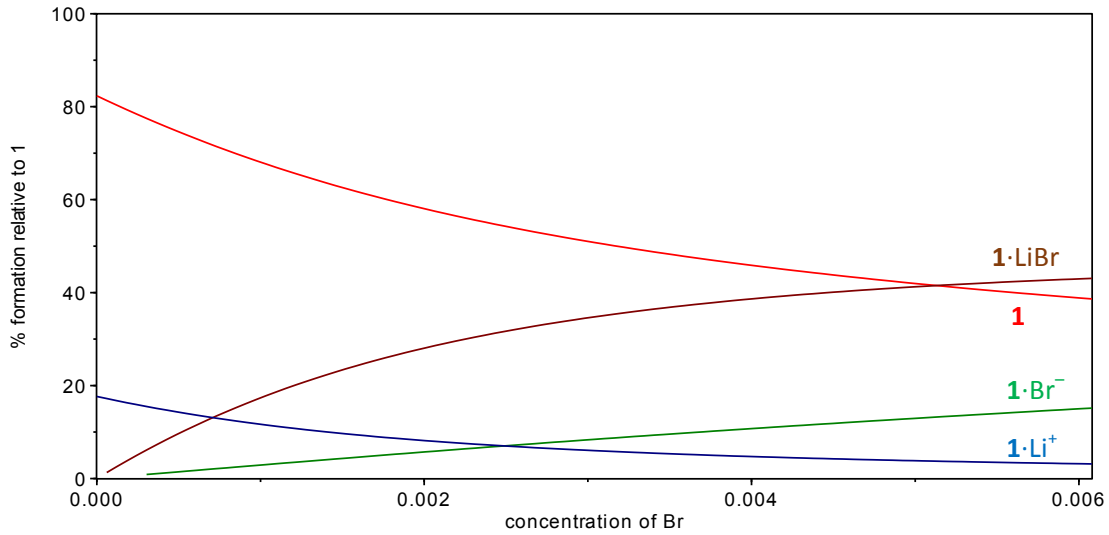

Figure S 55. Speciation diagram for the ^{1}H NMR titration of *E*-**1** (2 mM in acetonitrile-d_3) with TBABr in the presence of 1 equiv. of $Li(CH_3OCH_2CH_2OCH_3)_3BPh_4$.

4.5.3 Titration of *E*-**1** with LiBr in acetonitrile-d_3

Titration of *E*-**1** with TBABr in the presence of 1 equiv. of $Li(CH_3OCH_2CH_2OCH_3)_3BPh_4$ showed significant changes in the ^1H NMR chemical shifts of protons f, e, 3, and 7. These data were simultaneously fitted to the model shown in Scheme S 11, using HypNMR software.

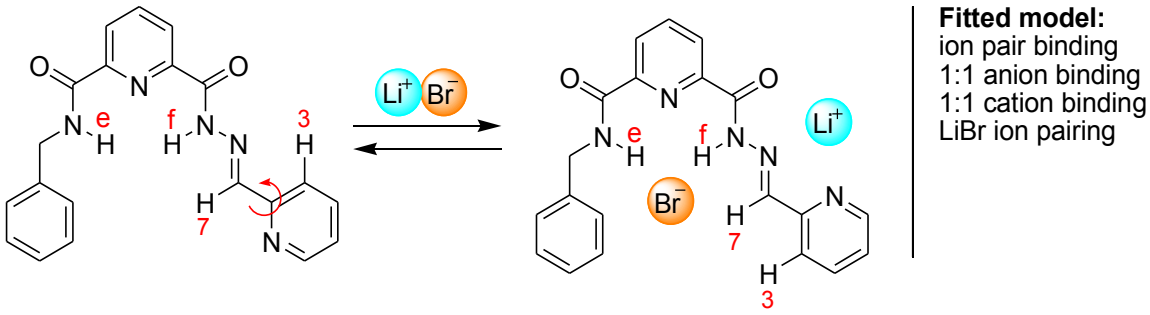

Scheme S 11. LiBr binding to *E*-**1**. Chemical shifts of the indicated protons were used for fitting.

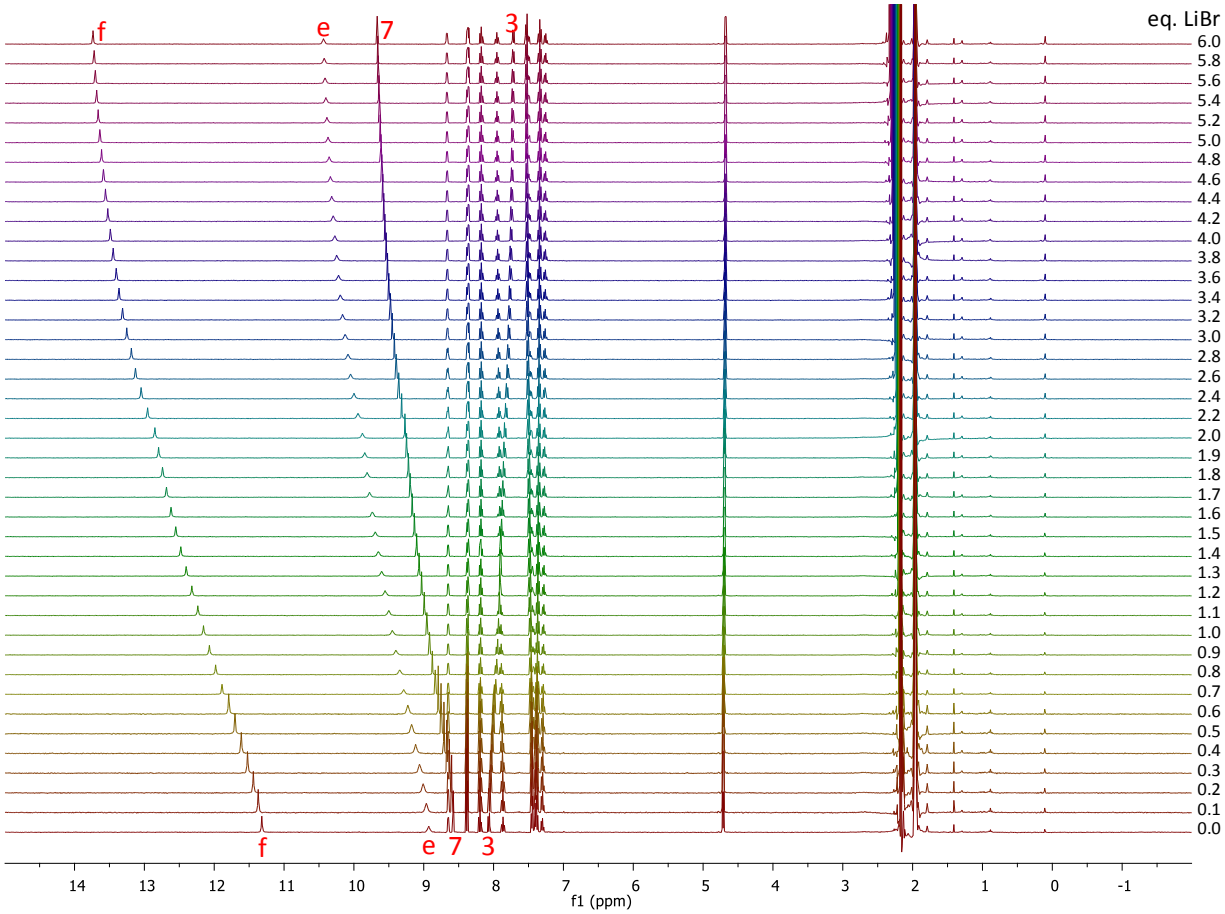

Figure S 56. ^1H NMR titration (acetonitrile-d_3) of *E*-**1** (2 mM) with LiBr. The assigned peaks were used for fitting.

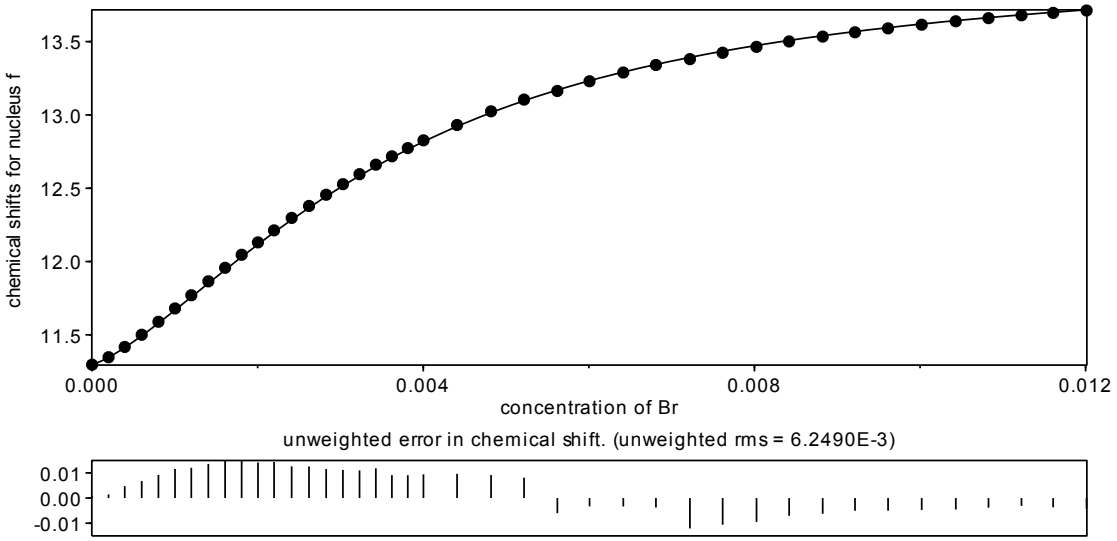

Figure S 57. Data points and fitting curve for ^{1}H NMR titration (acetonitrile-d_3) of *E*-**1** (2 mM) with LiBr.

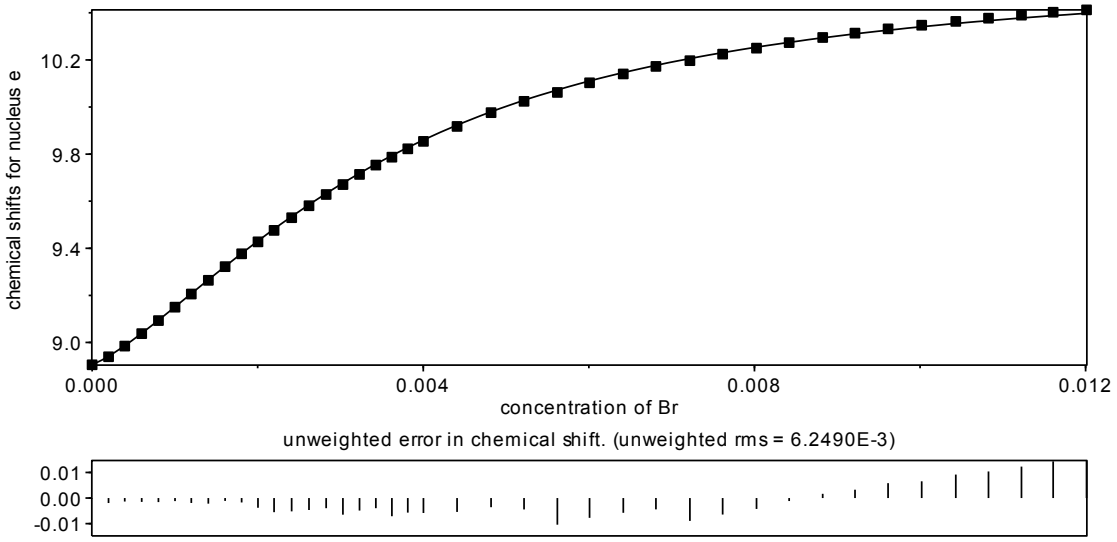

Figure S 58. Data points and fitting curve for ^{1}H NMR titration (acetonitrile-d_3) of *E*-**1** (2 mM) with LiBr.

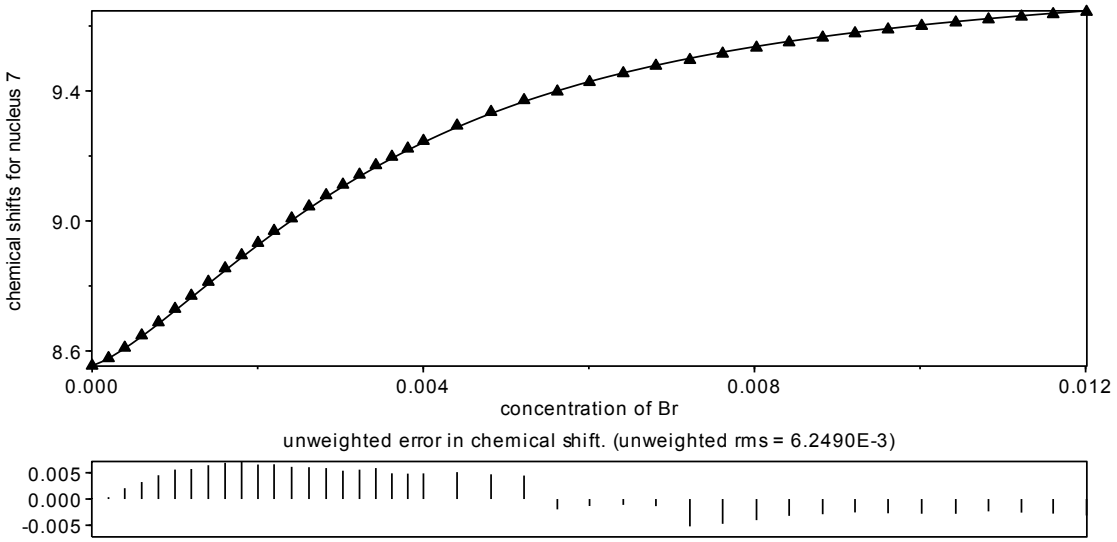

Figure S 59. Data points and fitting curve for ^{1}H NMR titration (acetonitrile-d_3) of *E*-**1** (2 mM) with LiBr.

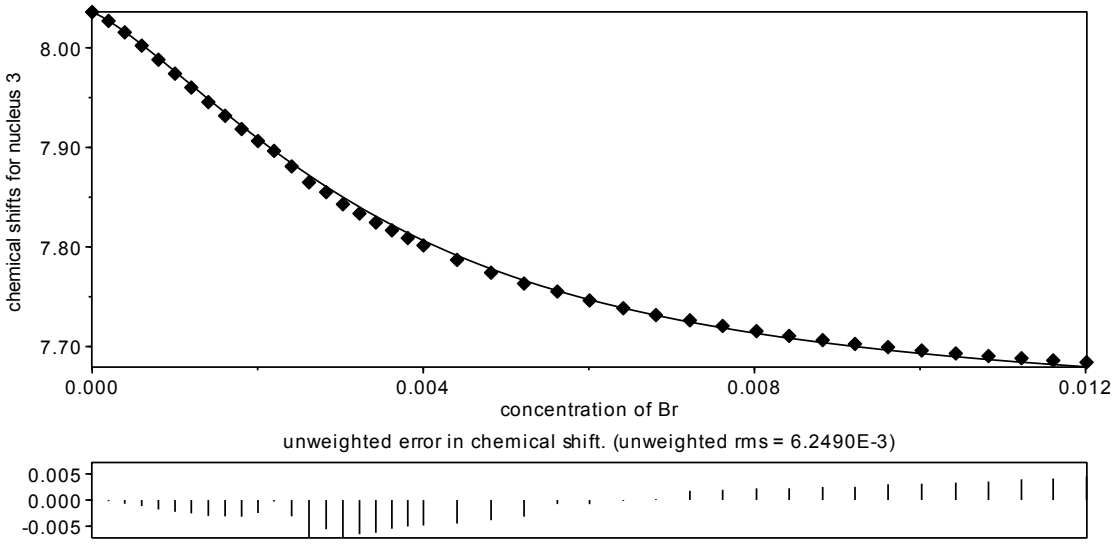

Figure S 60. Data points and fitting curve for ^{1}H NMR titration (acetonitrile-d_3) of *E*-**1** (2 mM) with LiBr.

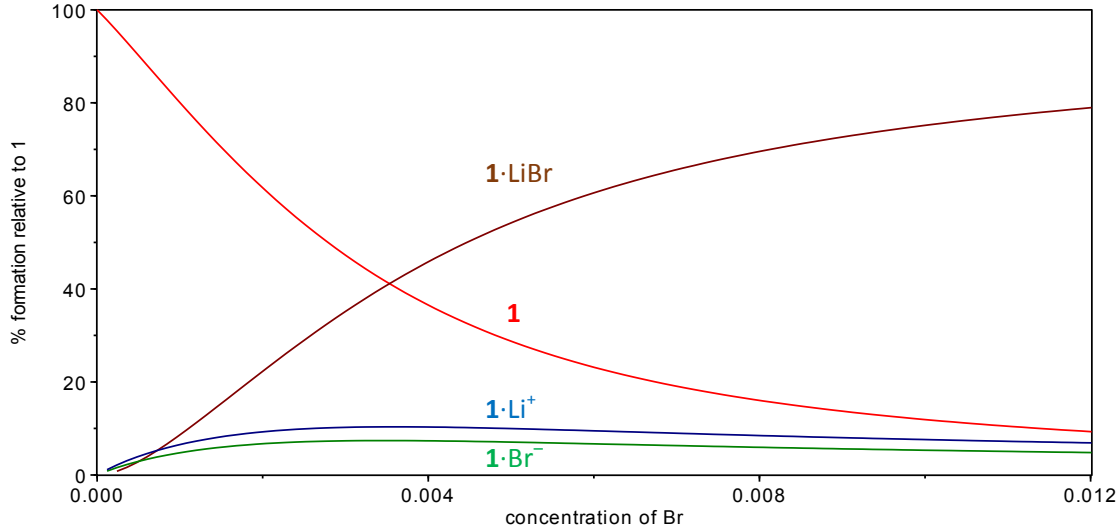

Figure S 61 Speciation diagram for the ^{1}H NMR titration of *E*-**1** (2 mM in acetonitrile-d_3) with LiBr.

4.5.4 Titration of *E*-**1** with I^- in the presence of 1 equiv. of Li^+ in acetonitrile-d_3

Titration of *E*-**1** with TBAI in the presence of 1 equiv. of $Li(CH_3OCH_2CH_2OCH_3)_3BPh_4$ showed significant changes in the ^1H NMR chemical shifts of protons f, e, and 7. These data were simultaneously fitted to the model shown in Scheme S 12, using HypNMR software.

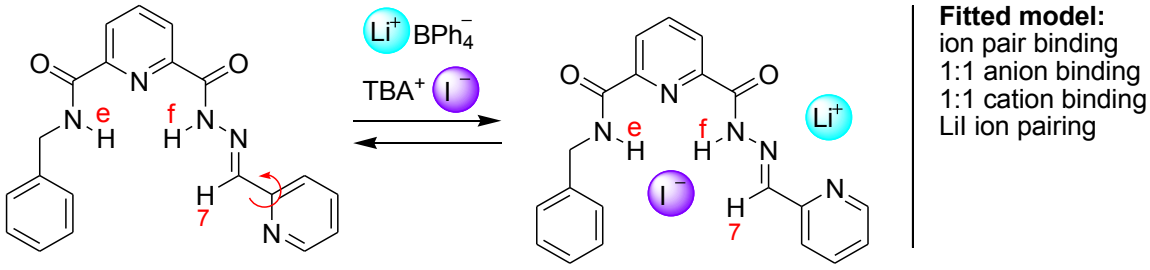

Scheme S 12. LiI binding to *E*-**1**. Chemical shifts of the indicated protons were used for fitting.

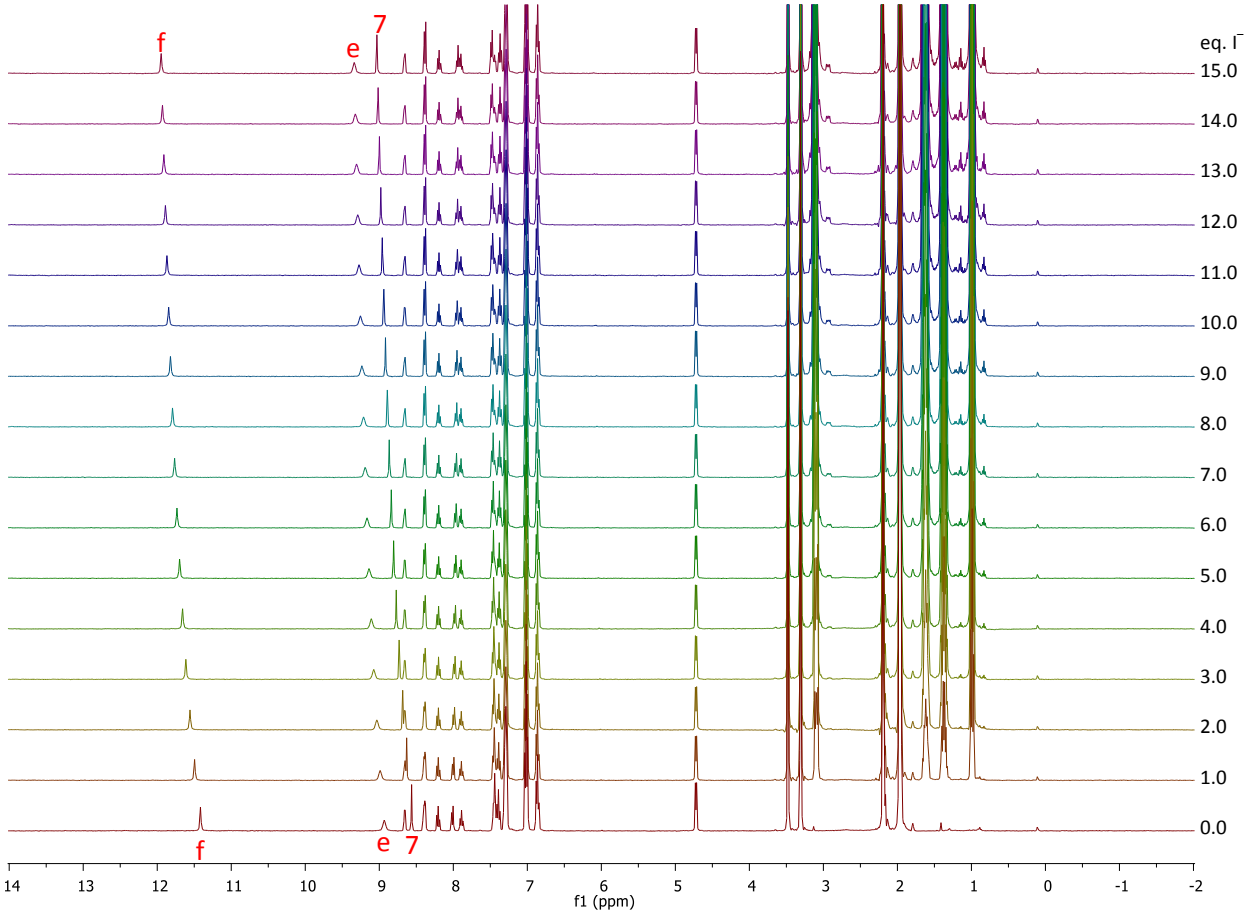

Figure S 62. ^1H NMR titration (acetonitrile-d_3) of *E*-**1** (2 mM) with TBAI in the presence of 1 equiv. of $Li(CH_3OCH_2CH_2OCH_3)_3BPh_4$. The assigned peaks were used for fitting.

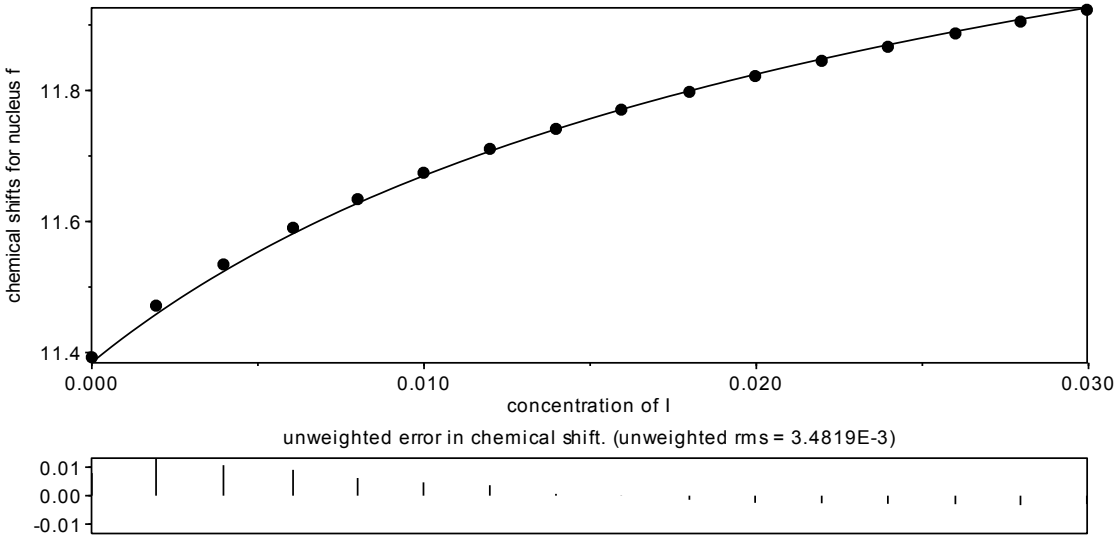

Figure S 63. Data points and fitting curve for ^{1}H NMR titration (acetonitrile-d_3) of *E*-**1** (2 mM) with TBAI in the presence of 1 equiv. of $Li(CH_3OCH_2CH_2OCH_3)_3BPh_4$.

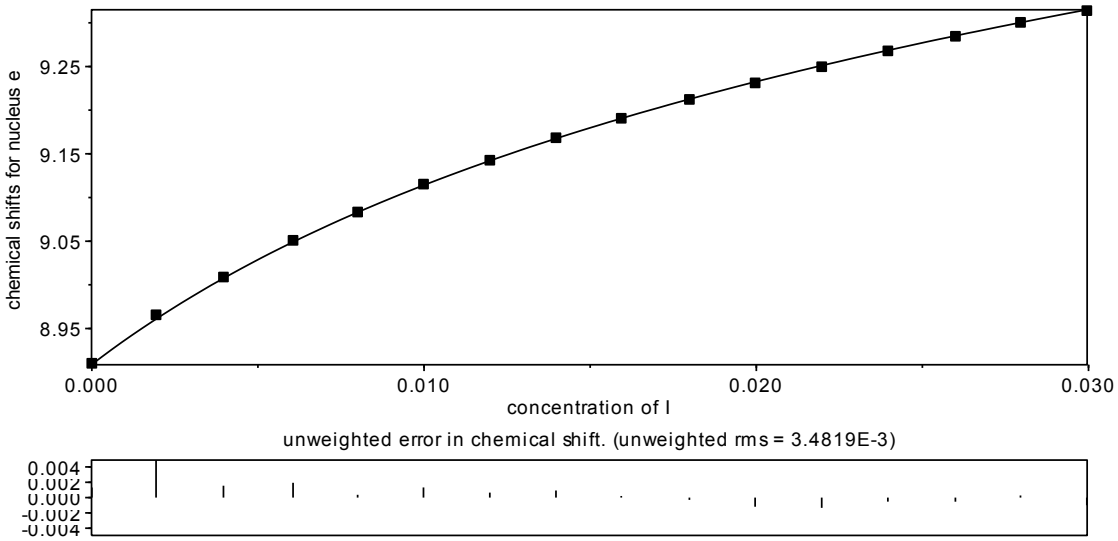

Figure S 64. Data points and fitting curve for ^{1}H NMR titration (acetonitrile-d_3) of *E*-**1** (2 mM) with TBAI in the presence of 1 equiv. of $Li(CH_3OCH_2CH_2OCH_3)_3BPh_4$.

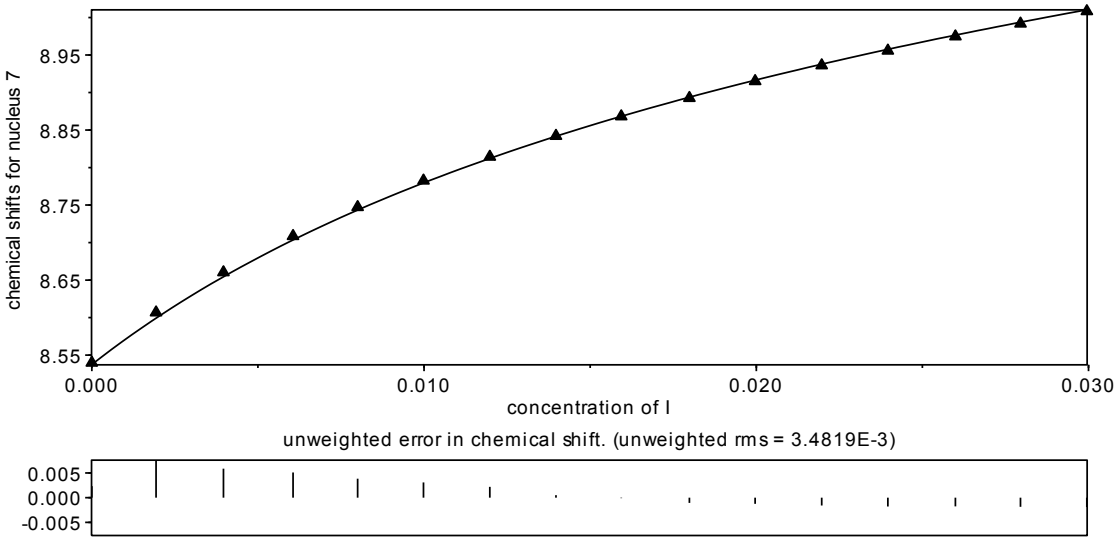

Figure S 65. Data points and fitting curve for ^{1}H NMR titration (acetonitrile-d_3) of *E*-**1** (2 mM) with TBAI in the presence of 1 equiv. of $Li(CH_3OCH_2CH_2OCH_3)_3BPh_4$.

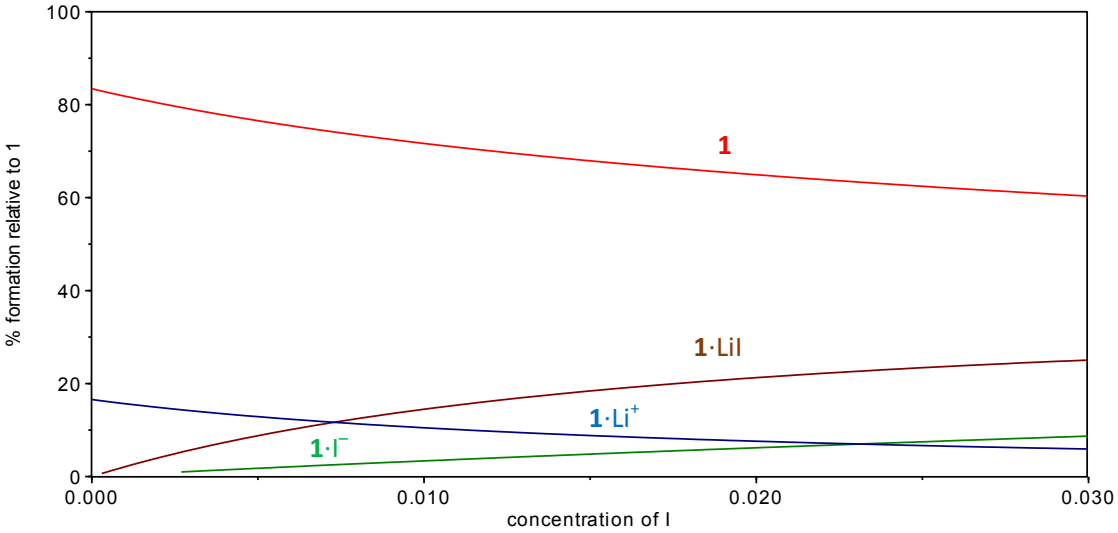

Figure S 66. Speciation diagram for the ^{1}H NMR titration of *E*-**1** (2 mM in acetonitrile-d_3) with TBAI in the presence of 1 equiv. of $Li(CH_3OCH_2CH_2OCH_3)_3BPh_4$.

4.5.5 Titration of *E*-**1** with LiI in acetonitrile-d_3

Titration of *E*-**1** with LiI showed significant changes in the ^{1}H NMR chemical shifts of protons f, e, 3, and 7. These data were simultaneously fitted to the model shown in Scheme S 13, using HypNMR software.

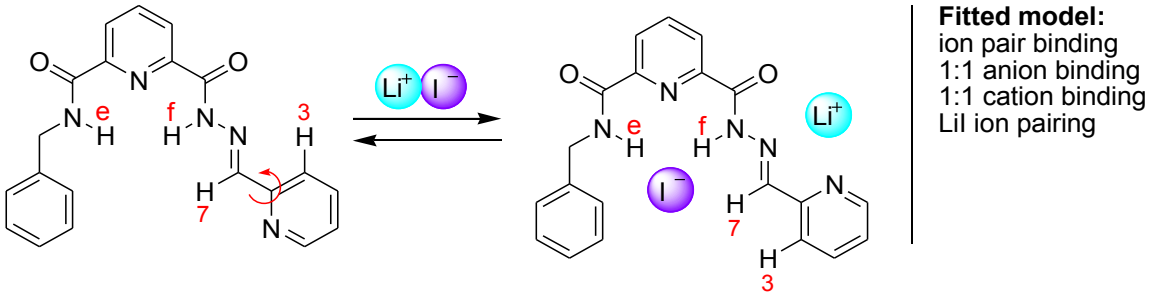

Scheme S 13. LiI binding to *E*-**1**. Chemical shifts of the indicated protons were used for fitting.

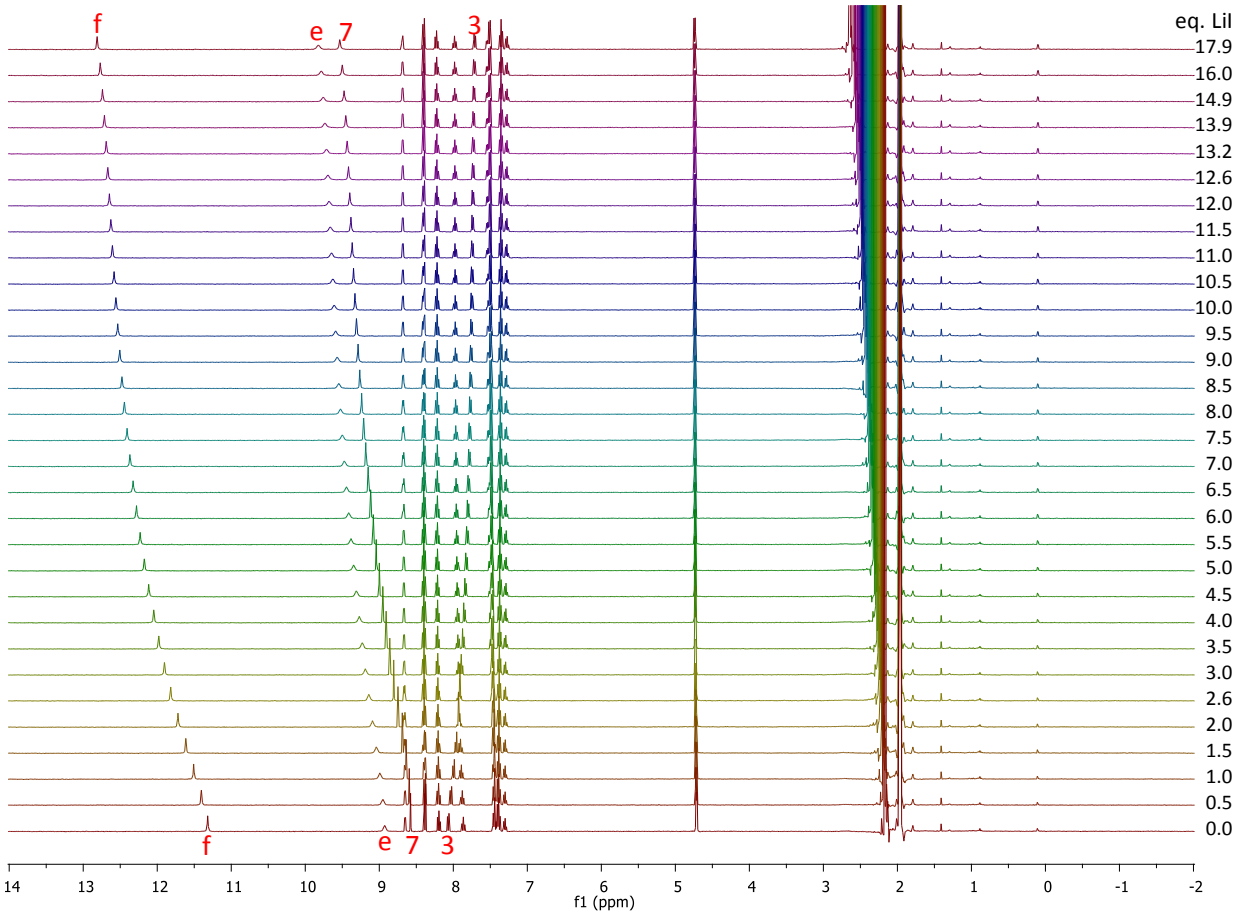

Figure S 67. ^{1}H NMR titration (acetonitrile-d_3) of *E*-**1** (2 mM) with LiI. The assigned peaks were used for fitting.

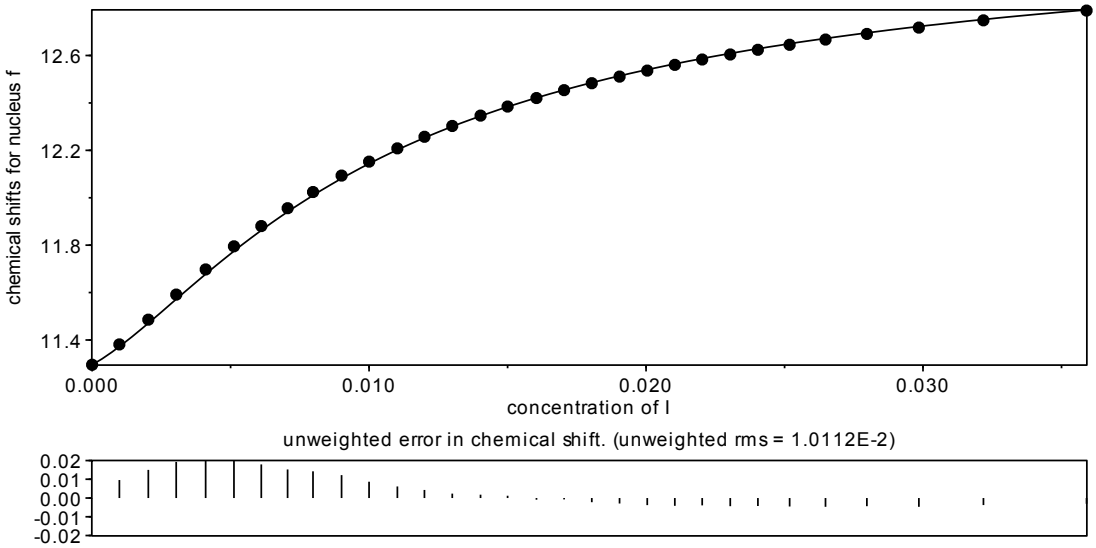

Figure S 68. Data points and fitting curve for ^{1}H NMR titration (acetonitrile-d_3) of *E*-**1** (2 mM) with LiI.

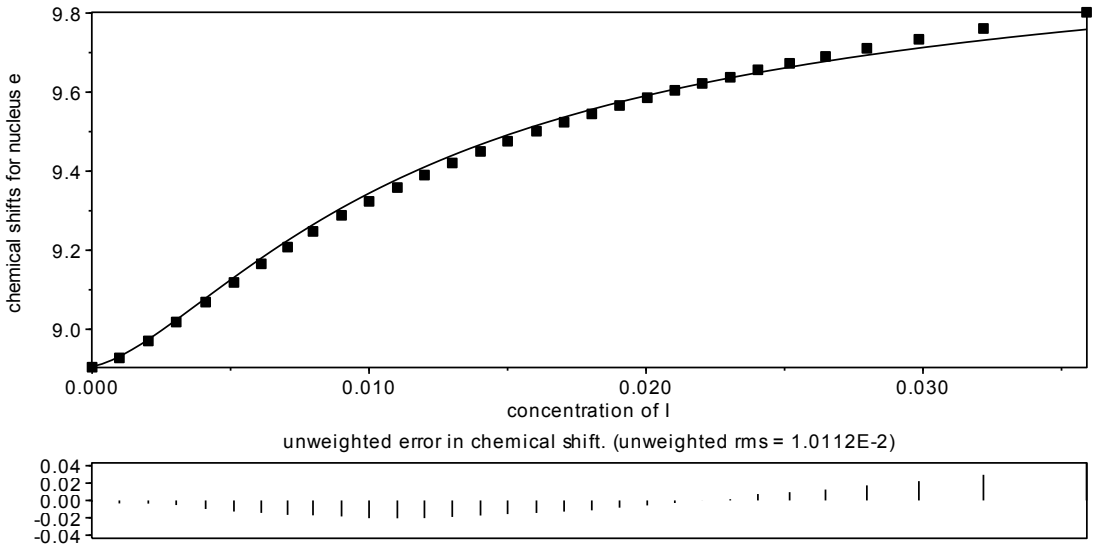

Figure S 69. Data points and fitting curve for ^{1}H NMR titration (acetonitrile-d_3) of *E*-**1** (2 mM) with LiI.

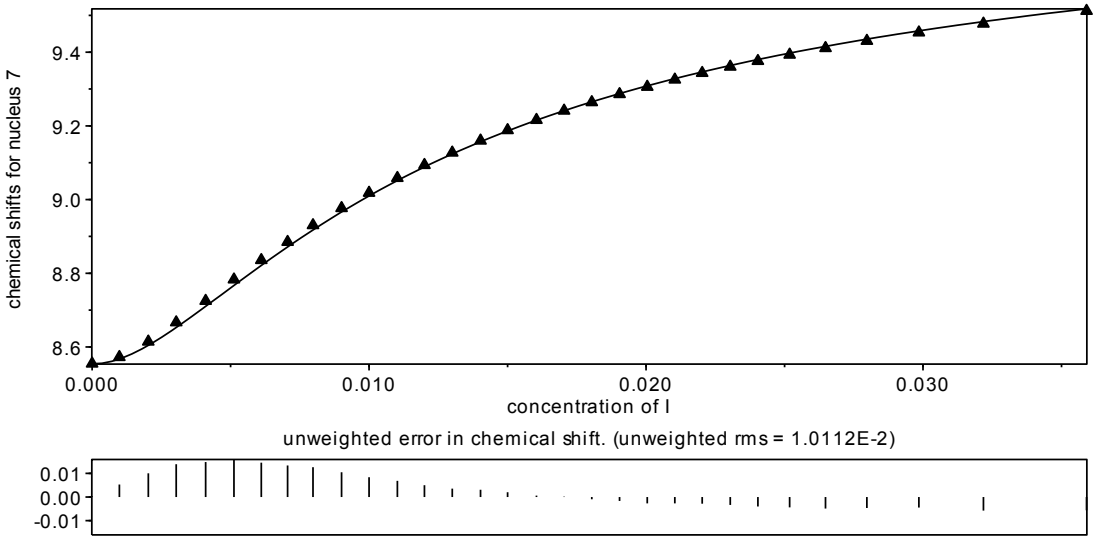

Figure S 70. Data points and fitting curve for ^{1}H NMR titration (acetonitrile-d_3) of *E*-**1** (2 mM) with LiI.

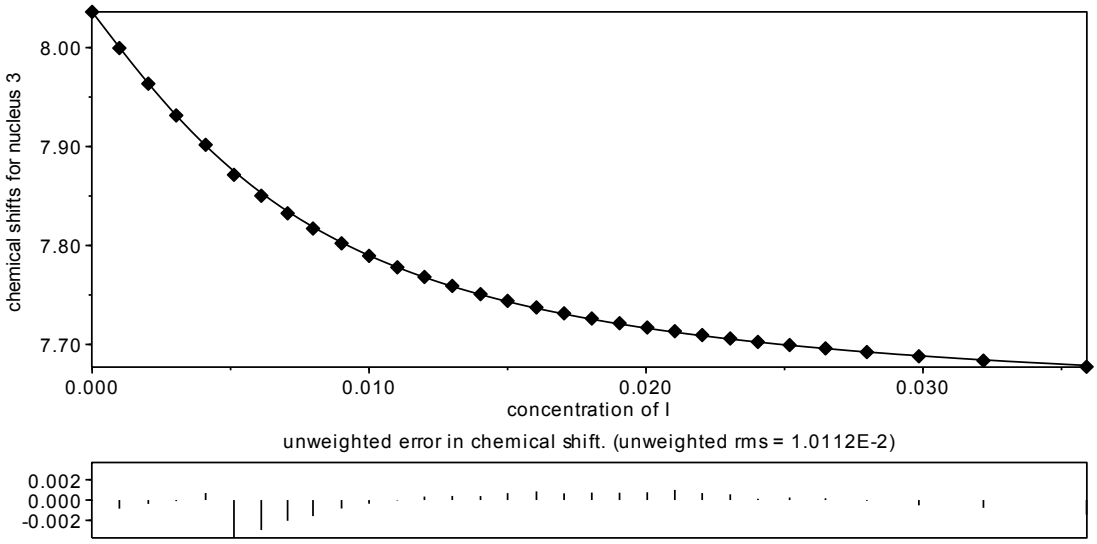

Figure S 71. Data points and fitting curve for ^{1}H NMR titration (acetonitrile-d_3) of *E*-**1** (2 mM) with LiI.

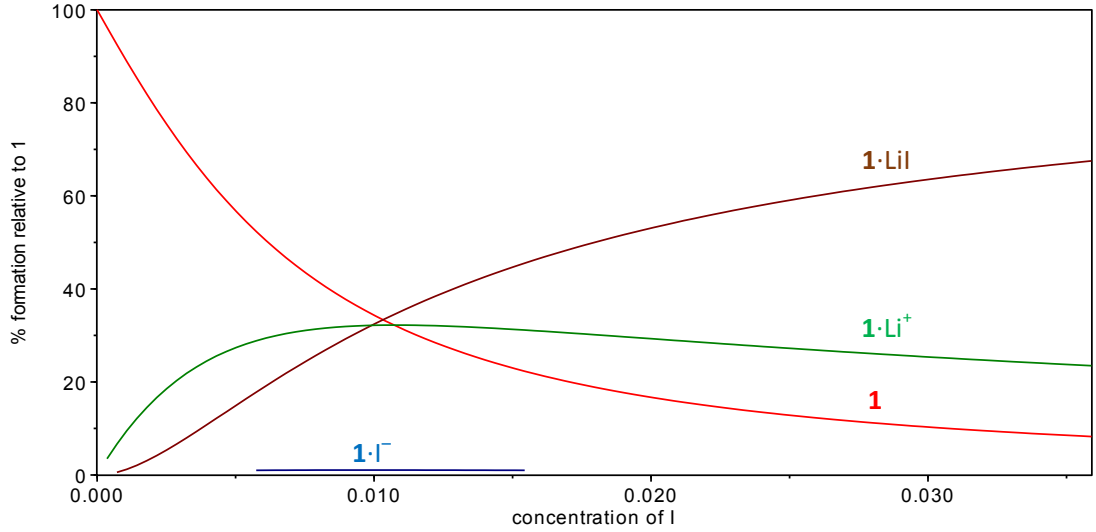

Figure S 72. Speciation diagram for the ^{1}H NMR titration of *E*-**1** (2 mM in acetonitrile-d_3) with LiI.

4.5.6 Titration of *E*-**1** with Br^- in the presence of 1 equiv. of Na^+ in acetonitrile-d_3

Titration of *E*-**1** with TBABr in the presence of 1 equiv. of $NaBPh_4$ showed significant changes in the ^1H NMR chemical shifts of protons f, e, and 7. These data were simultaneously fitted to the model shown in Scheme S 14, using HypNMR software.

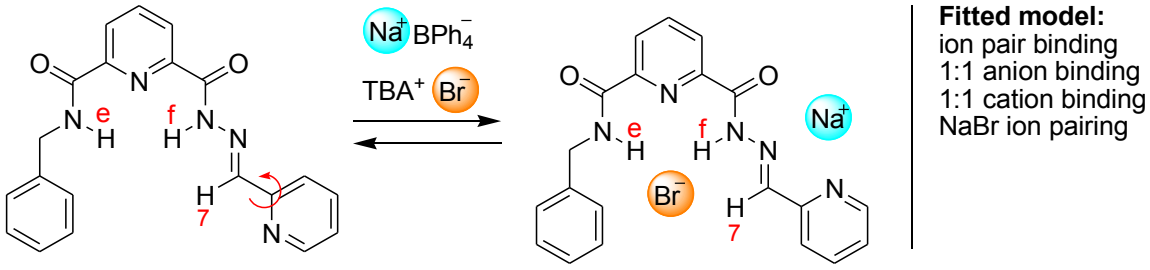

Scheme S 14. NaBr binding to *E*-**1**. Chemical shifts of the indicated protons were used for fitting.

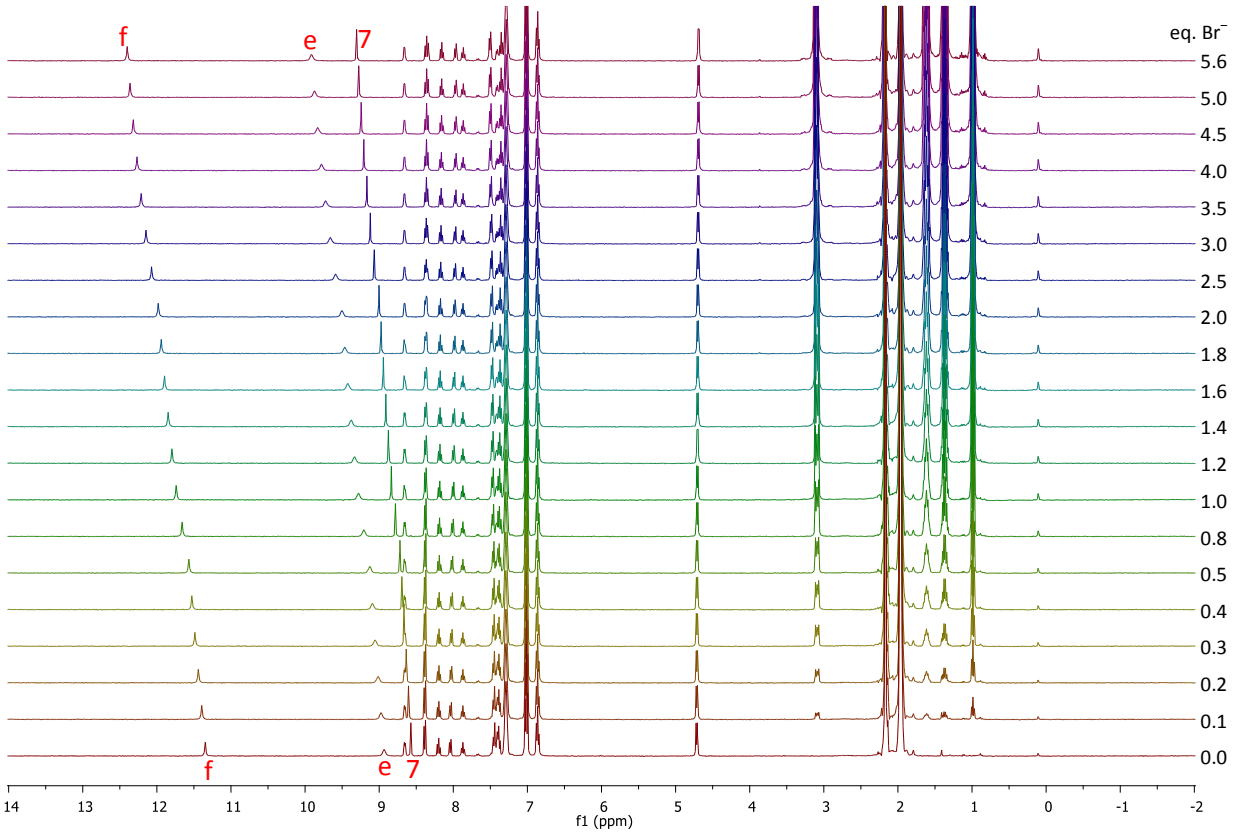

Figure S 73. ^1H NMR titration (acetonitrile-d_3) of *E*-**1** (2 mM) with TBABr in the presence of 1 equiv. of $NaBPh_4$. The assigned peaks were used for fitting.

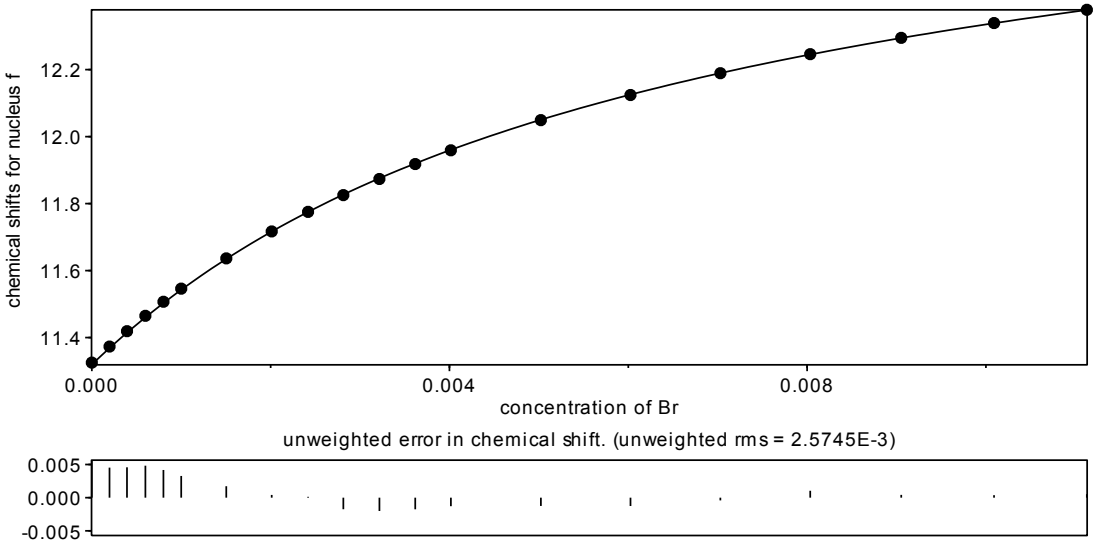

Figure S 74. Data points and fitting curve for ^{1}H NMR titration (acetonitrile-d_3) of *E*-**1** (2 mM) with TBABr in the presence of 1 equiv. of $NaBPh_4$.

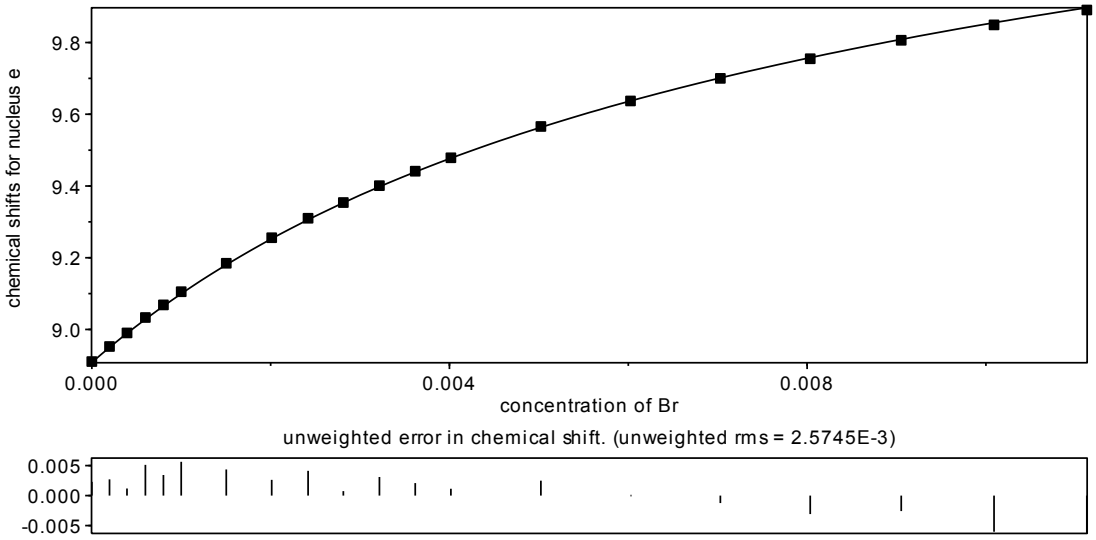

Figure S 75. Data points and fitting curve for ^{1}H NMR titration (acetonitrile-d_3) of *E*-**1** (2 mM) with TBABr in the presence of 1 equiv. of $NaBPh_4$.

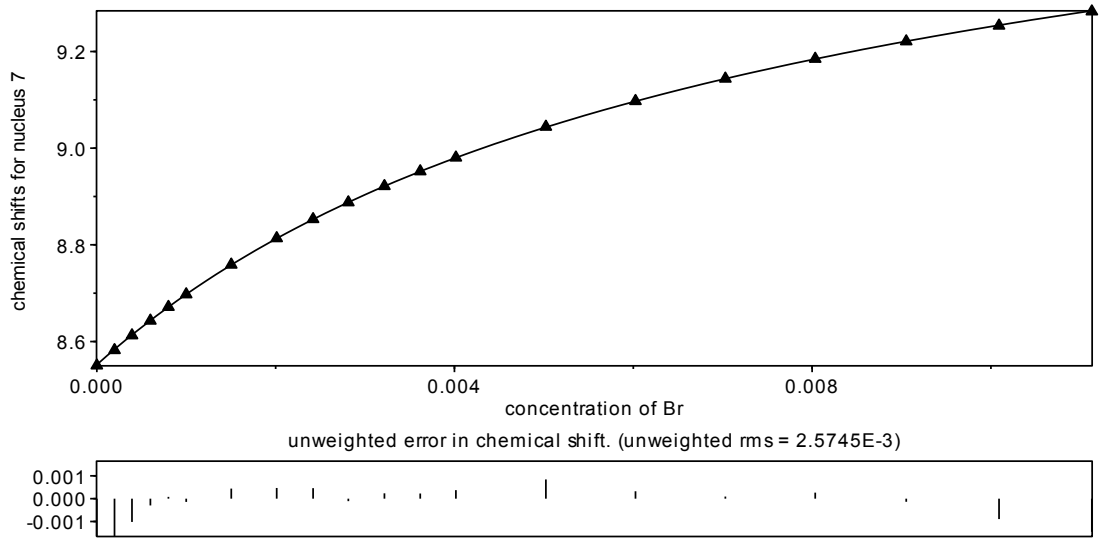

Figure S 76. Data points and fitting curve for ^{1}H NMR titration (acetonitrile-d_3) of *E*-**1** (2 mM) with TBABr in the presence of 1 equiv. of $NaBPh_4$.

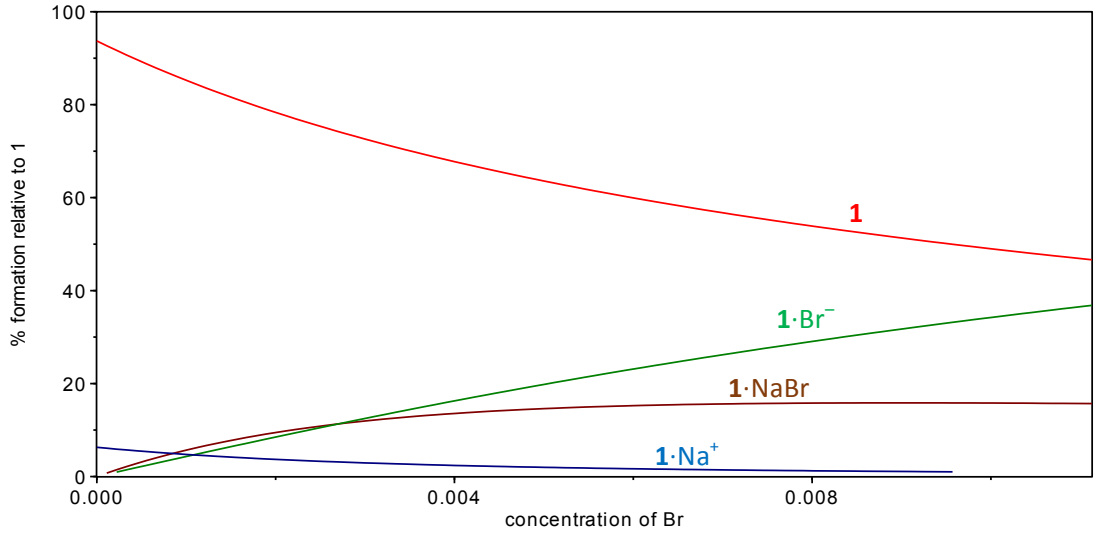

Figure S 77. Speciation diagram for the ^{1}H NMR titration of *E*-**1** (2 mM in acetonitrile-d_3) with TBABr in the presence of 1 equiv. of $NaBPh_4$.

4.5.7 Titration of *E*-**1** with I^- in the presence of 1 equiv. of Na^+ in acetonitrile-d_3

Titration of *E*-**1** with TBAI in the presence of 1 equiv. of $NaBPh_4$ showed significant changes in the ^1H NMR chemical shifts of protons f, e, and 7. These data were simultaneously fitted to the model shown in Scheme S 15, using HypNMR software.

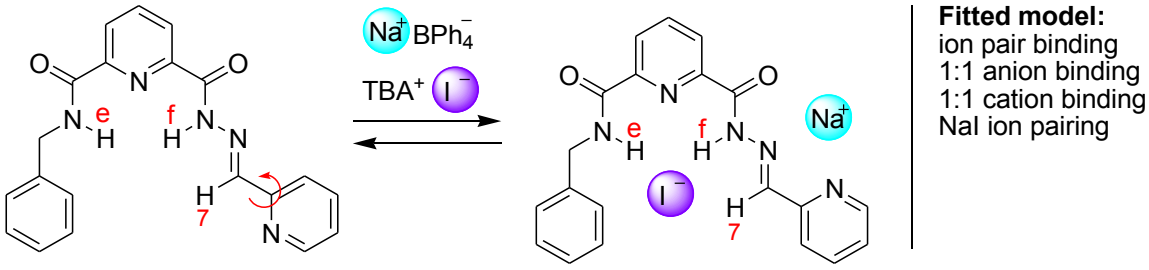

Scheme S 15. NaI binding to *E*-**1**. Chemical shifts of the indicated protons were used for fitting.

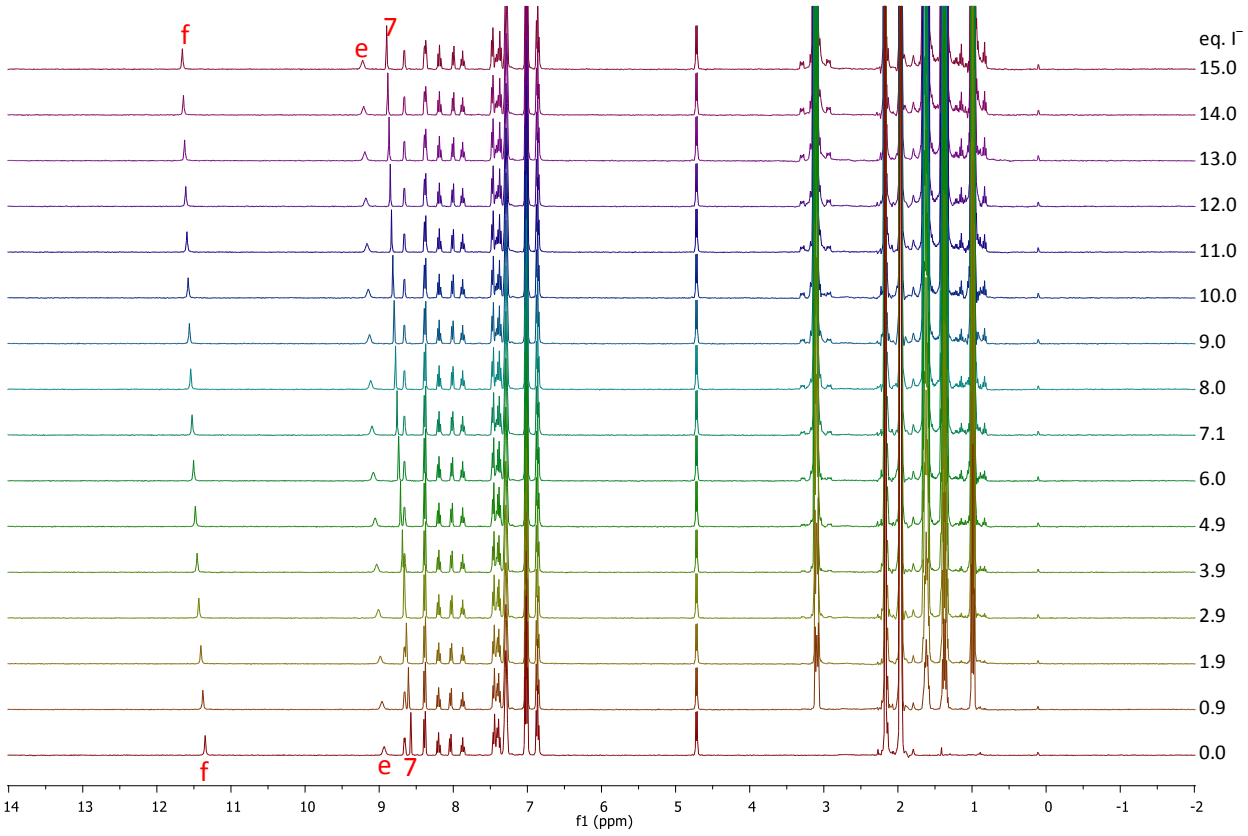

Figure S 78. ^1H NMR titration (acetonitrile-d_3) of *E*-**1** (2 mM) with TBAI (0–15 equiv., bottom to top) in the presence of 1 equiv. of $NaBPh_4$. The assigned peaks were used for manual fitting.

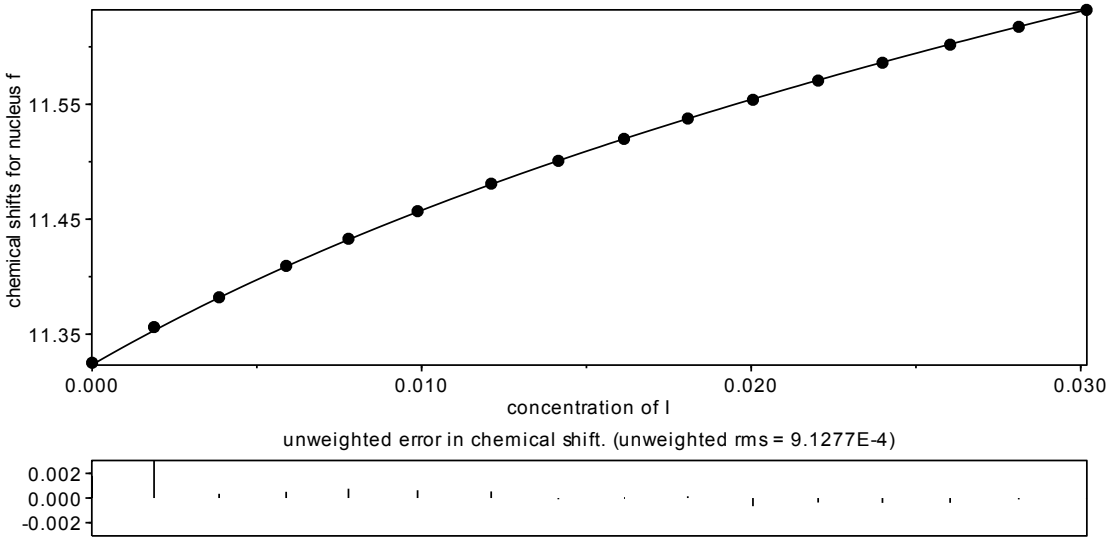

Figure S 79. Data points and fitting curve for ^{1}H NMR titration (acetonitrile-d_3) of *E*-**1** (2 mM) with TBAI in the presence of 1 equiv. of $NaBPh_4$.

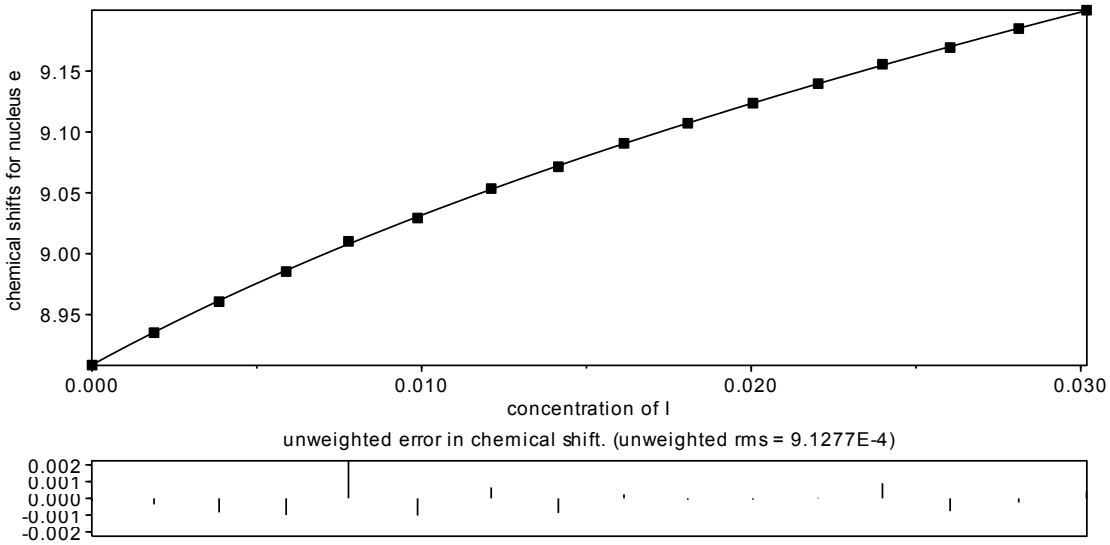

Figure S 80. Data points and fitting curve for ^{1}H NMR titration (acetonitrile-d_3) of *E*-**1** (2 mM) with TBAI in the presence of 1 equiv. of $NaBPh_4$.

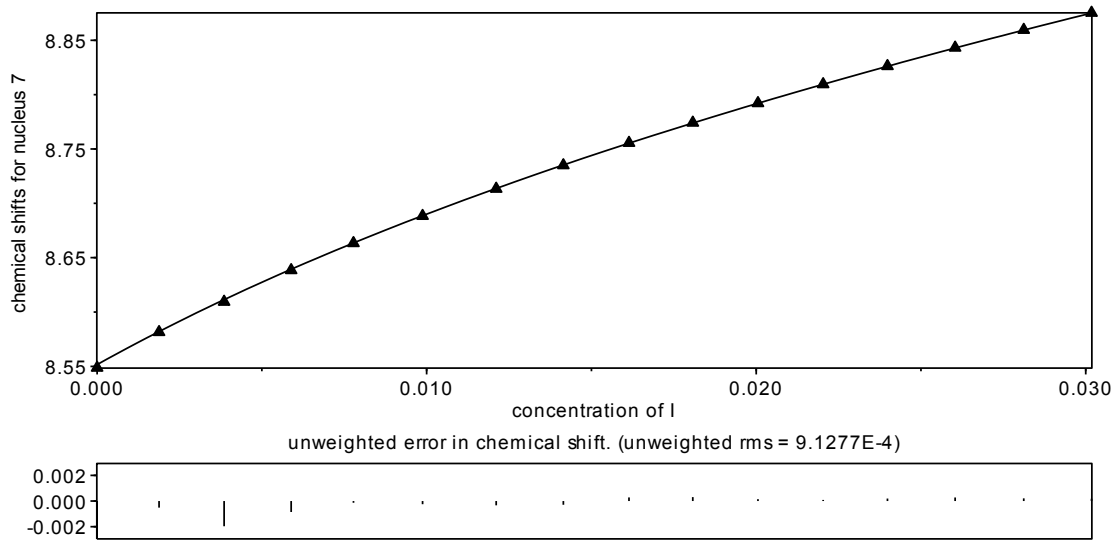

Figure S 81. Data points and fitting curve for ^{1}H NMR titration (acetonitrile-d_3) of *E*-**1** (2 mM) with TBAI in the presence of 1 equiv. of $NaBPh_4$.

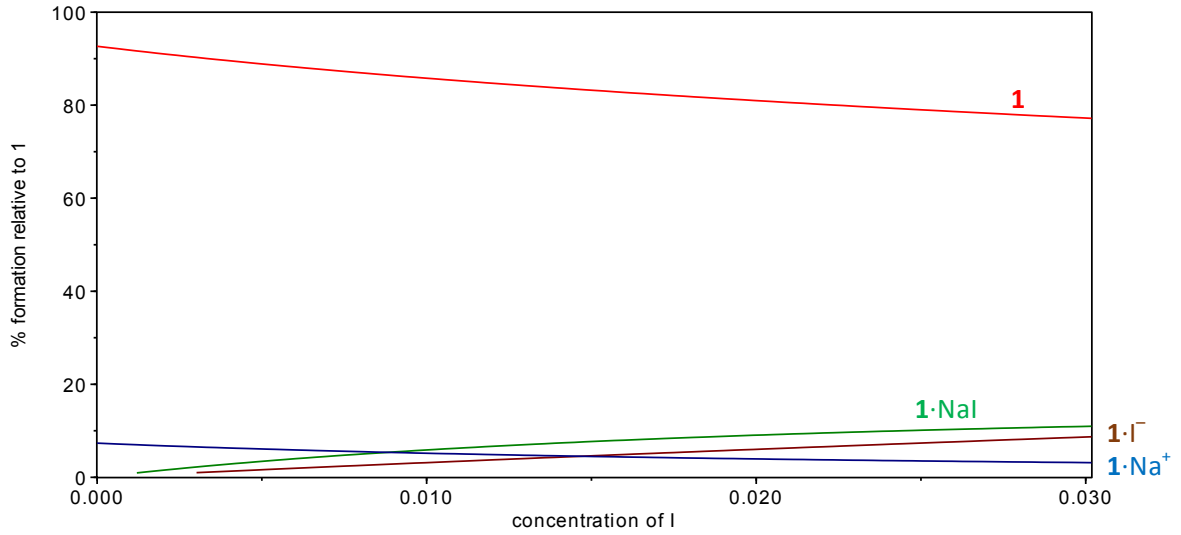

Figure S 82. Speciation diagram for the ^{1}H NMR titration of *E*-**1** (2 mM in acetonitrile-d_3) with TBAI in the presence of 1 equiv. of $NaBPh_4$.

4.5.8 Titration of *E*-**1** with NaI in acetonitrile-d_3

Titration of *E*-**1** with NaI showed significant changes in the ^{1}H NMR chemical shifts of protons f, e, 3, and 7. These data were simultaneously fitted to the model shown in Scheme S 16, using HypNMR software. Because *E*-**1**·NaI is prone to precipitation, solution of *E*-**1** was titrated with the solution of pure NaI (i.e. total concentration of *E*-**1** is not constant).

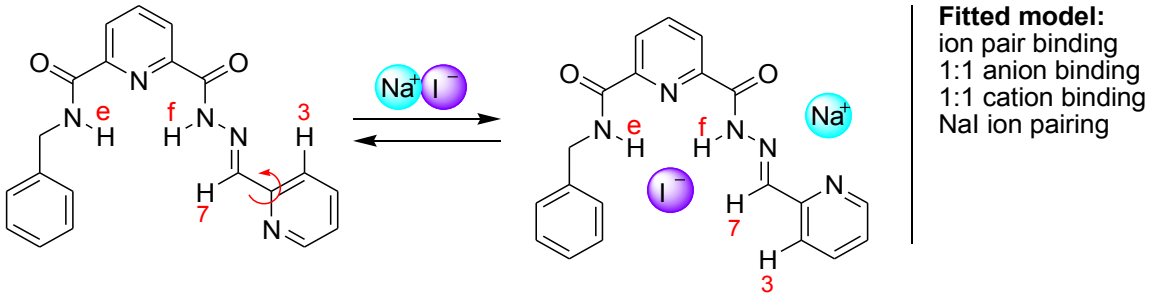

Scheme S 16. NaI binding to *E*-**1**. Chemical shifts of the indicated protons were used for fitting.

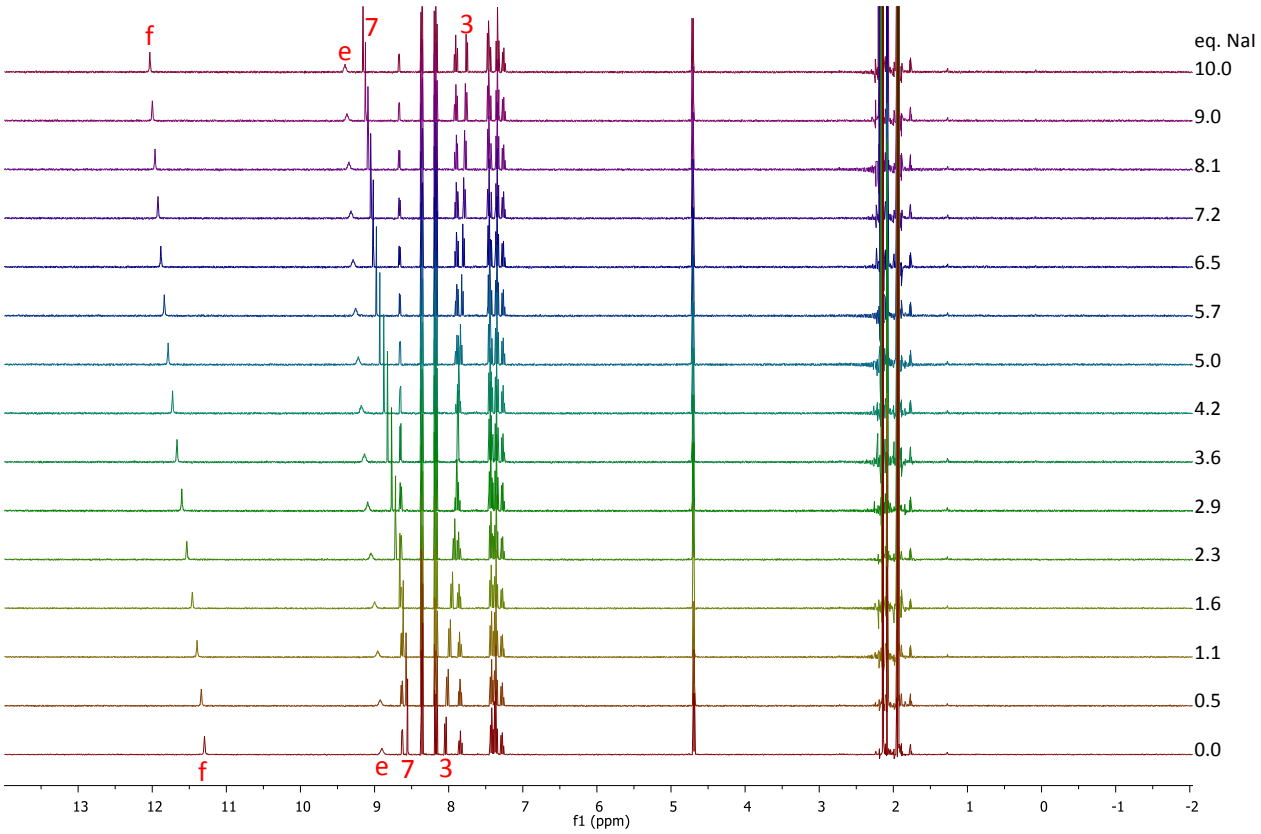

Figure S 83. ^{1}H NMR titration (acetonitrile-d_3) of *E*-**1** (4→2.9 mM) with NaI. The assigned peaks were used for fitting.

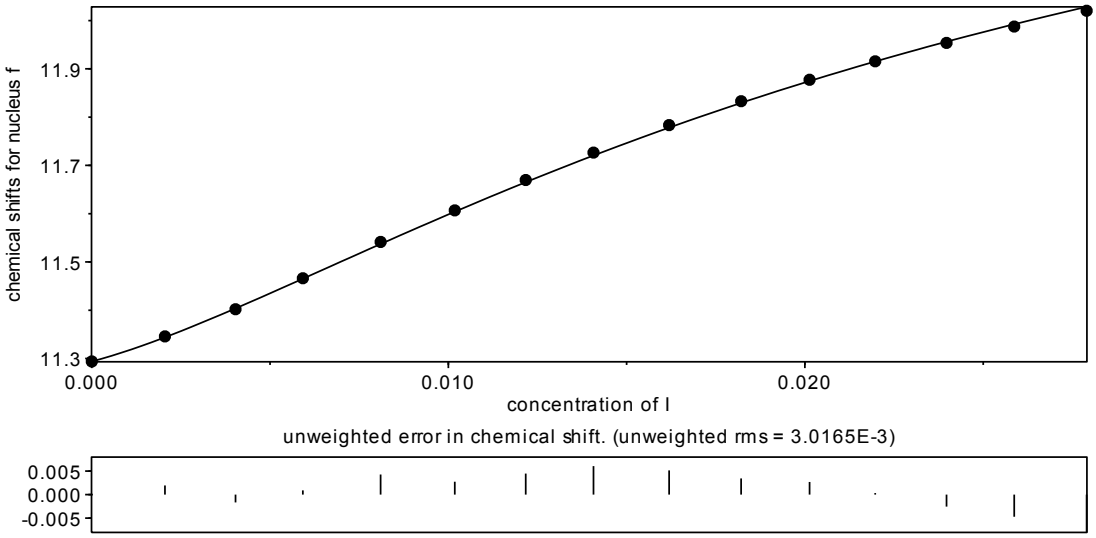

Figure S 84. Data points and fitting curve for ^{1}H NMR titration (acetonitrile-d_3) of *E*-**1** (4.0→2.9 mM) with NaI.

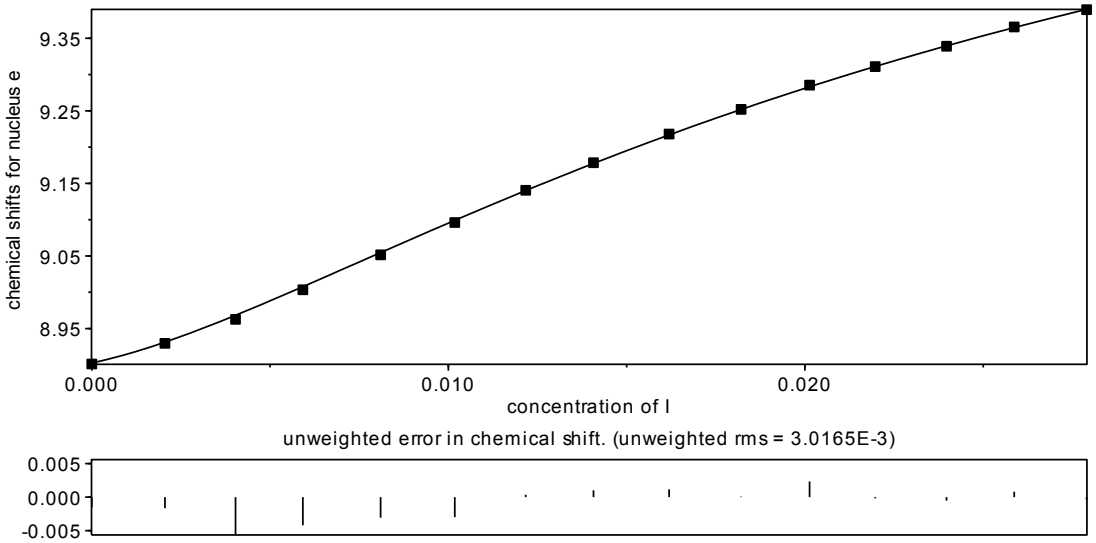

Figure S 85. Data points and fitting curve for ^{1}H NMR titration (acetonitrile-d_3) of *E*-**1** (4.0→2.9 mM) with NaI.

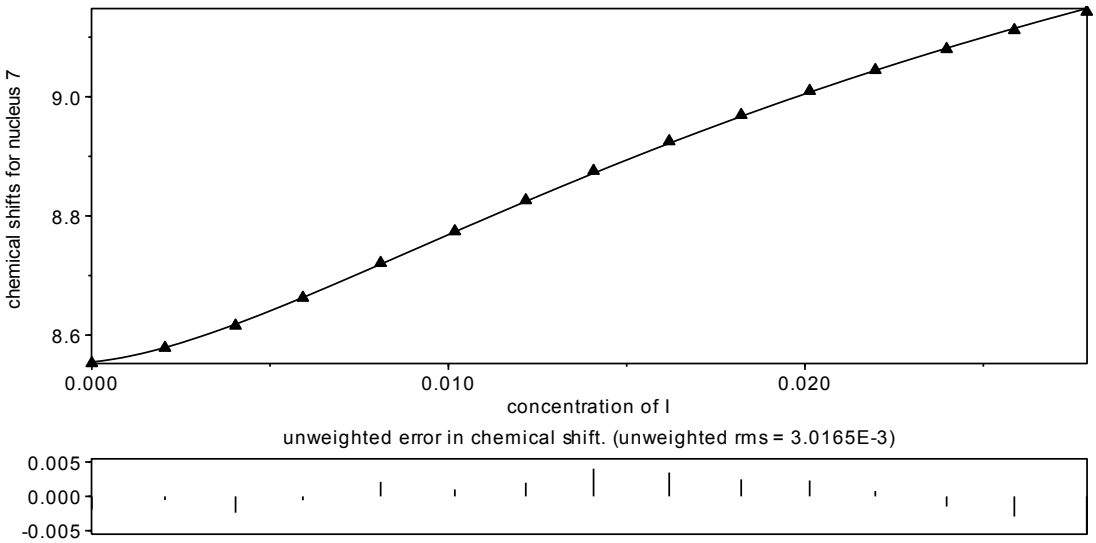

Figure S 86. Data points and fitting curve for ^{1}H NMR titration (acetonitrile-d_3) of *E*-**1** (4.0→2.9 mM) with NaI.

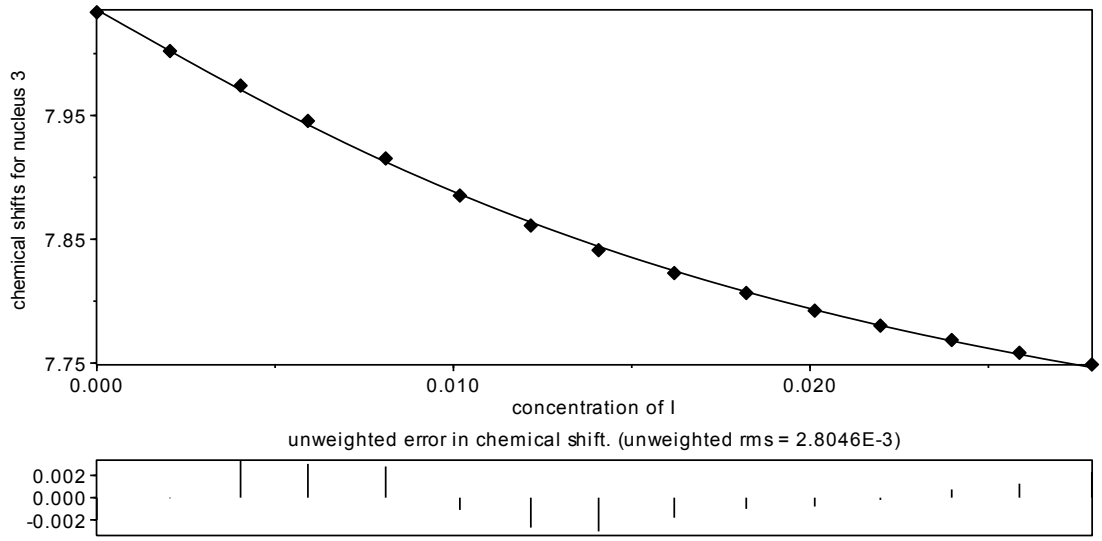

Figure S 87. Data points and fitting curve for ^{1}H NMR titration (acetonitrile-d_3) of *E*-**1** (4.0→2.9 mM) with NaI.

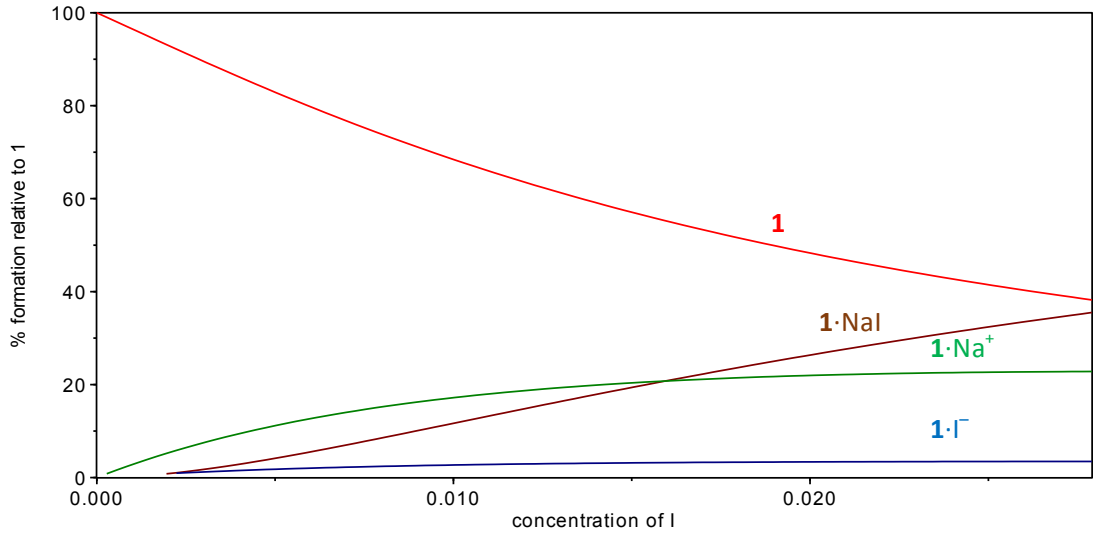

Figure S 88. Data points and fitting curve for ^{1}H NMR titration (acetonitrile-d_3) of *E*-**1** (4.0→2.9 mM) with NaI.

4.5.9 Titration of *E*-**1** with I^- in the presence of 1 equiv. of K^+ in acetonitrile-d_3

Titration of *E*-**1** with TBAI in the presence of 1 equiv. of $KBPh_4$ showed significant changes in the ^1H NMR chemical shifts of protons f, e, and 7. These data were simultaneously fitted to the model shown in Scheme S 17, using HypNMR software.

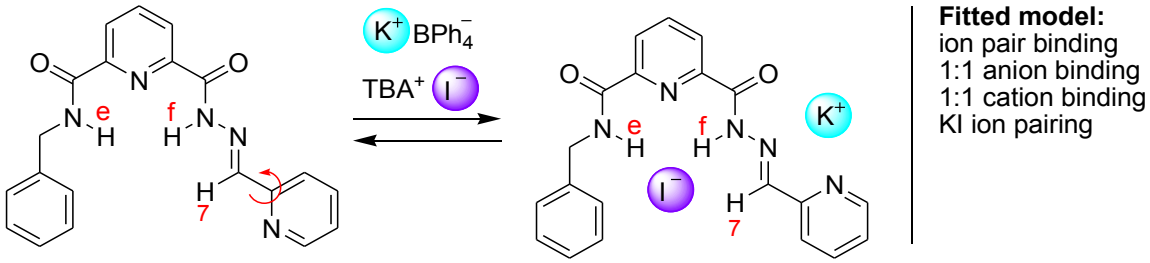

Scheme S 17. KI binding to *E*-**1**. Chemical shifts of the indicated protons were used for fitting.

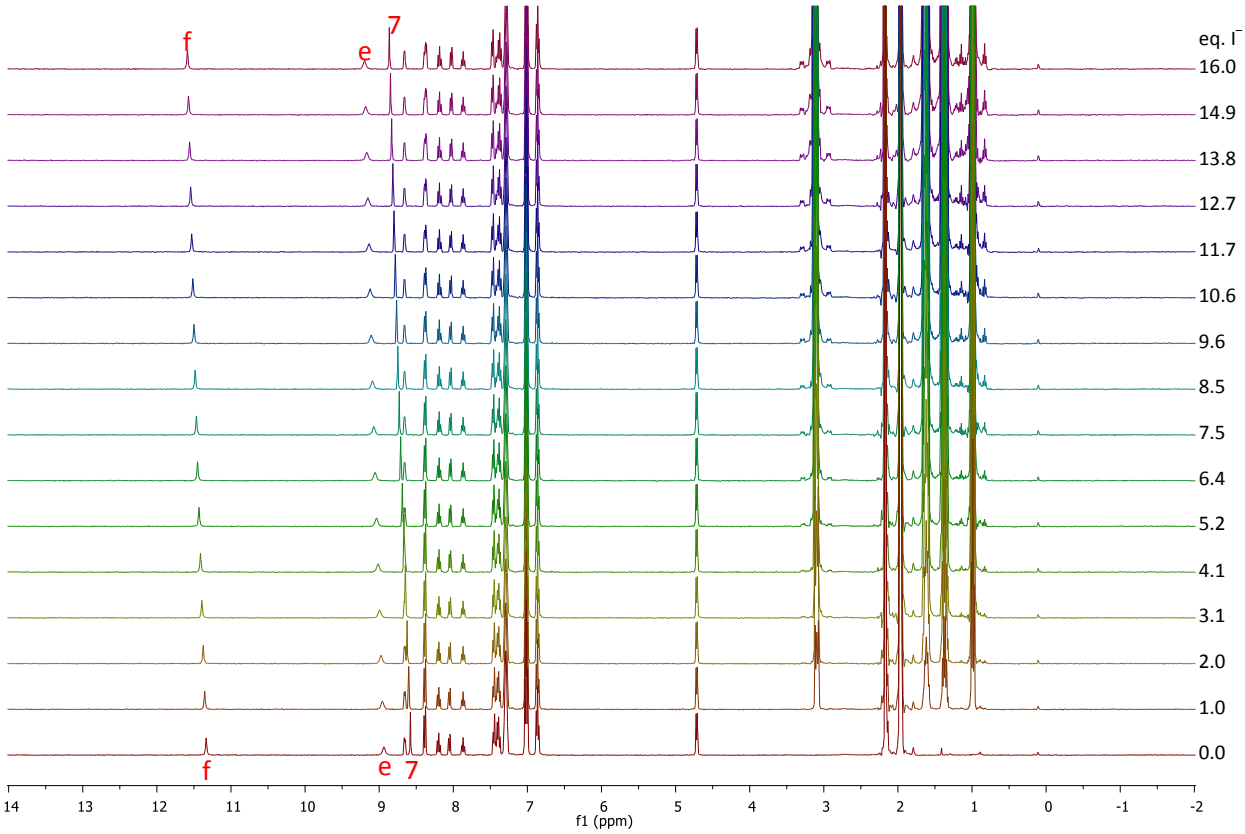

Figure S 89. ^1H NMR titration (acetonitrile-d_3) of *E*-**1** (2 mM) with TBAI in the presence of 1 equiv. of $KBPh_4$.

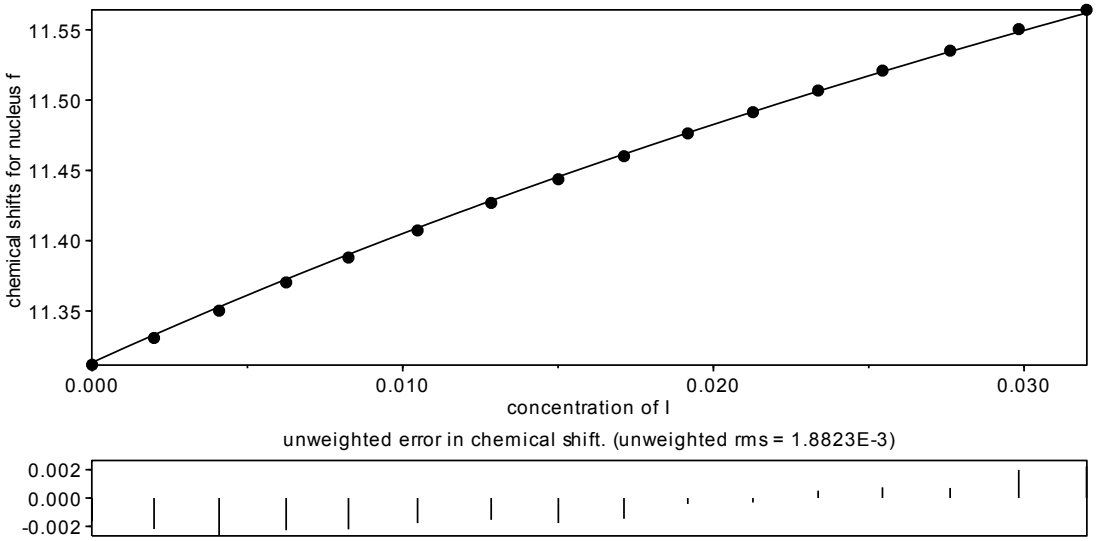

Figure S 90. Data points and fitting curve for ^{1}H NMR titration (acetonitrile-d_3) of *E*-**1** (2 mM) with TBAI in the presence of 1 equiv. of $KBPh_4$.

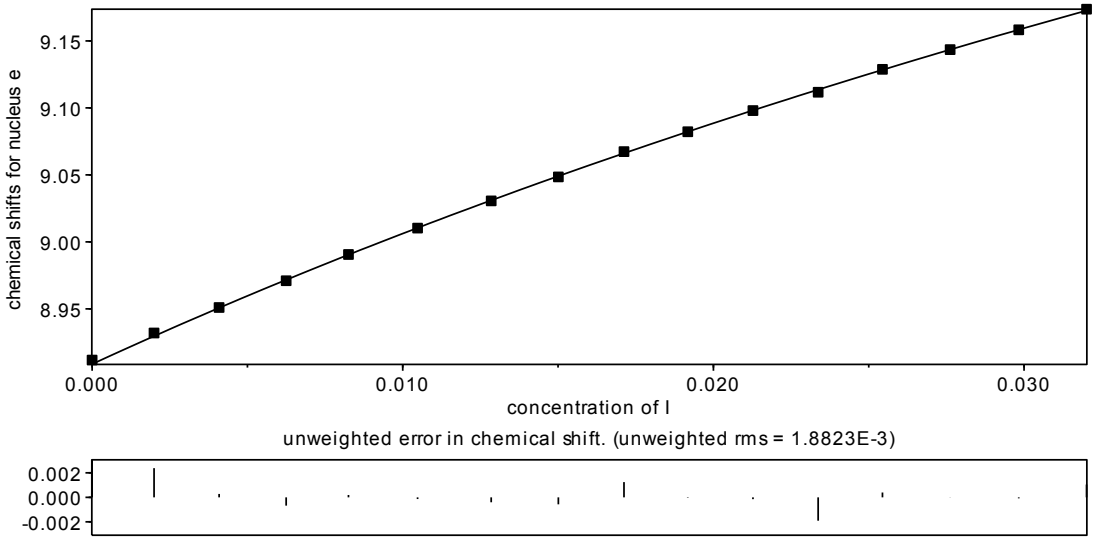

Figure S 91. Data points and fitting curve for ^{1}H NMR titration (acetonitrile-d_3) of *E*-**1** (2 mM) with TBAI in the presence of 1 equiv. of $KBPh_4$.

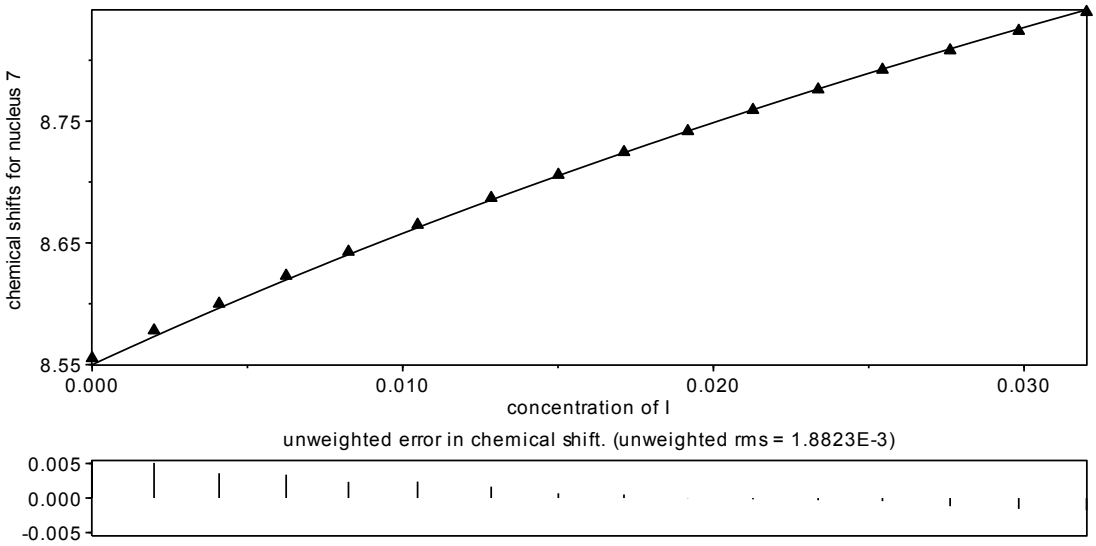

Figure S 92. Data points and fitting curve for ^{1}H NMR titration (acetonitrile-d_3) of *E*-**1** (2 mM) with TBAI in the presence of 1 equiv. of $KBPh_4$.

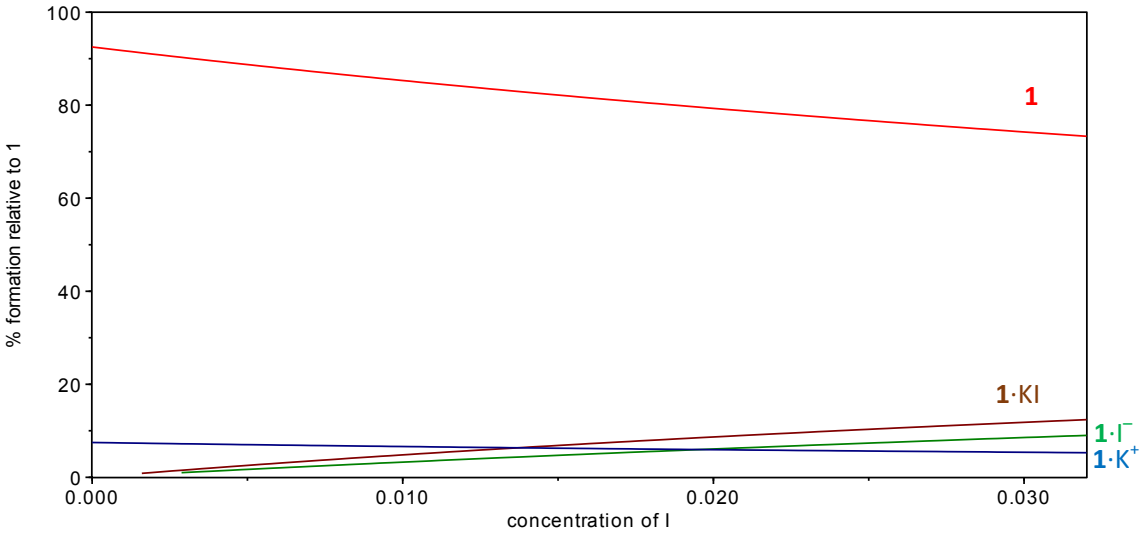

Figure S 93. Speciation during the ^{1}H NMR titration (acetonitrile-d_3) of *E*-**1** (2 mM) with TBAI in the presence of 1 equiv. of $KBPh_4$.

4.5.10 Titration of *Z*-**1** with LiBr in acetonitrile-d_3

Titration of *Z*-**1** with LiBr resulted in small changes in chemical shifts. Amide NH protons do not shift, indicating inaccessibility of the anion binding site. Slight changes in the chemical shift of proton 7 could be due to weak cation binding in the bidentate binding site but could not be adequately fitted to the model (Scheme S 18) due to the very weak interactions of *Z*-**1** with the investigated salt.

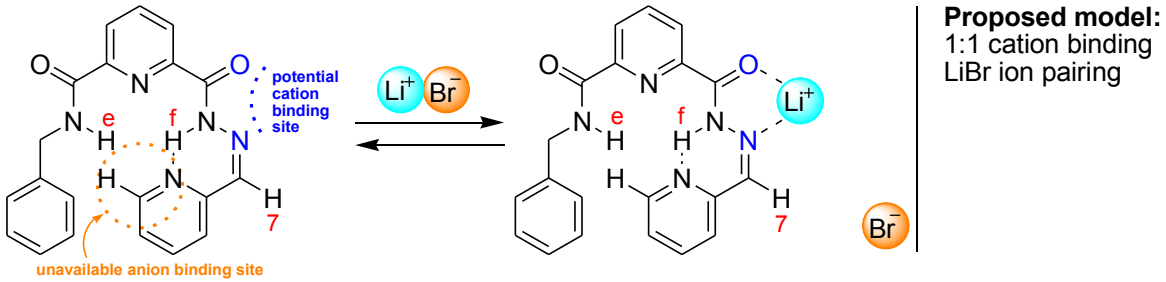

Scheme S 18. Possible Li^+ binding to *Z*-**1**. Chemical shifts of proton 7 was taken as an indication of potential cation binding.

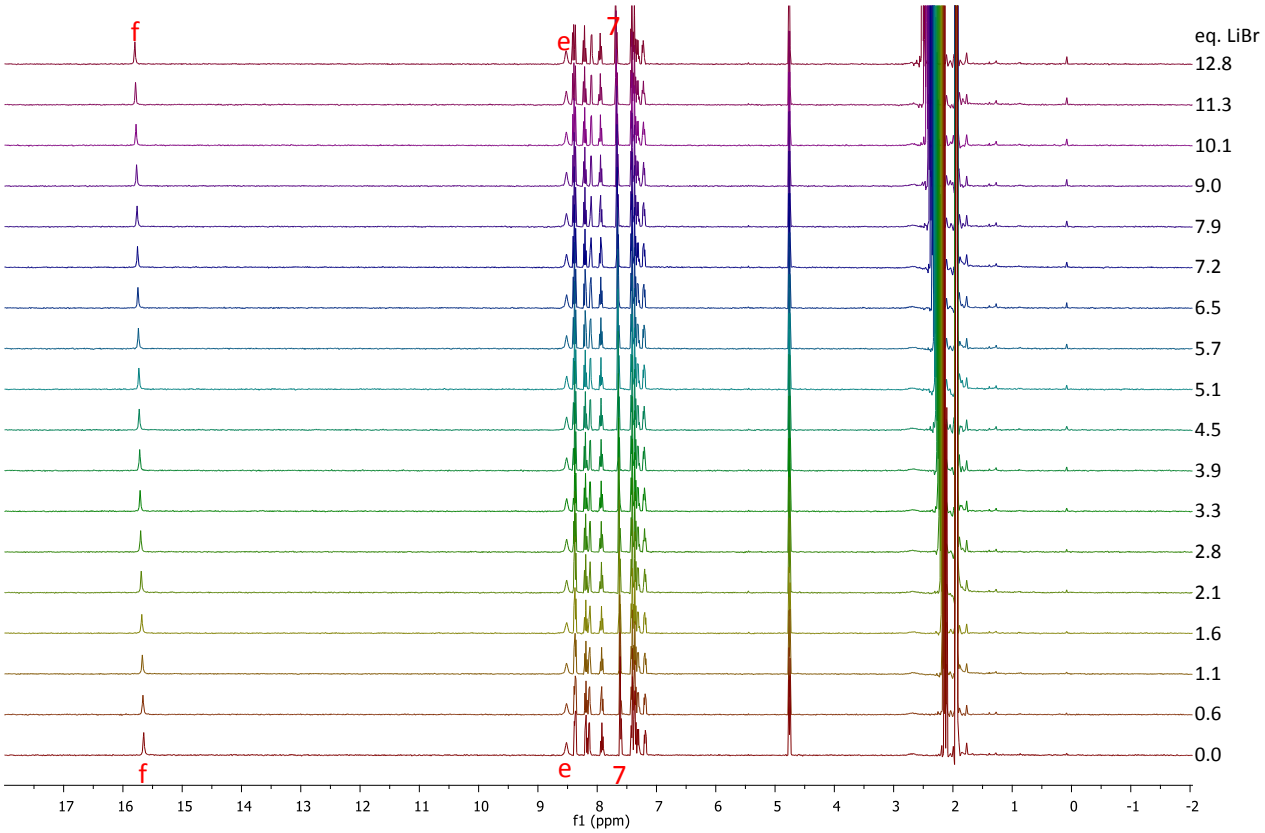

Figure S 94. ^{1}H NMR titration of *Z*-**1** (2 mM in acetonitrile-d_3) with LiBr.

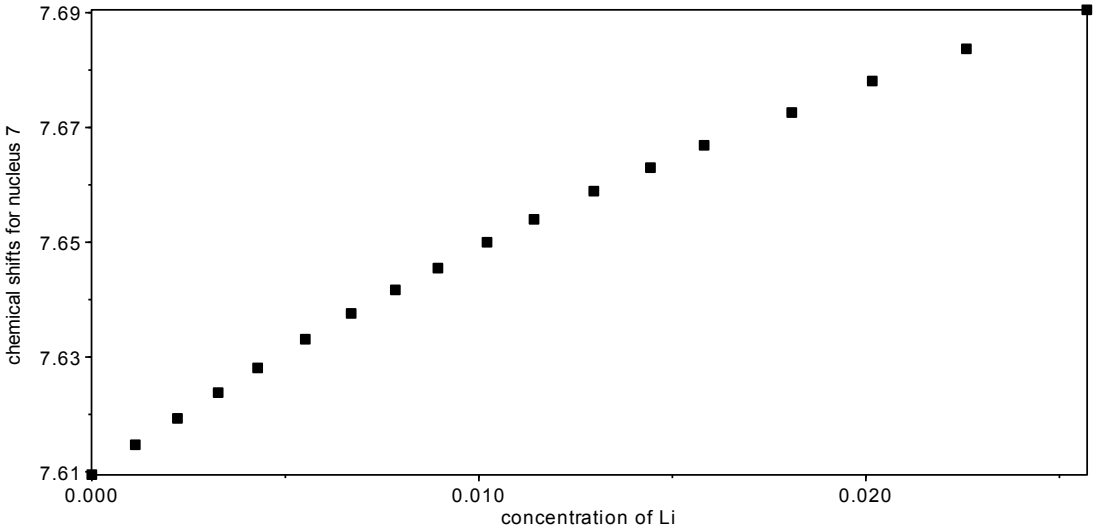

Figure S 95. Data points for ^{1}H NMR titration of *Z*-**1** (2 mM in acetonitrile-d_3) with LiBr.

4.5.11 Titration of *Z*-**1** with LiI in acetonitrile-d_3

Titration of *Z*-**1** with LiI resulted in small changes in chemical shifts. Amide NH protons do not shift, indicating inaccessibility of the anion binding site. Slight changes in the chemical shift of proton 7 could be due to weak cation binding in the bidentate binding site but could not be adequately fitted to the model (Scheme S 19) due to the very weak interactions of *Z*-**1** with the investigated salt.

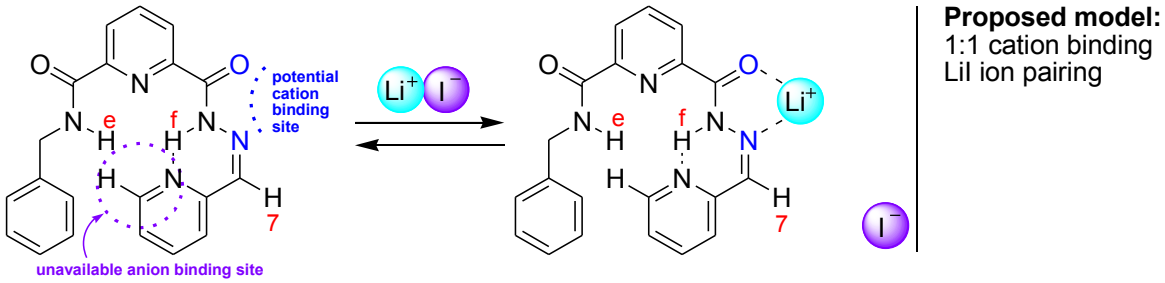

Scheme S 19. Proposed Li^+ binding to *Z*-**1**. Chemical shifts of proton 7 was taken as an indication of potential cation binding.

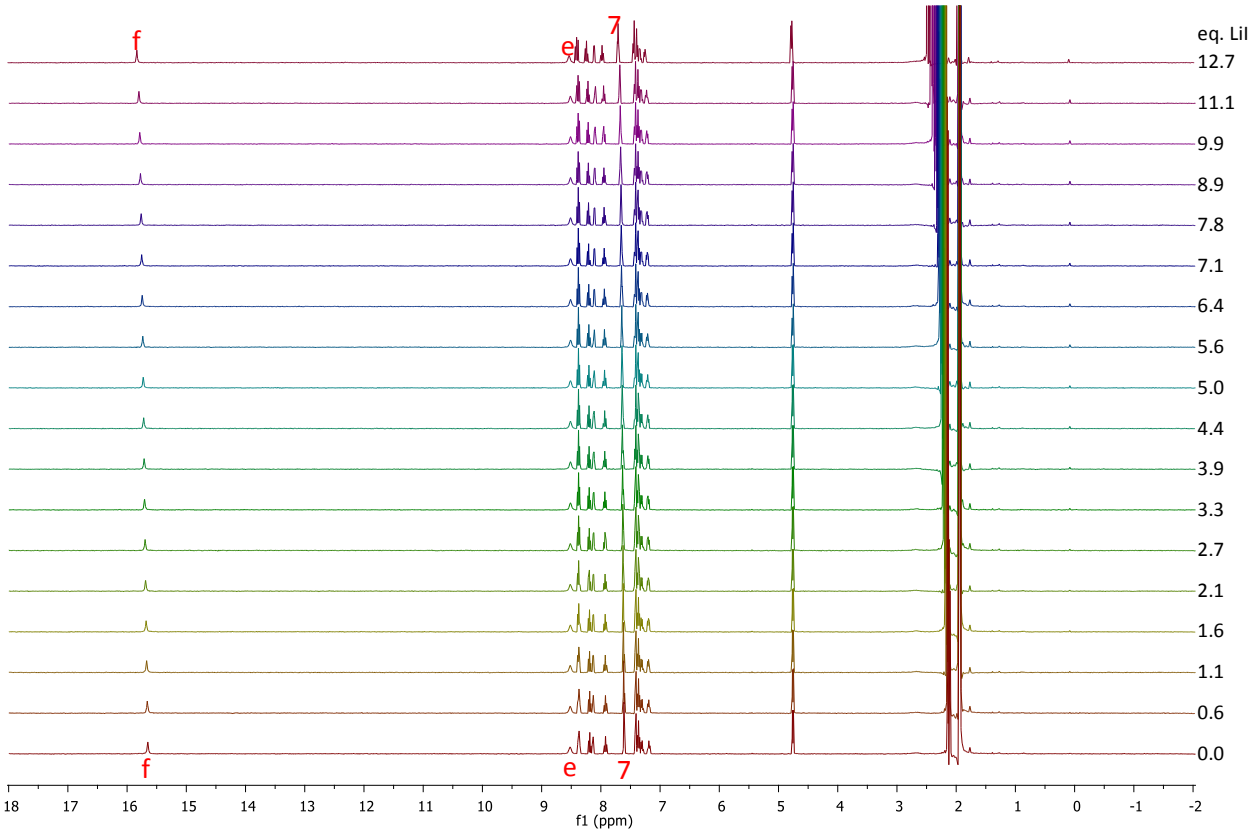

Figure S 96. ^{1}H NMR titration of *Z*-**1** (2 mM in acetonitrile-d_3) with LiI.

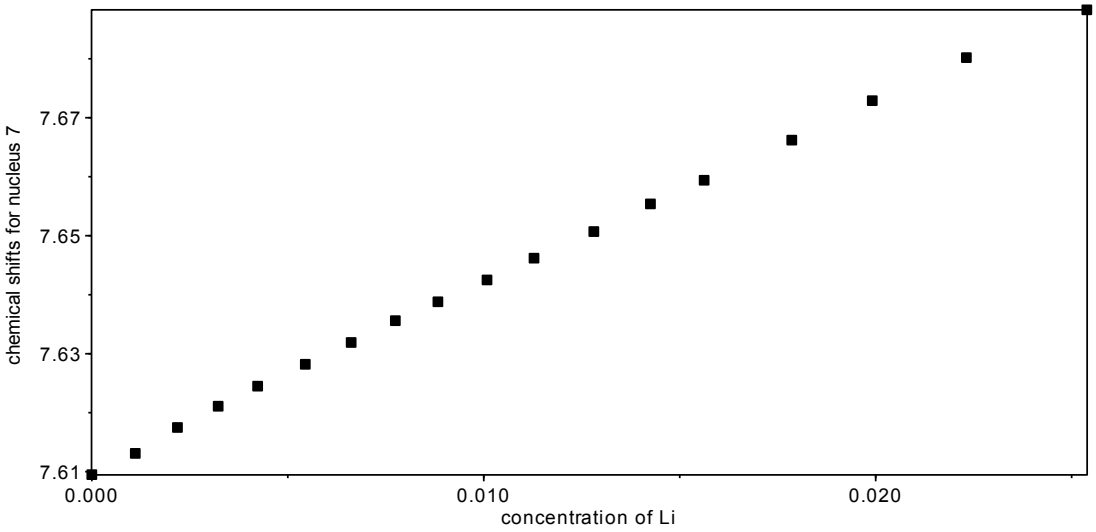

Figure S 97. Data points for ^{1}H NMR titration of *Z*-**1** (2 mM in acetonitrile-d_3) with LiI.

4.5.12 Titration of *Z*-**1** with NaI in acetonitrile-d_3

Titration of *Z*-**1** with NaI showed small changes in chemical shifts. Amide NH proton does not shift, indicating inaccessibility of the anion binding site. Changes in chemical shift of proton 7 were taken as indicative of cation binding but could not be adequately fitted to the model (Scheme S 20), supporting very weak interactions of *Z*-**1** and the investigated salt.

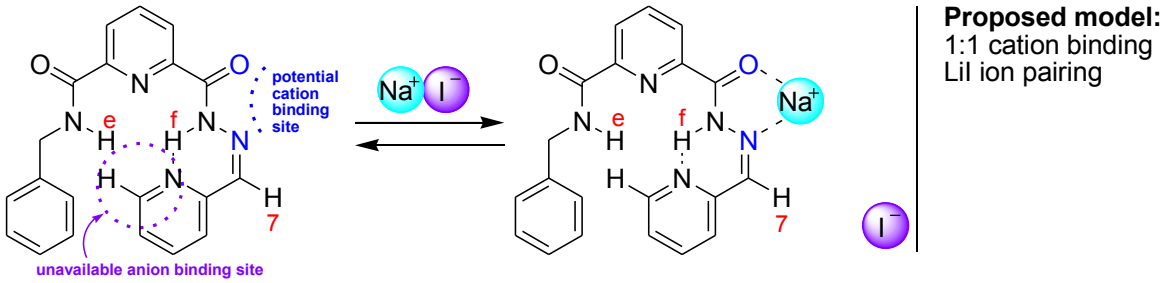

Scheme S 20. Possible Na^+ binding to *Z*-**1**. Chemical shifts of proton 7 was taken as an indication of potential cation binding.

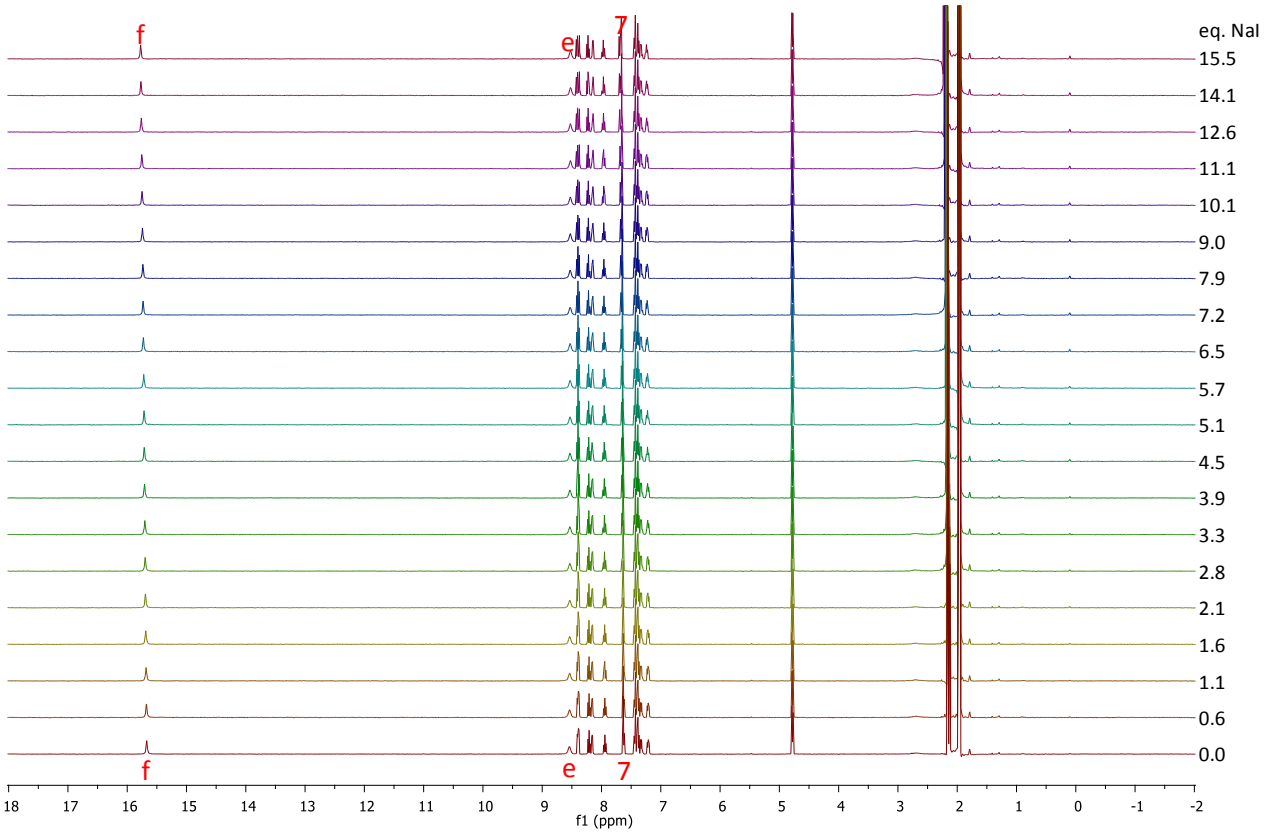

Figure S 98. ^{1}H NMR titration of *Z*-**1** (2 mM in acetonitrile-d_3) with NaI.

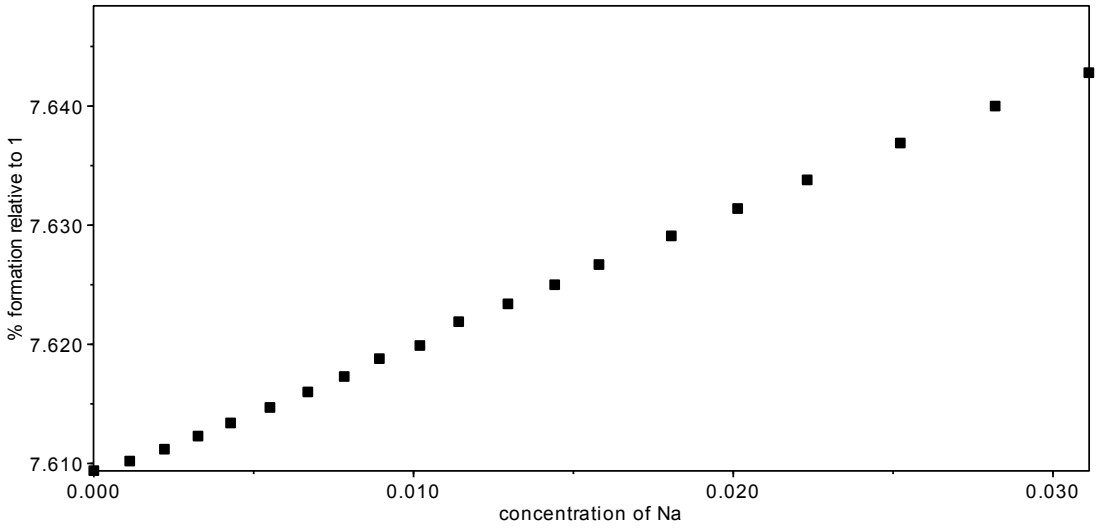

Figure S 99. Data points for ^{1}H NMR titration of *Z*-**1** (2 mM in acetonitrile-d_3) with NaI.

5 Photoisomerization Reactions

Photoswitching reactions were done in quartz NMR tubes using a self-constructed photo reactor equipped with 8 × 9 W UV-bulbs (Philips PL-S 9W/01/2P, λ_{max} ≈ 315 nm, *ca.* 20 nm band width, or Philips PL-S 9W/2P BLB, λ_{max} ≈ 365 nm, *ca.* 20 nm band width), a ventilator for air cooling and a digital thermometer for monitoring of internal temperature. The UV irradiance in the reactor was measured with the Delta Photo/radiometer HD 2102.2 equipped with the LP471 UVA probe, and was found to be ≈ 90 and ≈ 490 mW m^{-2} for 315 and 365 nm UV lamps, respectively. The lamps were switched on and left for 45 min to warm up prior to inserting the sample into the photoreactor. The samples were irradiated for 5 min while rotating (7.5 rpm) to insure homogenous irradiation, after which the ^{1}H NMR spectra were recorded.

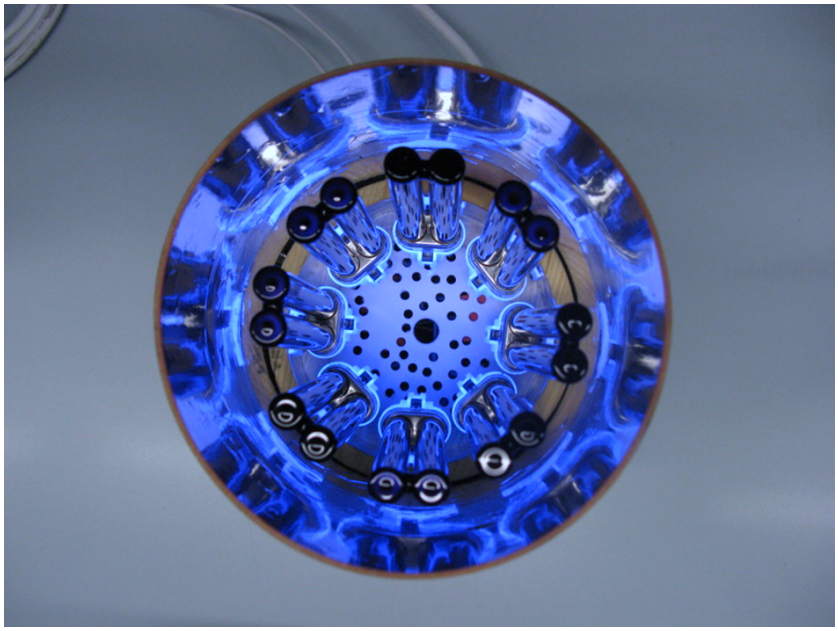

Figure S 100. A self-constructed photoreactor (top view).

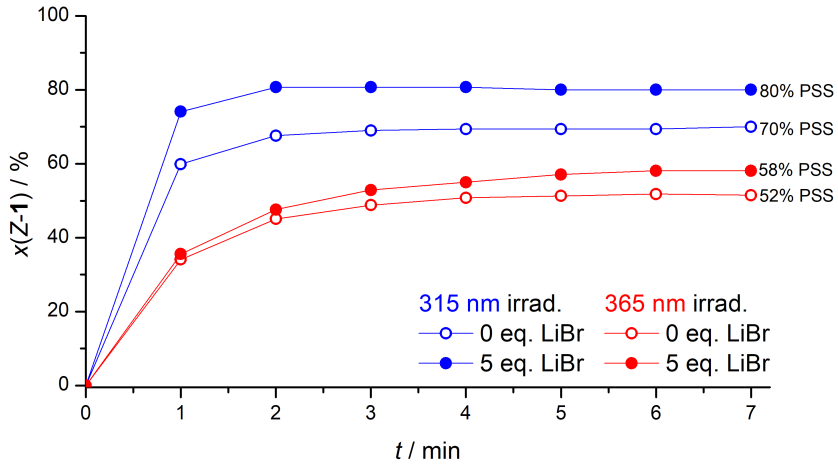

Figure S 101. Photoisomerization of *E*-**1** to *Z*-**1** in acetonitrile-d_3 (2 mM) using different wavelengths, with and without the presence of LiBr, showing the photostationary state (PSS) reached in few minutes under UV irradiation. The fraction of *Z*-**1** was calculated by ^{1}H NMR integration of the corresponding benzyl CH_2 protons.

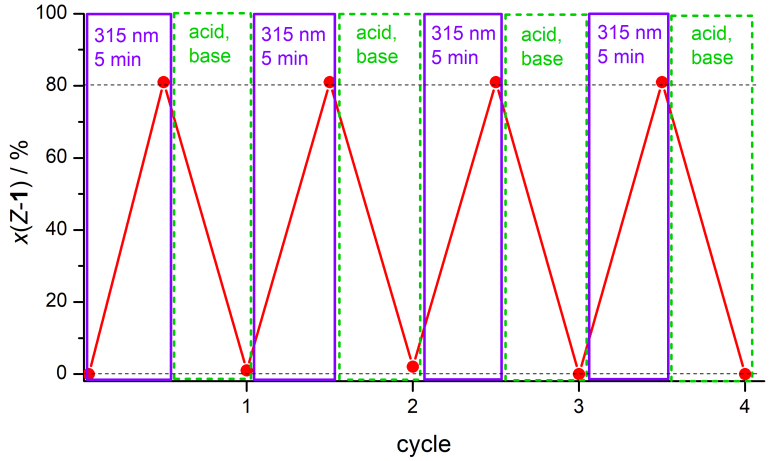

Figure S 102. Photo and acid switching cycles between *E*-**1** and *Z*-**1** isomers in acetonitrile-d_3 (2 mM, 0.800 µL) containing 5 equivalents of LiBr. Acid-switching reaction is completed within few minutes upon addition of acetonitrile solutions of triflic acid, 1 eq, and subsequent neutralization with acetonitrile solution of DIPEA, 1 equiv. (sample dilution was less than 2 %). The fraction of *Z*-**1** was calculated by ^{1}H NMR integration of the corresponding benzyl CH_2 protons.

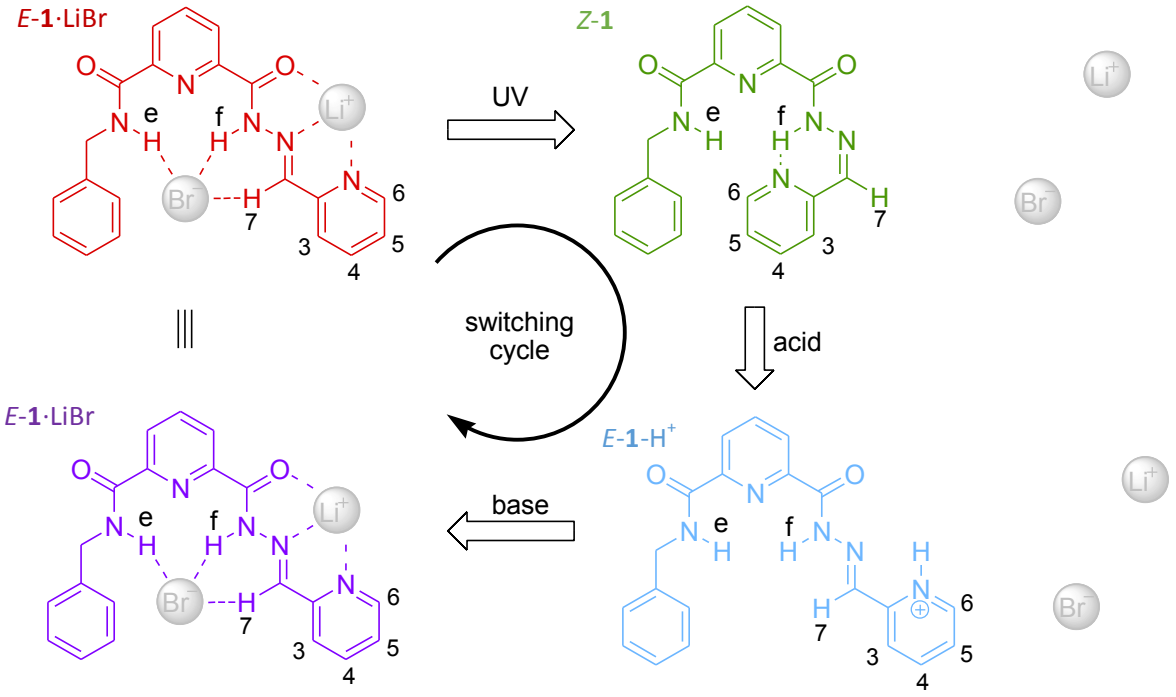

Scheme S 21. Proposed photo- and acid-induced switching cycle of the receptor **1** between the binding *E* and non-binding *Z* isomers, with respect to LiBr binding. Protonated *E*-**1**-H^+ may also exhibit anion binding due to the positive charge.

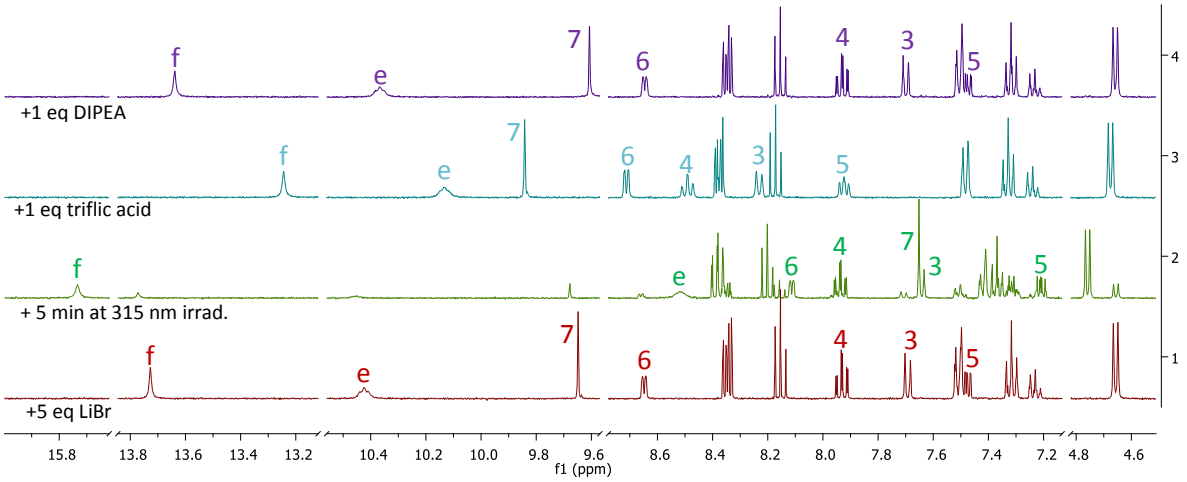

Figure S 103. ^{1}H NMR (acetonitrile-d_3) spectra of one photo/acid switching cycle (bottom to top) in the *E*/*Z* isomerization of *E*-**1** (2 mM) in the presence of LiBr (5 eq). One cycle involves 3 steps: 1) photo-isomerization of *E*-**1** to *Z*-**1** (315 nm, 5 min, 80% PSS); 2) acid-induced quantitative back-isomerization to protonated *E*-**1**; 3) neutralization of the protonated *E*-**1** with DIPEA restoring the non-protonated *E*-**1**.

6 UV Spectra

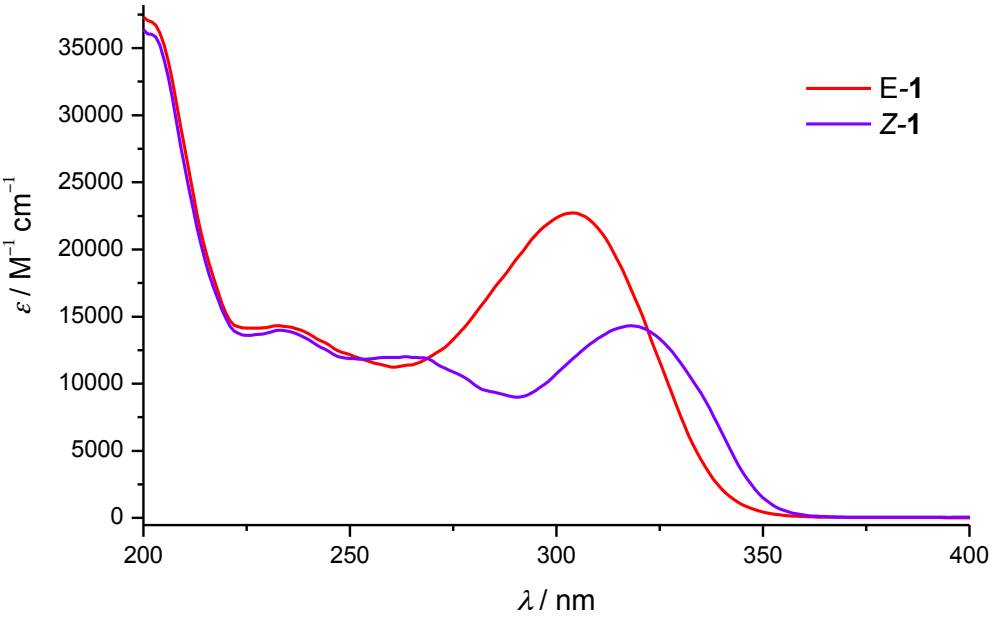

Figure S 104. UV spectra of *E*-**1** and *Z*-**1** isomers in acetonitrile.

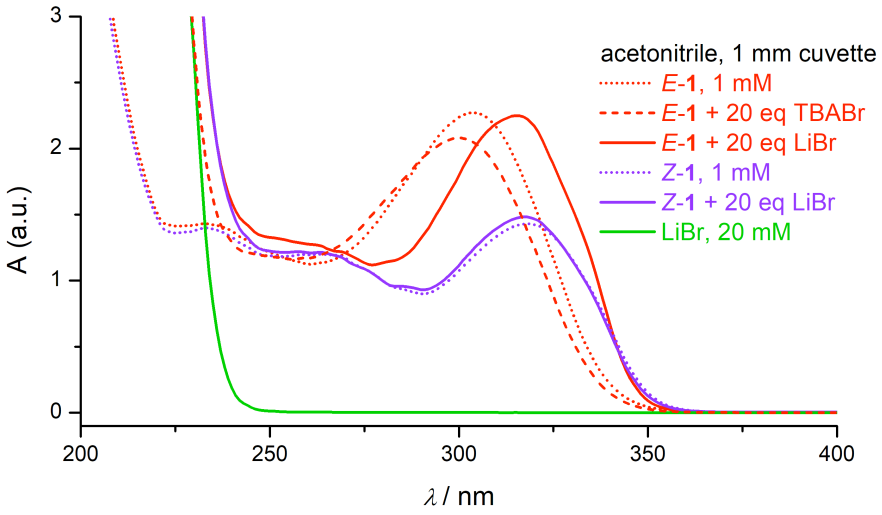

Figure S 105. UV spectra of *E*-**1** and *Z*-**1** in acetonitrile (1 mM). Bromide anion binding to *E*-**1** induces a small blue shift (4 nm) of the absorption maximum at ≈ 300 nm. The fully bound receptor with LiBr ion pair shows a red shift of 11 nm, indicative of ion pair binding (i.e. coordination of lithium to the acylhydrazone moiety). In contrast, *Z*-**1** with 20 equiv. of LiBr shows only small changes due to weak interactions. Other investigated salts (LiCl, NaBr, ammonium salts) were not soluble enough, or were too weakly bound (iodide salts) to record a meaningful UV spectrum in acetonitrile.

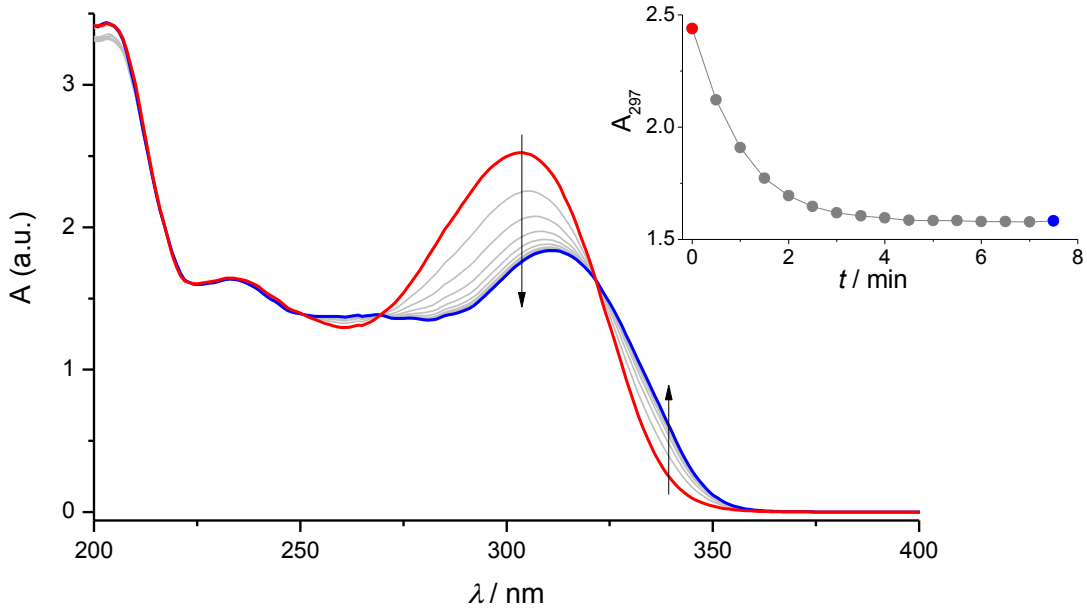

Figure S 106. UV spectra showing *E*-**1** to *Z*-**1** isomerization in acetonitrile (0.122 mM) during irradiation at 315 nm in a spectrofluorimeter (1 cm cuvette, 20 nm slit, 20 °C).

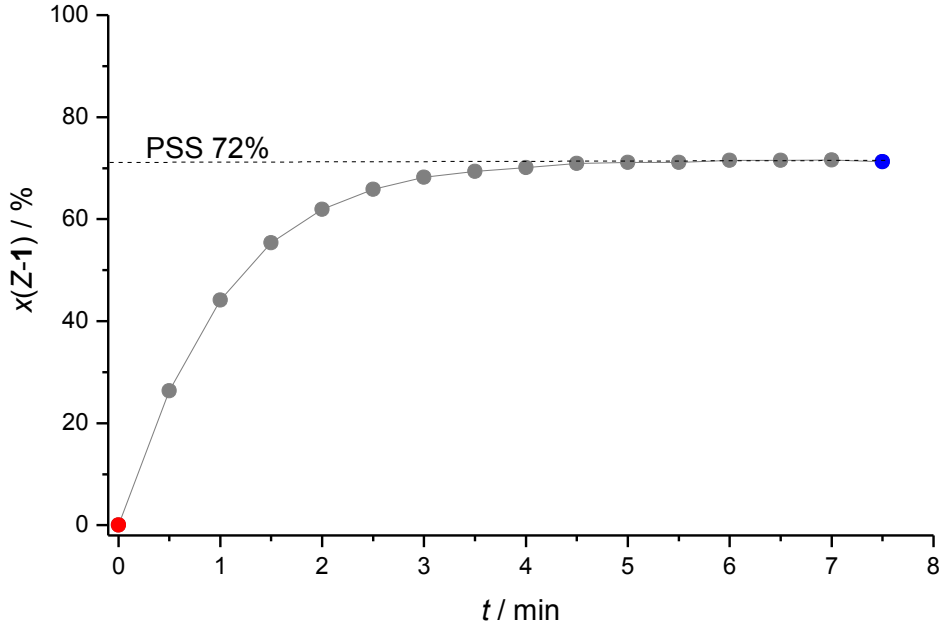

Figure S 107. Changes in the mole fraction of *Z*-**1** during photoisomerization of *E*-**1** to *Z*-**1** upon irradiation at 315 nm in a spectrofluorimeter (0.122 mM in acetonitrile-d_3, 1 cm cuvette, 20 nm slit, 20 °C).

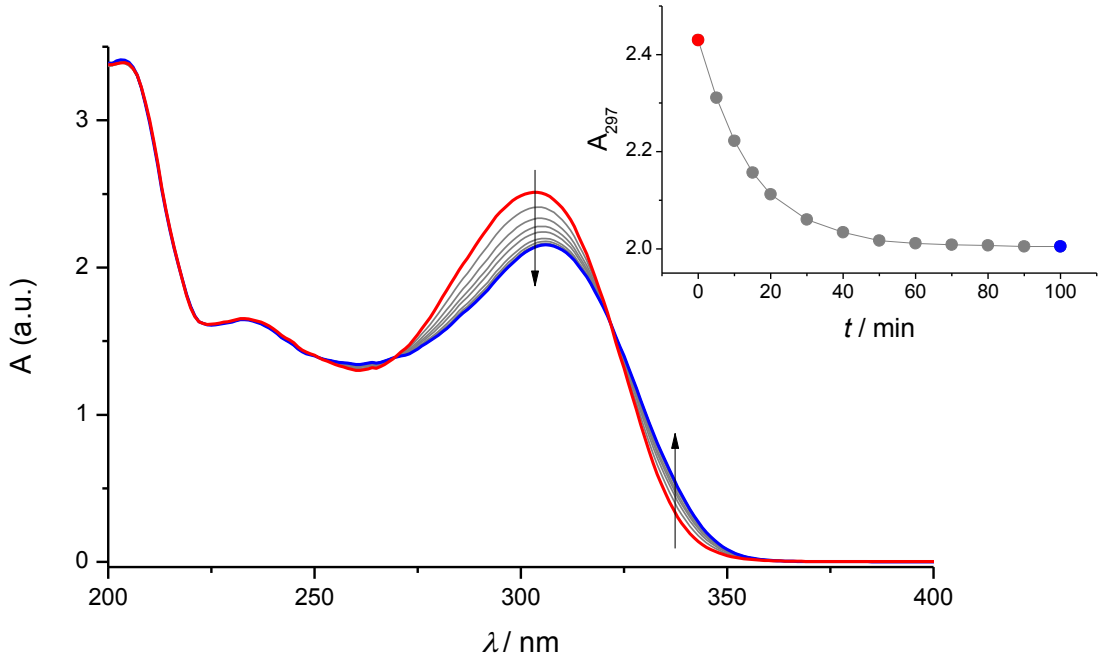

Figure S 108. UV spectra showing *E*-**1** to *Z*-**1** isomerization in acetonitrile (0.122 mM) during irradiation at 365 nm in a spectrofluorimeter (1 cm cuvette, 20 nm slit, 20 °C).

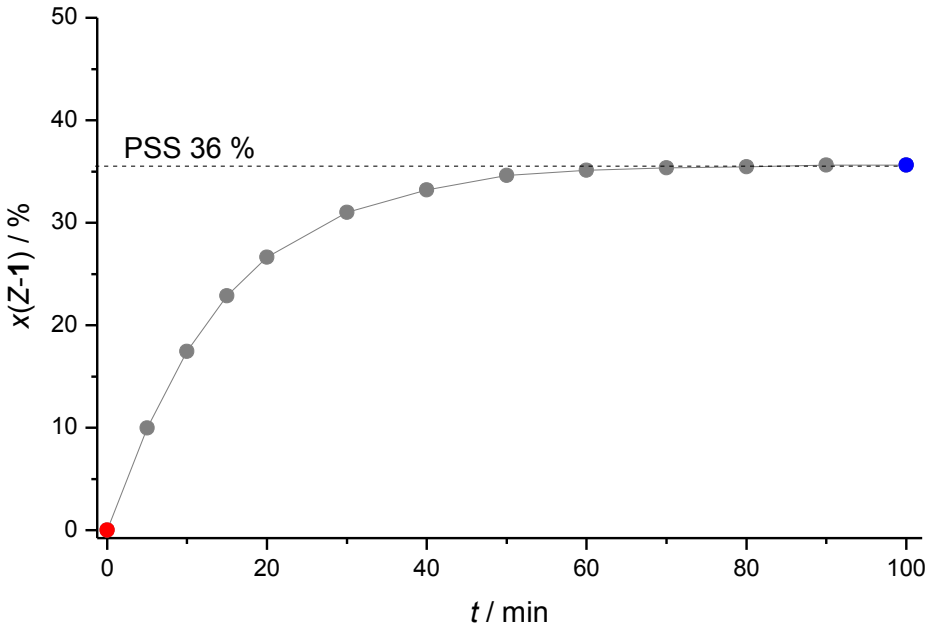

Figure S 109. Changes in the mole fraction of *Z*-**1** during photoisomerization of *E*-**1** to *Z*-**1** upon irradiation at 365 nm in a spectrofluorimeter (0.122 mM in acetonitrile-d_3, 1 cm cuvette, 20 nm slit, 20 °C).

6.1 Actinometry and Quantum Yield Determination

Ferrioxalate actinometry and quantum yield determinations were done according to the established procedures.[S10] All samples were irradiated in 1 cm quartz cuvettes under controlled conditions (315 nm, 2.5 nm bandwidth, 20 °C, "wavelength scan" mode), using spectrofluorimeter as the light source. The quantum yields thus obtained were: $\Phi_{E\rightarrow Z}$ = 0.26, and $\Phi_{Z\rightarrow E}$= 0.16, for *E* to *Z* and *Z* to *E* photoisomerisation reactions respectively.

For a given photoreaction

$$\mathrm{A} \xrightarrow{h\nu} \mathrm{B},$$

the quantum yield, Φ, is given by

$$\Phi = \frac{n_{\mathrm{B}}}{n_{h\nu}},$$

where n_{B} is the number of moles of the formed product B and $n_{h\nu}$ is the number of moles of photons absorbed by the solution during the irradiation period within which low conversions are obtained (< 5%). Under the same experimental conditions and when all incident light is absorbed (absorbance > 2), two different photoreactions will absorb the same amount of photons, $n_{h\nu}$. Therefore, it is possible to calculate the quantum yield of one reaction if the quantum yield of the other reaction is known:

$$\Phi_1 = \frac{n_{\mathrm{B1}}}{n_{h\nu}} \quad \text{and} \quad \Phi_2 = \frac{n_{\mathrm{B2}}}{n_{h\nu}} \quad \text{give} \quad \Phi_1 = \frac{n_{\mathrm{B1}}}{n_{\mathrm{B2}}}\Phi_2,$$

or, in terms of the rates of formation:

$$\Phi_1 = \frac{n_{\mathrm{B1}}}{n_{\mathrm{B2}}}\Phi_2 = \frac{\frac{\Delta n_{\mathrm{B1}} t}{\Delta t}}{\frac{\Delta n_{\mathrm{B2}} t}{\Delta t}}\Phi_2 = \frac{\frac{\Delta c_{\mathrm{B1}} V_1 t}{\Delta t}}{\frac{\Delta c_{\mathrm{B2}} V_2 t}{\Delta t}}\Phi_2,$$

where $\frac{\Delta c_{\mathrm{B}}}{\Delta t}$ represent the rate of product formation, which can be determined experimentally as a slope of the least squares regression line fitted to the *concentration* vs. *time* plot for the formation of the product. Given the same irradiation time and irradiated volumes, the equation simplifies to

$$\Phi_1 = \frac{\frac{\Delta c_{\mathrm{B1}}}{\Delta t}}{\frac{\Delta c_{\mathrm{B2}}}{\Delta t}}\Phi_2,$$

In the case presented herein, we used a well-known ferrioxalate photoreduction reaction as a reference standard, in which the concentration of the Fe^{2+} product can be easily followed spectrophotometrically and the quantum yield is known to be 1.24. Thus:

$$\Phi_{E\rightarrow Z} = \frac{\text{rate of } Z\mathbf{1} \text{ formation}}{\text{rate of } \mathrm{Fe^{2+}} \text{ formation}} \cdot \Phi_{\mathrm{Fe^{3+}\rightarrow Fe^{2+}}} = \frac{1.81\cdot 10^{-8}}{8.49\cdot 10^{-8}} \cdot 1.24 = 0.26,$$

and

$$\Phi_{Z\rightarrow E} = \frac{\text{rate of } E\mathbf{1} \text{ formation}}{\text{rate of } \mathrm{Fe^{2+}} \text{ formation}} \cdot \Phi_{\mathrm{Fe^{3+}\rightarrow Fe^{2+}}} = \frac{1.11\cdot 10^{-8}}{8.49\cdot 10^{-8}} \cdot 1.24 = 0.16.$$

For detailed procedures, see below.

6.1.1 Actinometry

All manipulations with light-sensitive solutions were done in the dark and aluminum foil was used to protect the samples from light. To avoid any contact of the acidic solutions with metal needles the solutions were transferred using Pasteur pipettes and weighed.

Freshly made solution of triply-recrystallized potassium ferrioxalate trihydrate (0.006 M) in H_2SO_4 (0.05 M, prepared from Milli-Q water) was weighted into seven 1 cm quartz cuvettes (3 mL into each). Six samples were irradiated in a spectrofluorimeter (315 nm, 2.5 nm bandwidth, 20 °C, "wavelength scan" mode) for a specific period of time: 250, 500, 750, 1000, 1250, and 1500 s with stirring. One sample was not irradiated ("blank"). Immediately after irradiation, 0.5 mL of the 0.1 % phenanthroline buffer solution (1.65 M CH_3COONa in 0.5 M H_2SO_4) was added and, after exactly 1 h, UV-vis spectrum was recorded with respect to pure water in the reference beam. From the measured absorbances at 510 nm the concentrations of the Fe^{2+}-phenanthroline complex were calculated (ε_{510} = 11100 M^{-1} cm^{-1}). The Fe^{2+} concentrations thus obtained were corrected for dilution with phenanthroline buffer (that is multiplied by the factor 3.5 mL/3 mL) to yield the Fe^{2+} concentrations in the irradiated samples, which were then plotted versus time and fitted to the linear equation. The obtained slope represents the rate of formation of ferrous ions from which the quantum yields of *E*-**1** and *Z*-**1** photoisomerisation reactions (performed under the same conditions) were calculated using the known quantum yield of the ferrioxalate actinometer:[S10a] Φ = 1.24.

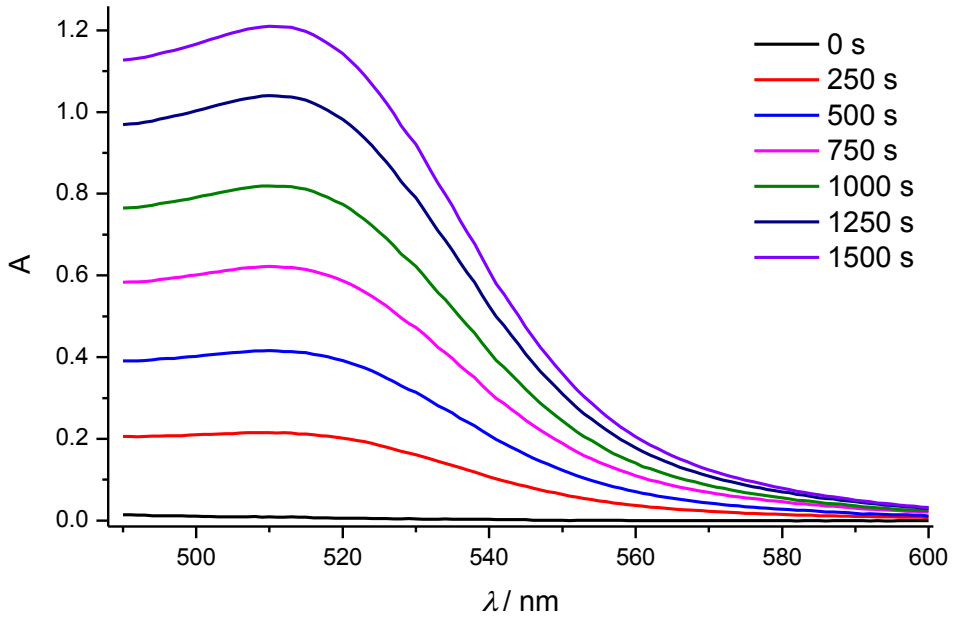

Figure S 110. UV-Vis spectra acquired during the ferrioxalate actinometry measurements. The absorbance at 510 nm is proportional to the concentration of the formed phenanthroline complex with ferrous ions.

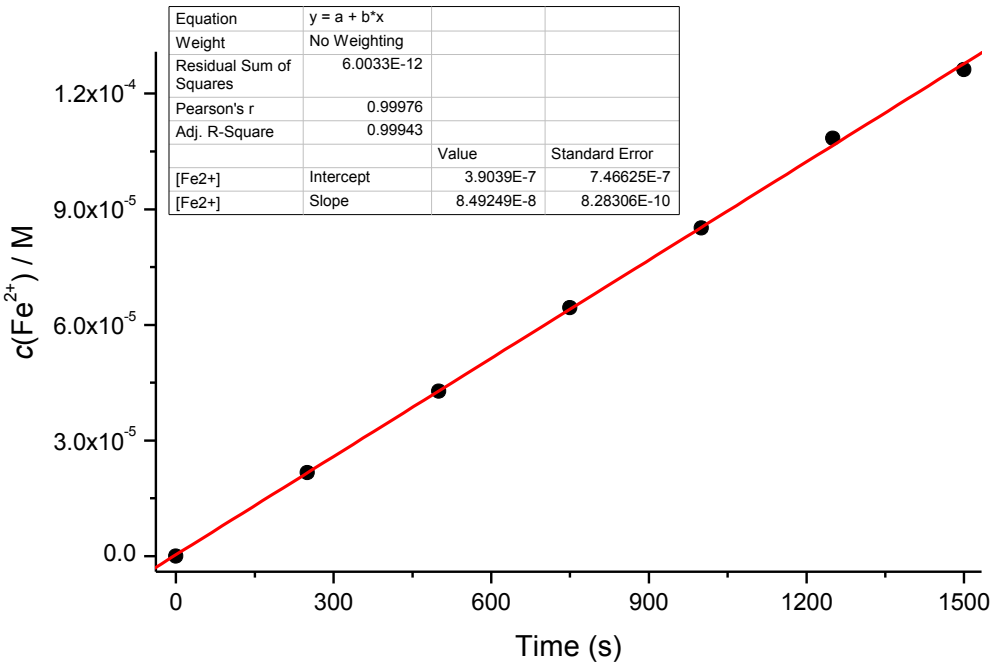

Figure S 111. Concentration vs. time plot for the formation of ferrous ions during the irradiation at 315 nm.

6.1.2 *E*-**1** to *Z*-**1** Photoisomerization

Solution of *E*-**1** (0.122 mM, 3 mL) in acetonitrile-d_3 was irradiated at 315 nm with constant stirring in a 1 cm quartz cuvette (2.5 nm bandwidth, 20 °C, "wavelength scan" mode) and after each irradiation period the concentration of *Z*-**1** was calculated from the UV spectra. The concentrations thus obtained were plotted versus time and fitted to the linear equation. The obtained slope represents the rate of formation of *Z*-**1** and was used in the calculation of the quantum yield.

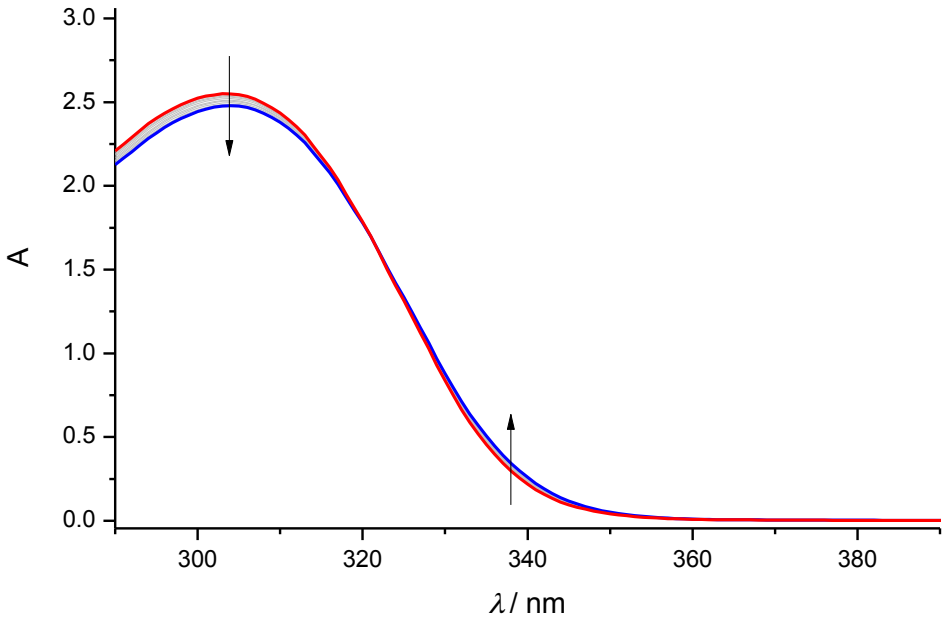

Figure S 112. UV-Vis spectra acquired during the irradiation of *E*-**1** (0.122 mM, 3 mL, 1 cm cuvette) at 315 nm for 500 s.

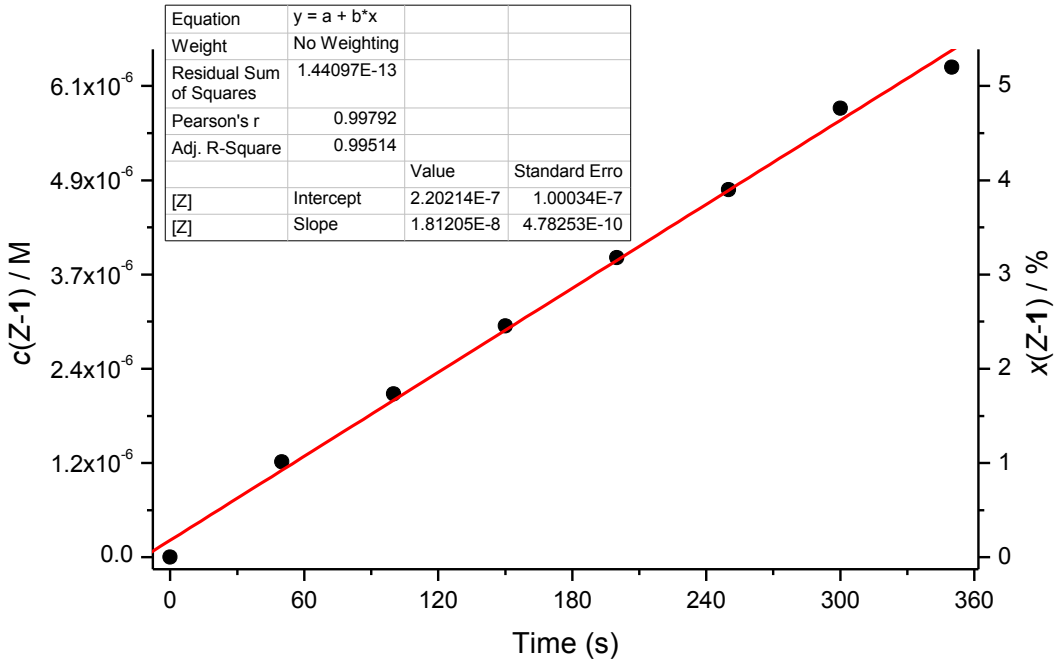

Figure S 113. Concentration vs. time plot for the formation of *Z*-**1** during the irradiation at 315 nm.

6.1.3 *Z*-**1** to *E*-**1** Photoisomerization

Solution of *Z*-**1** (0.15 mM, 3 mL) in acetonitrile-d_3 was irradiated at 315 nm with constant stirring in a 1 cm quartz cuvette (2.5 nm bandwidth, 20 °C, "wavelength scan" mode) and after each irradiation period the concentration of *E*-**1** was calculated from the UV spectra. The concentrations thus obtained were plotted versus time and fitted to the linear equation. The obtained slope represents the rate of formation of *E*-**1** and was used in the calculation of the quantum yield.

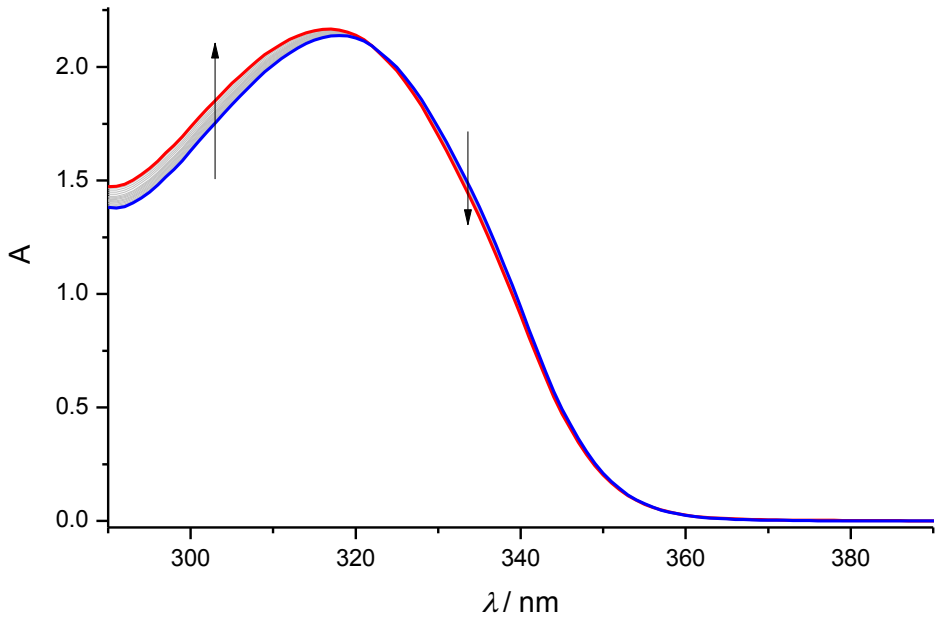

Figure S 114. UV-Vis spectra acquired during the irradiation of *Z*-**1** (0.15 mM, 3 mL, 1 cm cuvette) at 315 nm for 1000 s.

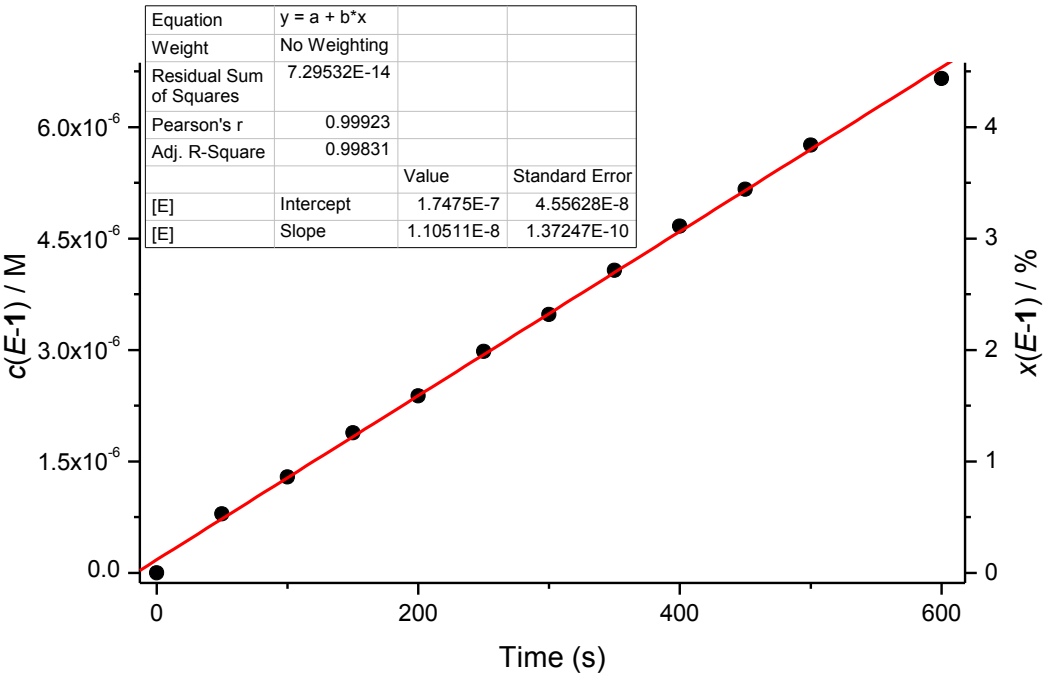

Figure S 115. Concentration vs. time plot for the formation of *E*-**1** during the irradiation of *Z*-**1** at 315 nm.

7 X-ray Measurements

7.1 General Procedure for Crystallizations

For crystallizations of pure receptor isomers, methanolic solution thereof was left to slowly evaporate. For complexes with salts, solution of *E*-**1** with excess of salt was added to nine separate 0.5 mL Eppendorf vials in 10 to 50 µL aliquots (every 5 µL) and diluted to 55 µL with pure solvent. The vials were capped and left standing. After few days, colorless needle-like crystalline material precipitated from the vials. Suitable crystals were chosen for the X-ray measurement. Typically, only one or two vials in a narrow concentration range contained crystals suitable for X-ray measurements, others containing too small or excessively twinned crystals.

7.2 X-ray Structures

Table S 2. Crystallographic parameters for *E*-**1**, *Z*-**1**, and *E*-**1** complexes with different salts.

Compound	*E*-**1**	*Z*-**1**	*E*-**1**·$LiClO_4$	*E*-**1**·NaI	*E*-**1**·KI	*E*-**1**·NH_4Br	*E*-**1**·NH_4I
CCDC number	1861118	1870353	1861119	1861120	1861121	1861122	1861123
Empirical formula	$C_{20}H_{17}N_5O_2$	$C_{20}H_{17}N_5O_2$	$C_{20}H_{17}ClLiN_5O_6$	$C_{20}H_{17}IN_5NaO_2$	$C_{20}H_{17}IKN_5O_2$	$C_{20}H_{21}BrN_6O_2$	$C_{20}H_{21}IN_6O_2$
Formula weight	359.39	359.39	465.78	509.27	525.39	457.34	504.33
Temperature/K	100(2)	100.00(10)	103(5)	100(2)	100(2)	100(2)	100(2)
Crystal system	monoclinic	orthorhombic	monoclinic	monoclinic	monoclinic	monoclinic	triclinic
Space group	$P2_1/n$	$Pna2_1$	$P2_1/n$	$P2_1/n$	$P2_1/c$	$P2_1/n$	P-1
a / Å	7.44527(12)	16.4964(2)	7.4234(5)	6.8614(2)	10.4474(4)	21.1019(7)	10.1486(4)
b / Å	9.34308(12)	20.5023(3)	18.5015(10)	19.3391(6)	14.5733(4)	7.5385(2)	10.7029(5)
c / Å	30.9935(5)	5.05085(7)	14.8435(8)	15.0522(4)	13.6575(4)	27.2240(8)	11.0170(5)
α / °	90	90	90	90	90	90	78.363(4)
β / °	94.8031(15)	90	91.626(5)	98.006(3)	91.382(3)	111.514(4)	81.711(4)
γ / °	90	90	90	90	90	90	62.200(4)
Volume / $Å^3$	2148.39(5)	1708.27(4)	2037.8(2)	1977.86(11)	2078.79(11)	4029.0(2)	1035.05(9)
Z	4	4	4	4	4	8	2
ρ_{calc} / g cm^{-3}	1.111	1.397	1.518	1.71	1.679	1.508	1.618
μ / mm^{-1}	0.611	0.769	2.109	13.17	14.12	3.03	12.397
F(000)	752	752	960	1008	1040	1872	504
Crystal size / mm^3	0.23 × 0.19 × 0.14	0.724 × 0.049 × 0.025	0.145 × 0.043 × 0.037	0.13 × 0.04 × 0.02	0.13 × 0.07 × 0.05	0.15 × 0.08 × 0.08	0.19 × 0.13 × 0.08
Radiation	CuKα (λ = 1.54184)	CuKα (λ = 1.54184)	CuKα (λ = 1.54184)	CuKα (λ = 1.54184)	CuKα (λ = 1.54184)	CuKα (λ = 1.54184)	CuKα (λ = 1.54184)
2*Θ* range for data collection / °	5.724 to 134.156	6.878 to 134.138	7.638 to 134.152	7.488 to 148.992	8.466 to 148.982	4.574 to 134.16	8.208 to 134.15
Index ranges	-8 ≤ h ≤ 8, -11 ≤ k ≤ 11, -37 ≤ l ≤ 37	-19 ≤ h ≤ 19, -24 ≤ k ≤ 24, -6 ≤ l ≤ 6	-4 ≤ h ≤ 8, -21 ≤ k ≤ 22, -17 ≤ l ≤ 15	-8 ≤ h ≤ 8, -23 ≤ k ≤ 24, -18 ≤ l ≤ 18	-13 ≤ h ≤ 12, -18 ≤ k ≤ 18, -15 ≤ l ≤ 17	-25 ≤ h ≤ 25, -4 ≤ k ≤ 9, -32 ≤ l ≤ 32	-12 ≤ h ≤ 12, -12 ≤ k ≤ 12, -13 ≤ l ≤ 13
Reflections collected	27597	21290	7065	17188	17752	13885	13116
Independent reflections	3824 [R_{int} = 0.0304, R_{sigma} = 0.0155]	3033 [R_{int} = 0.0522, R_{sigma} = 0.0285]	3620 [R_{int} = 0.0527, R_{sigma} = 0.0952]	4053 [R_{int} = 0.0509, R_{sigma} = 0.0440]	4248 [R_{int} = 0.0494, R_{sigma} = 0.0387]	7170 [R_{int} = 0.0302, R_{sigma} = 0.0442]	3689 [R_{int} = 0.0376, R_{sigma} = 0.0304]
Data/restraints/ parameters	3824/2/250	3033/1/250	3620/2/304	4053/2/268	4248/1/268	7170/24/559	3689/3/280
Goodness-of-fit on F^2	1.165	1.056	1.011	1.003	1.11	1.028	1.052
Final *R* indexes [*I*>=2*σ* (*I*)]	R_1 = 0.0513, wR_2 = 0.1242	R_1 = 0.0287, wR_2 = 0.0717	R_1 = 0.0546, wR_2 = 0.1121	R_1 = 0.0301, wR_2 = 0.0715	R_1 = 0.0565, wR_2 = 0.1483	R_1 = 0.0360, wR_2 = 0.0867	R_1 = 0.0228, wR_2 = 0.0578
Final *R* indexes [all data]	R_1 = 0.0527, wR_2 = 0.1249	R_1 = 0.0312, wR_2 = 0.0733	R_1 = 0.1009, wR_2 = 0.1364	R_1 = 0.0394, wR_2 = 0.0757	R_1 = 0.0618, wR_2 = 0.1514	R_1 = 0.0467, wR_2 = 0.0936	R_1 = 0.0238, wR_2 = 0.0589
Largest diff. peak/hole / e $Å^{-3}$	0.33/-0.21	0.14/-0.15	0.33/-0.37	0.70/-1.47	3.53/-1.27	0.85/-0.45	0.55/-0.45

All the crystal structures of *E*-**1** complexes with simple salts exhibit intermolecular aromatic stacking of the acylhydrazone moieties, forming π-stacked dimers as depicted in Figure S 116. The π-stacked dimeric structures extend to complex networks through diverse hydrogen bonding patterns and ion interactions (Figure S 117). According to the Bernstein-Davis notation,[S11] all anions are bound to *E*-**1** by the $R_2^1(10)$ hydrogen-bond motif, lying in the plane of the central pyridine pincer, with the exception of NH_4I complex where iodide ion is found outside the plane by 2.238 Å. All the cations are bound through intramolecular *O,N,N*-interactions with the acylhydrazone moiety, either in a coordinative fashion (alkali cations) or by hydrogen bonding (ammonium cations). Cations form additional intermolecular interactions with anions and amide carbonyl of the *E*-**1**, with the exception of *E*-**1** complex with NH_4Br where amide carbonyls are not involved. Pairs of ion pairs are found in the structures of *E*-**1** complexes with NaI and NH_4Br, forming discrete rhombohedral moieties (see below), and additional anion-cation zig-zag pattern is found in the case of NH_4Br. The remaining complexes, namely, with KI, NH_4I, and $LiClO_4$, exhibit discrete ion pairs in the crystal structure.

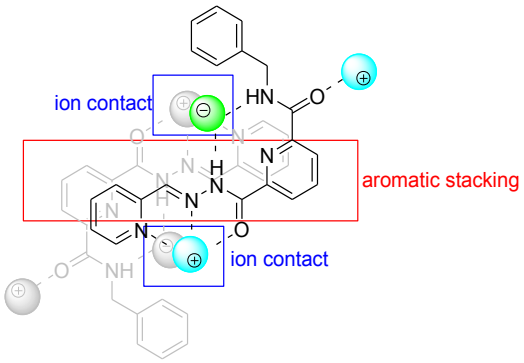

Figure S 116. General motif exhibited in the crystal structures of *E*-**1** with simple salts, through which 1D, 2D, and 3D networks are formed in the solid state. Dashed lines indicate coordinative or hydrogen bonding to *E*-**1**, depending on the nature of ion (e.g. alkali metal or ammonium cation). In the case of ammonium salts, the ion contact also represents hydrogen bonding between the ions.

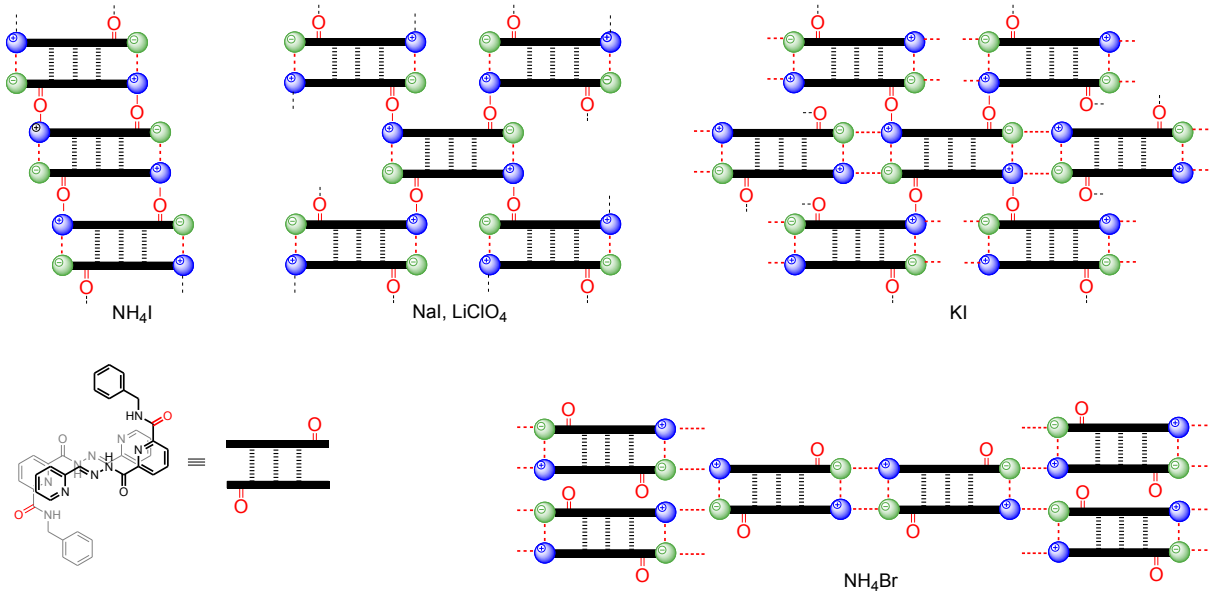

Figure S 117. Schematic representations of various packing patterns in the crystal structures of *E*-**1** complexes with different salts, formed through hydrogen bonding and ion interactions.

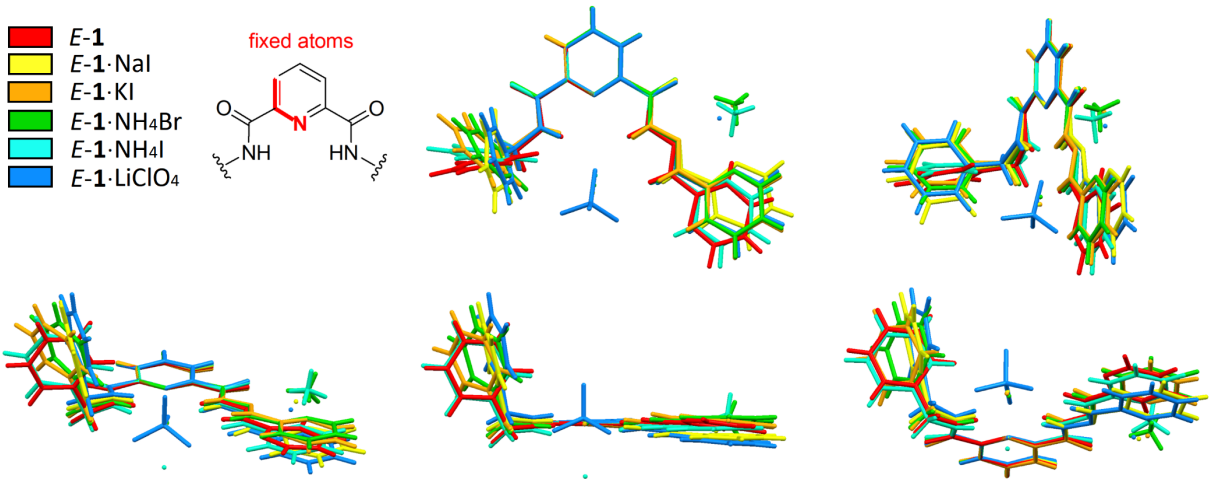

Figure S 118. Different perspectives of overlapped molecular structures from the solid state structures of *E*-**1** and its complexes with various salts.

Table S 3. Comparison of selected parameters from the crystal structures of *E*-**1** and its complexes with simple salts.

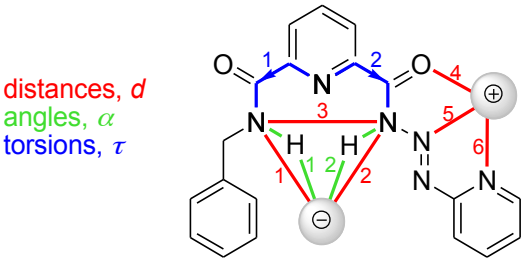

parameter	*E*-**1**	*E*-**1**·$LiClO_4$	*E*-**1**·NaI	*E*-**1**·KI	*E*-**1**·NH_4I	*E*-**1**·NH_4Br	
d_1 / Å	–	2.986	3.580	3.579	3.612	3.347	3.392
α_1 / °	–	156	144	133	145	147	150
d_2 / Å	–	2.997	3.793	3.816	3.796	3.473	3.496
α_2 / °	–	158	160	157	146	154	156
d_3 / Å	4.535	4.659	4.719	4.758	4.591	4.705	4.720
τ_1 / °	–0.5	10.4	7.5	6.9	–10.6	–3.5	–4.1
τ_2 / °	–3.0	6.9	7.9	–6.0	2.7	–3.8	–0.8
d_4 / Å	–	2.508	2.419	2.700	2.908	2.813	2.791
d_5 / Å	–	2.104	2.473	2.795	2.986	2.930	2.945
d_6 / Å	–	2.264	2.514	2.860	2.923	2.892	2.892
d(N–N) / Å	1.380	1.375	1.372	1.376	1.371	1.377	1.378
d(N=N) / Å	1.276	1.284	1.270	1.286	1.280	1.273	1.276

Crystallization of *E*-**1**

E-**1** (≈ 10 mg) was shortly heated with 1 mL of methanol, and the undissolved material was filtered off through cotton. Suitable crystals for X-ray analysis were obtained upon slow evaporation of the solvent.

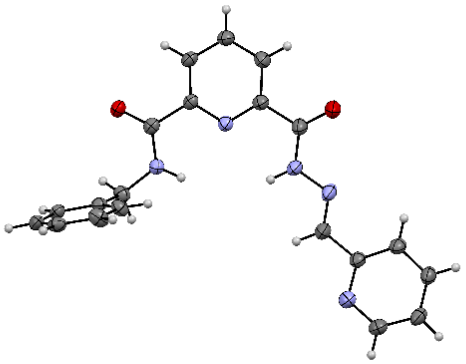

Figure S 119. Molecular structure of *E*-**1.** Ellipsoids are shown at 50 % probability level.

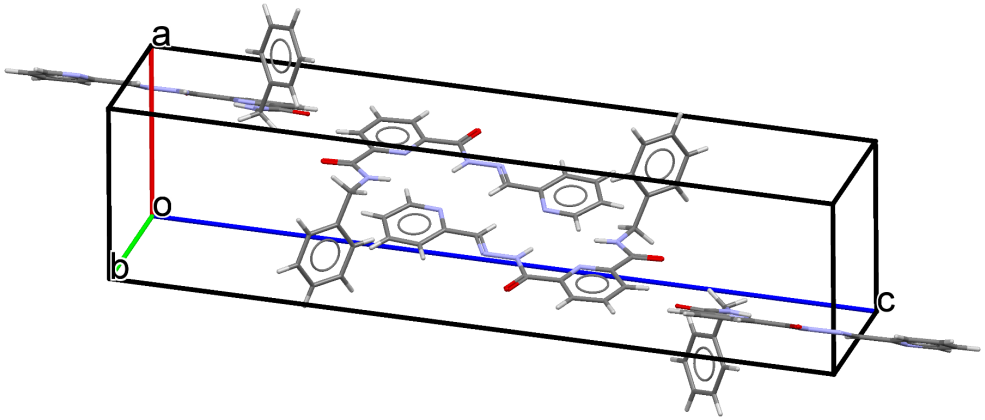

Figure S 120. Crystal packing of *E*-**1**. Due to the high disorder of solvent molecules, the MASK procedure in the Olex2 program was used.

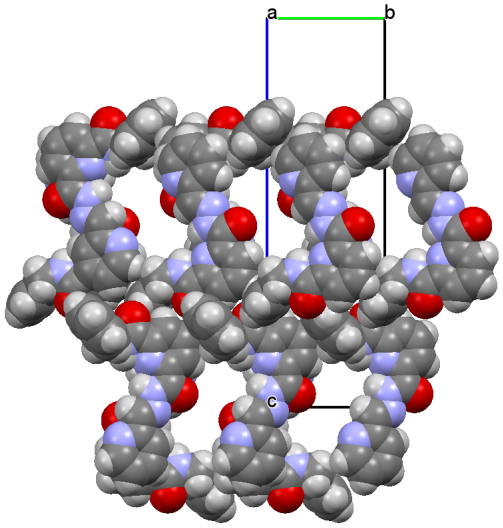

Figure S 121. Channels formed in the crystal of *E*-**1**, occupied by disordered solvent molecules.

Crystallization of *Z*-**1**

Z-**1** (≈ 10 mg) was shortly heated with 1 mL of methanol, and the undissolved material was filtered off through cotton. Crystals suitable for X-ray analysis were obtained upon slow evaporation of the solvent.

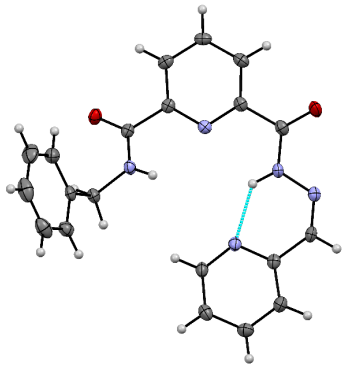

Figure S 122. Molecular structure of *Z*-**1.** Ellipsoids are shown at 50 % probability level.

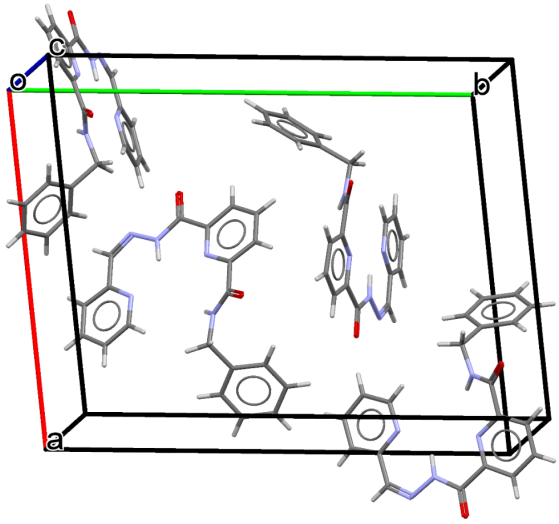

Figure S 123. Crystal packing of *Z*-**1**.

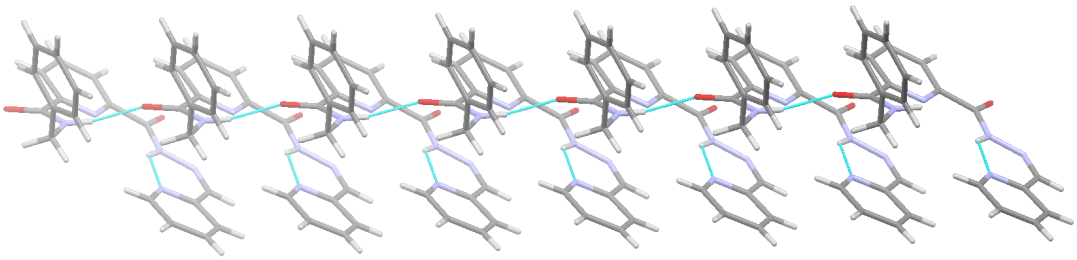

Figure S 124. Hydrogen bonding $C_1^1(4)$ pattern in the crystal structure of *Z*-**1**.

Crystallization of *E*-**1** with NaI

Sodium iodide (15 mg, 0.1 mmol) was dissolved in 0.5 mL of acetonitrile *E*-**1** solution (12 mM, 6 µmol), followed by the general procedure for crystallization.

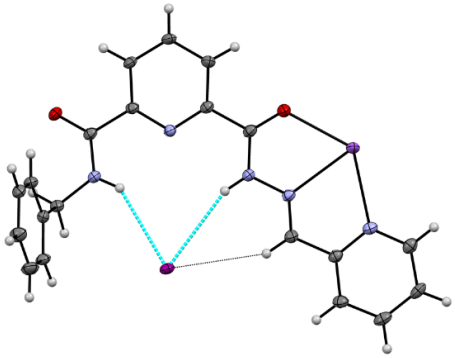

Figure S 125. Molecular structure of *E*-**1**·NaI complex in the solid state. Ellipsoids are shown at 50 % probability level.

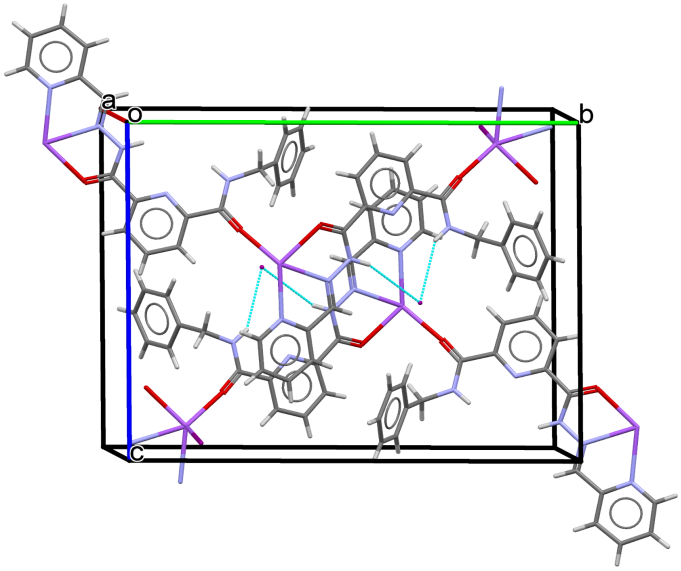

Figure S 126. Crystal packing of *E*-**1**·NaI complex

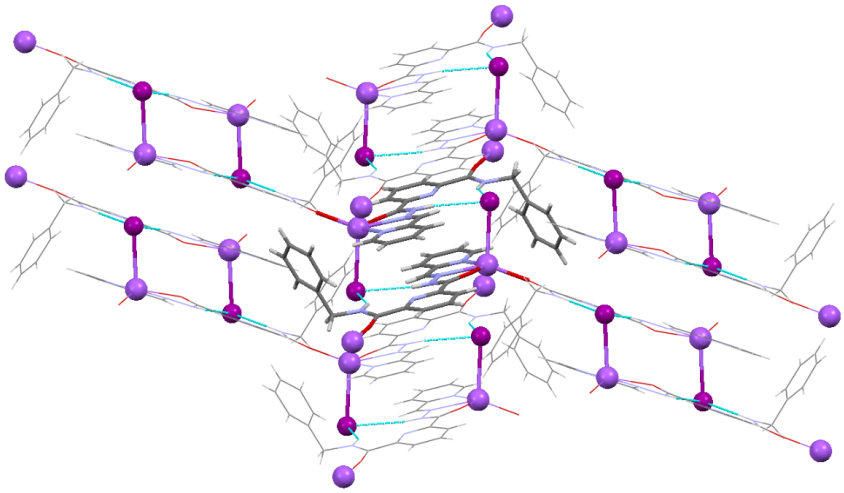

Figure S 127. Stacked dimer motif (capped sticks model) in the crystal structure of *E*-**1**·NaI, exhibiting discrete ion pairs in the solid state (ball model), forming a complex 2D network of hydrogen bonds and ion interactions.

Crystallization of *E*-**1** with KI

Potassium iodide (≈ 20 mg) and *E*-**1** (5.8 mg, 16 µmol, 22 mM) with 0.75 mL of acetonitrile were shortly heated to boiling, and the undissolved material was filtered off through cotton. The solution was further treated according to the general procedure for crystallization.

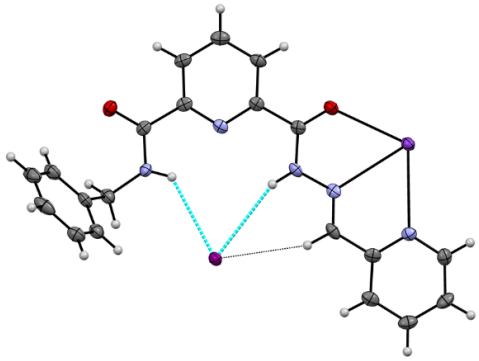

Figure S 128. Molecular structure of *E*-**1**·KI complex in the solid state. Ellipsoids are shown at 50 % probability level.

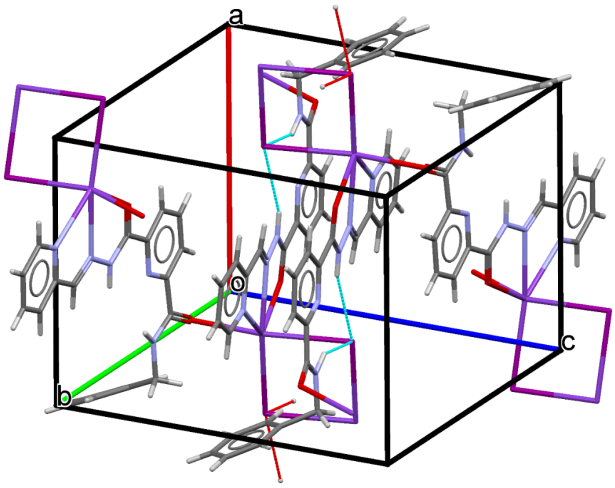

Figure S 129. Crystal packing of *E*-**1**·KI complex.

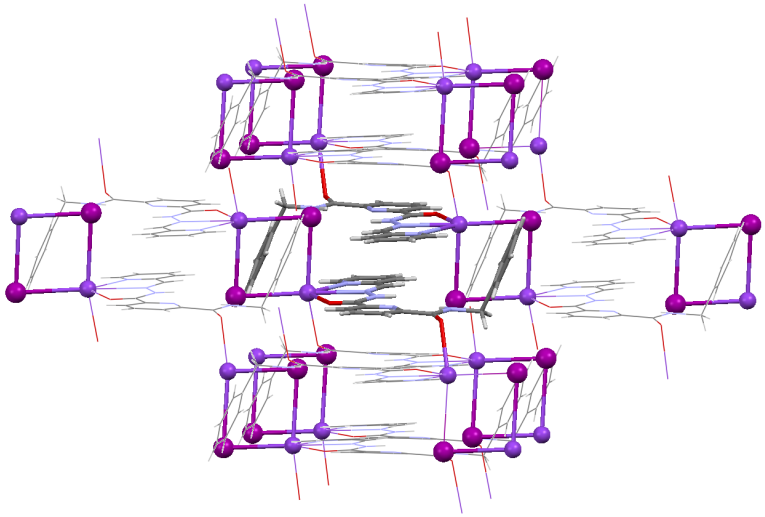

Figure S 130. Stacked dimer motif (capped sticks model) in the crystal structure of *E*-**1**·KI, exhibiting discrete pairs of ion pairs in the solid state (ball model), forming a complex 3D network of hydrogen bonds and ion interactions.

Crystallization of *E*-**1** with NH_4I

Ammonium iodide (10 mg) and 0.5 mL of acetonitrile *E*-**1** solution (11 mM, 6 µmol) were shortly heated to boiling and the undissolved material was filtered off through cotton. The solution was further treated according to the general procedure for crystallization.

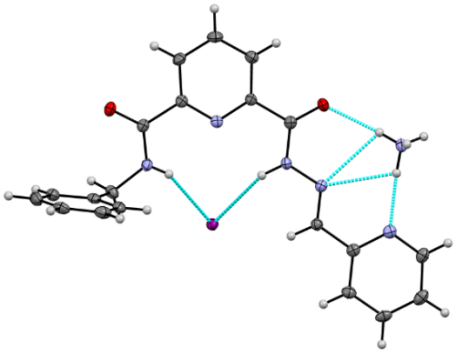

Figure S 131. Molecular structure of *E*-**1**·NH_4I complex in the solid state. Ellipsoids are shown at 50 % probability level.

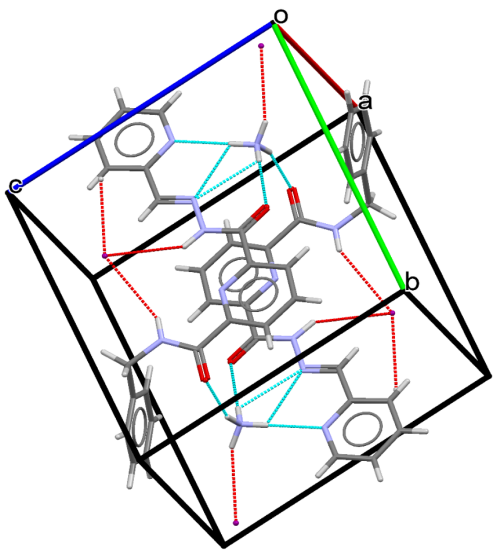

Figure S 132. Crystal packing of *E*-**1**·NH_4I complex.

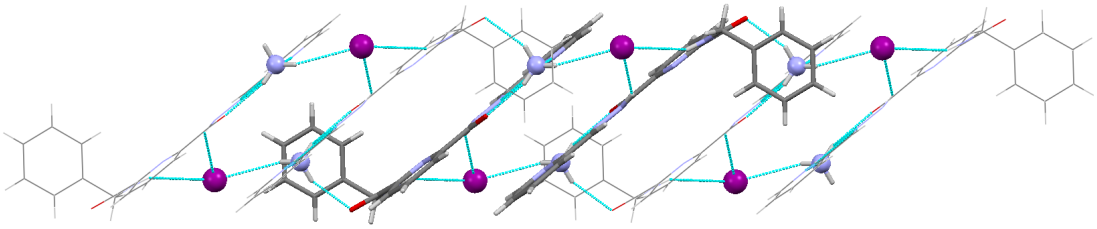

Figure S 133. Stacked dimer motif (capped sticks model) in the crystal structure of *E*-**1**·NH_4I, exhibiting discrete ion pairs in the solid state (ball model), forming a complex 1D network of hydrogen bonds and ion interactions.

Crystallization of *E*-**1** with NH_4Br

Ammonium bromide (10 mg) and 0.5 mL of acetonitrile *E*-**1** solution (11 mM, 6 µmol) were shortly heated to boiling and the undissolved material was filtered off through cotton. The solution was further treated according to the general procedure for crystallization.

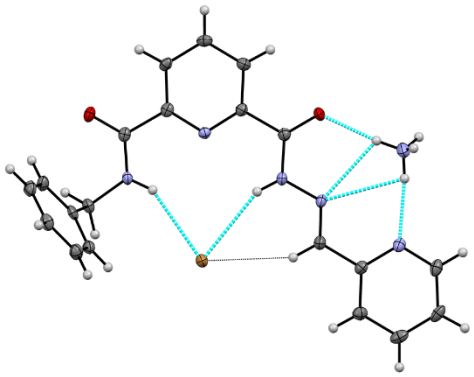

Figure S 134. Molecular structure of *E*-**1**·NH_4Br complex in the solid state. Ellipsoids are shown at 50 % probability level.

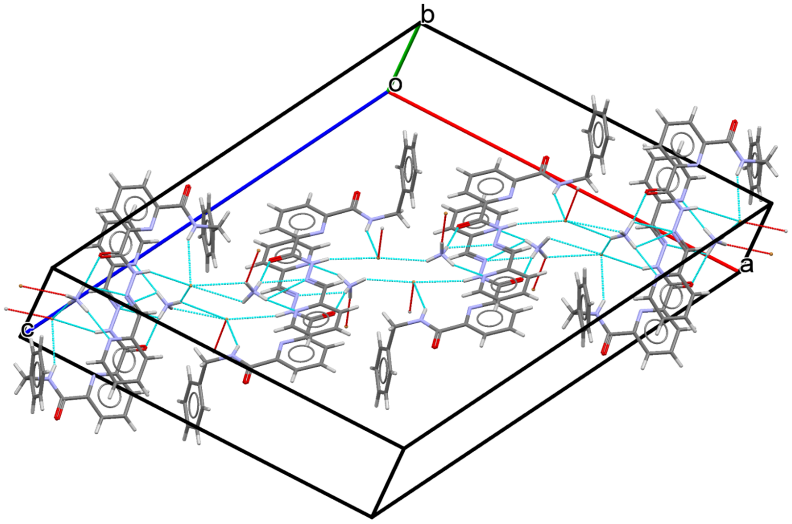

Figure S 135. Crystal packing of *E*-**1**·NH_4Br complex.

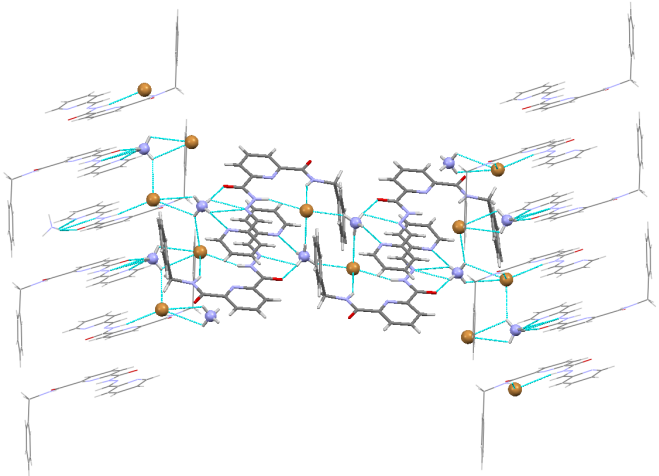

Figure S 136. Stacked dimer motif (capped sticks model) in the crystal structure of *E*-**1**·NH_4Br, exhibiting discrete pairs of ion pairs and zig-zag chains through hydrogen bonding in the solid state (ball model), forming a complex hydrogen bonded 2D network.

Crystallization of *E*-**1** with $LiClO_4$

Lithium perchlorate (2.74 mg, 25.8 µmol) was dissolved in 1 mL of 10% acetonitrile/chloroform (v/v) *E*-**1** solution (5.5 mM, 5.5 µmol), followed by the general procedure for crystallization. Suitable crystals for X-ray analysis were obtained upon slow evaporation of the solvent.

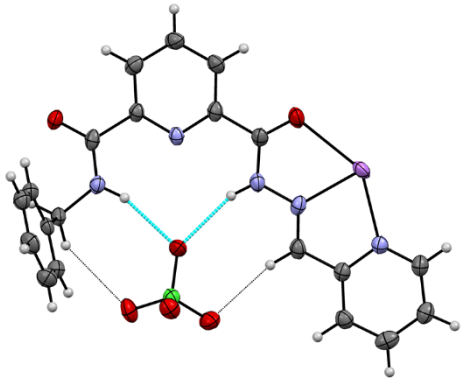

Figure S 137. Molecular structure of *E*-**1**·$LiClO_4$ complex in the solid state. Ellipsoids are shown at 50 % probability level.

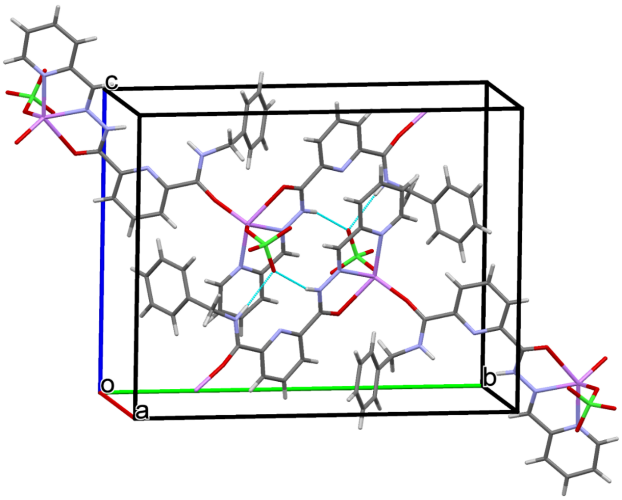

Figure S 138. Crystal packing of *E*-**1**·$LiClO_4$ complex.

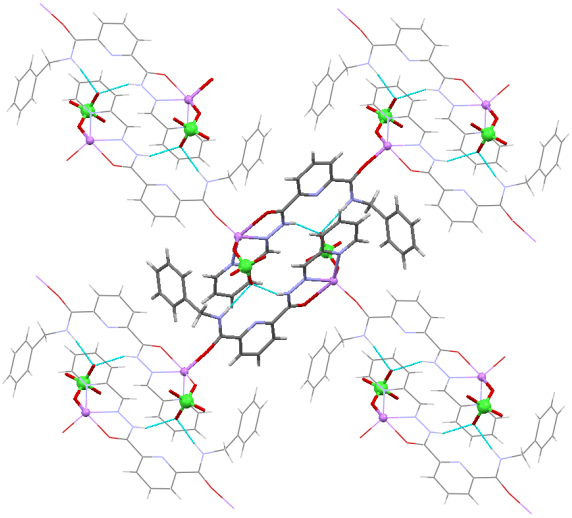

Figure S 139. Stacked dimer motif (capped sticks model) in the crystal structure of *E*-**1**·$LiClO_4$, exhibiting discrete ion pairs in the solid state (ball model), forming a complex hydrogen bonded 2D network.

7.3 Hydrogen Bonding Analysis with PLATON Software

All molecular interactions in the crystals of *E*-**1** complexes with simple salts were identified using PLATON program.[S12]

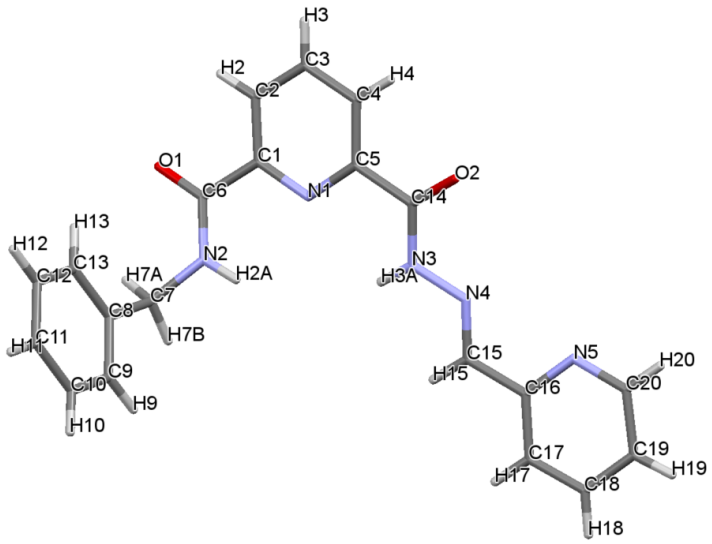

Figure S 140. Numbering scheme of the *E*-**1** molecule in the crystal structures.

E-**1**·NaI:

```
==========================================================================================================================

Analysis of Potential Hydrogen Bonds and Schemes with d(D...A) < R(D)+R(A)+0.50, d(H...A) < R(H)+R(A)-0.12 Ang., D-H...A > 100.0 Deg

==========================================================================================================================

Note: - ARU codes in [] are with reference to the Coordinates printed above (Possibly transformed, when MOVE .NE. 1.555)

==========================================================================================================================

Nr Typ Res Donor --- H....Acceptor [    ARU  ]     D - H      H...A      D...A  D - H...A    A..H..A* A'..H..A" Sum(XY,YZ)  Sum(XZ)

--------------------------------------------------------------------------------------------------------------------------

 1 Intra 1 N(2)  --H(2A)  ..I(1)   [       ]    0.85(3)    2.86(3)   3.580(3)     144(3)

 2 Intra 1 N(2)  --H(2A)  ..N(1)   [       ]    0.85(3)    2.33(3)   2.711(4)     108(2)' 108.3(12)'            360(4)

 3 Intra 1 N(3)  --H(3A)  ..I(1)   [       ]    0.88(3)    2.96(3)   3.793(3)     160(4)


H-Bond classification [G.A.Jeffrey, H.Maluszynska & J.Mitra., Int.J.Biol.Macromol.(1985),7,336-348]

--------------------------------------------------------------------------------------------------------------------------

2-Centre   (linear)     D-H...X most prob. angle 160 deg  - also: G.A.Jeffrey & W.Saenger, Hydrogen Bonding in Biological Structures

3-Centre (bifurcated)   SUM of 3 angl. about H = 360 deg                Springer-Verlag, Berlin, 1991, pp 20.

4-Centre (trifurcated)
```

E-**1**·KI:

==========

Analysis of Potential Hydrogen Bonds and Schemes with d(D...A) < R(D)+R(A)+0.50, d(H...A) < R(H)+R(A)-0.12 Ang., D-H...A > 100.0 Deg

==========

Note: - ARU codes in [] are with reference to the Coordinates printed above (Possibly transformed, when MOVE .NE. 1.555)

==========

Nr Typ Res Donor --- H....Acceptor [ARU] D - H H...A D...A D - H...A A..H..A* A'..H..A" Sum(XY,YZ) Sum(XZ)

---

1 Intra 1 N(2) --H(2A) ..I(1) [ ] 0.87(6) 2.93(6) 3.579(6) 133(5)

2 Intra 1 N(2) --H(2A) ..N(1) [ ] 0.87(6) 2.23(6) 2.743(8) 118(5)' 109(2)' 360(7)

3 Intra 1 N(3) --H(3A) ..I(1) [ ] 0.89(9) 2.97(9) 3.817(6) 158(7)

4 Intra 1 C(15) --H(15) ..I(1) [ ] 0.93 3.01 3.860(6) 153

For C--H...Acceptor Interactions See: Th. Steiner, Cryst. Rev, (1996), 6, 1-57

H-Bond classification [G.A.Jeffrey, H.Maluszynska & J.Mitra., Int.J.Biol.Macromol.(1985),7,336-348]

2-Centre (linear) D-H...X most prob. angle 160 deg - also: G.A.Jeffrey & W.Saenger, Hydrogen Bonding in Biological Structures

3-Centre (bifurcated) SUM of 3 angl. about H = 360 deg Springer-Verlag, Berlin, 1991, pp 20.

4-Centre (trifurcated)

E-**1**·NH_4Br:

```
==========================================================================================================================

Analysis of Potential Hydrogen Bonds and Schemes with d(D...A) < R(D)+R(A)+0.50, d(H...A) < R(H)+R(A)-0.12 Ang., D-H...A > 100.0 Deg

==========================================================================================================================

Note: - ARU codes in [] are with reference to the Coordinates printed above (Possibly transformed, when MOVE .NE. 1.555)

==========================================================================================================================

Nr Typ Res Donor --- H....Acceptor [    ARU  ]     D - H      H...A      D...A  D - H...A    A..H..A* A'..H..A" Sum(XY,YZ)  Sum(XZ)

--------------------------------------------------------------------------------------------------------------------------

 1      1 N2A   --H2AA   ..Br1A  [       ] 0.852(18)    2.63(2)   3.392(2)     149(3)

 2 Intra 1 N2A   --H2AA   ..N1A   [       ] 0.852(18)    2.36(3)   2.734(3)     107(2)'  102.5(7)'            359(4)

 3      1 N3A   --H3AA   ..Br1A  [       ]   0.85(3)    2.70(3)   3.496(2)     156(3)

 4 Intra 1 N3A   --H3AA   ..N1A   [       ]   0.85(3)    2.40(3)   2.738(3)     104(3)'   99.4(9)'            359(4)

 5      2 N2B   --H2BA   ..Br1B  [       ]   0.85(2)    2.61(3)   3.347(2)     147(3)

 6 Intra 2 N2B   --H2BA   ..N1B   [       ]   0.85(2)    2.32(3)   2.727(3)     110(3)'  103.2(8)'            360(4)

 7      2 N3B   --H3BA   ..Br1B  [       ]   0.84(3)    2.69(3)   3.473(2)     155(3)

 8 Intra 2 N3B   --H3BA   ..N1B   [       ]   0.84(3)    2.39(3)   2.744(3)     106(3)'   98.9(9)'            360(4)

 9      5 N6A   --H6AA   ..N4A   [       ] 0.879(18)    2.62(2)   2.944(4)  103.2(19)

10      5 N6A   --H6AA   ..N5A   [       ] 0.879(18)  2.023(18)   2.889(4)     169(2)'   70.9(6)'            343(3)

11      5 N6A   --H6AB   ..O2A   [       ] 0.878(13)  1.918(12)   2.792(3)     173(3)

12      5 N6A   --H6AB   ..N4A   [       ] 0.878(13)    2.49(3)   2.944(4)     113(2)'   72.5(6)'            359(4)

13      5 N6A   --H6AC   ..Br1B  [  3656.04]   0.88(3)    2.70(2)   3.407(4)     138(2)

        5 N6A   --H6AD   .. ?                 0.88(2)

14      6 N6B   --H6BA   ..O2B   [       ]   0.87(2)  1.957(19)   2.814(3)     166(3)

15      6 N6B   --H6BA   ..N4B   [       ]   0.87(2)    2.56(3)   2.930(3)     107(2)'   70.7(8)'            344(4)

16      6 N6B   --H6BB   ..Br1A  [       ]   0.88(3)    2.61(3)   3.364(3)     144(2)

17      6 N6B   --H6BC   ..N5B   [       ] 0.877(18)    2.08(2)   2.892(4)     154(3)

18      6 N6B   --H6BD   ..Br1A  [  3656.03]  0.879(17)  2.516(15)   3.392(3)     174(3)

19      1 C3A   --H3A    ..O1B   [  2656.02]     0.93      2.45   3.298(3)      151

20 Intra 2 C9B   --H9B    ..O1B   [       ]     0.93      2.60   3.174(4)      121

21      2 C11B  --H11B   ..O1B   [  1545.02]     0.93      2.60   3.160(4)      120

22      1 C15A  --H15A   ..Br1A  [       ]     0.93      2.79   3.648(3)      153

23      2 C15B  --H15B   ..Br1B  [       ]     0.93      2.77   3.629(3)      153

24      1 C18A  --H18A   ..O1A   [  4454.01]     0.93      2.51   3.358(4)      151
```

Translation of ARU-Code to CIF and Equivalent Position Code

==========

[2656.] = [2_656] =3/2-x,1/2+y,3/2-z

[4454.] = [4_565] =-1/2+x,1/2-y,-1/2+z

[3656.] = [3_656] =1-x,-y,1-z

[1545.] = [1_545] =x,-1+y,z

For C--H...Acceptor Interactions See: Th. Steiner, Cryst. Rev, (1996), 6, 1-57

==========

H-Bond classification [G.A.Jeffrey, H.Maluszynska & J.Mitra., Int.J.Biol.Macromol.(1985),7,336-348]

2-Centre (linear) D-H...X most prob. angle 160 deg - also: G.A.Jeffrey & W.Saenger, Hydrogen Bonding in Biological Structures

3-Centre (bifurcated) SUM of 3 angl. about H = 360 deg Springer-Verlag, Berlin, 1991, pp 20.

4-Centre (trifurcated)

E-**1**·NH_4I:

```
==========================================================================================================================

Analysis of Potential Hydrogen Bonds and Schemes with d(D...A) < R(D)+R(A)+0.50, d(H...A) < R(H)+R(A)-0.12 Ang., D-H...A > 100.0 Deg

==========================================================================================================================

Note: - ARU codes in [] are with reference to the Coordinates printed above (Possibly transformed, when MOVE .NE. 1.555)

==========================================================================================================================

Nr Typ Res Donor --- H....Acceptor [    ARU  ]     D - H      H...A      D...A  D - H...A    A..H..A* A'..H..A" Sum(XY,YZ)  Sum(XZ)

--------------------------------------------------------------------------------------------------------------------------

 1      1 N(2)  --H(2A)  ..I(1)   [        ]    0.81(4)    2.91(4)   3.612(2)     145(3)

 2 Intra 1 N(2)  --H(2A)  ..N(1)   [        ]    0.81(4)    2.37(3)   2.711(3)     106(3)' 100.8(12)'            352(4)

 3      1 N(3)  --H(3A)  ..I(1)   [        ]    0.92(3)    3.00(3)   3.797(2)     146(2)

 4 Intra 1 N(3)  --H(3A)  ..N(1)   [        ]    0.92(3)    2.34(3)   2.679(3)     102(2)'  99.3(11)'            347(3)

 5      3 N(6)  --H(6A)  ..I(1)   [  2676.02]    0.88(3)    2.81(3)   3.606(2)     151(2)

 6      3 N(6)  --H(6B)  ..O(2A)  [        ]    0.87(2)  2.062(19)   2.907(3)     164(2)

 7      3 N(6)  --H(6B)  ..N(4)   [        ]    0.87(2)    2.62(3)   2.987(3)     107(2)'   68.7(8)'            340(3)

 8      3 N(6)  --H(6C)  ..O(1)   [  2666.01]    0.89(3)    2.01(3)   2.841(3)     155(3)

 9      3 N(6)  --H(6D)  ..N(4)   [        ]    0.88(2)    2.54(2)   2.987(3)     112(2)

10      3 N(6)  --H(6D)  ..N(5)   [        ]    0.88(2)    2.05(2)   2.924(3)     172(3)'   71.8(5)'            356(4)


Translation of ARU-Code to CIF and Equivalent Position Code

============================================================

  [  2666.] = [  2_666] =1-x,1-y,1-z

  [  2676.] = [  2_676] =1-x,2-y,1-z


H-Bond classification [G.A.Jeffrey, H.Maluszynska & J.Mitra., Int.J.Biol.Macromol.(1985),7,336-348]

--------------------------------------------------------------------------------------------------------------------------

2-Centre   (linear)     D-H...X most prob. angle 160 deg  - also: G.A.Jeffrey & W.Saenger, Hydrogen Bonding in Biological Structures

3-Centre (bifurcated)   SUM of 3 angl. about H = 360 deg                Springer-Verlag, Berlin, 1991, pp 20.

4-Centre (trifurcated)
```

E-**1**·$LiClO_4$:

==========

Analysis of Potential Hydrogen Bonds and Schemes with d(D...A) < R(D)+R(A)+0.50, d(H...A) < R(H)+R(A)-0.12 Ang., D-H...A > 100.0 Deg

==========

Note: - ARU codes in [] are with reference to the Coordinates printed above (Possibly transformed, when MOVE .NE. 1.555)

==========

Nr Typ Res Donor --- H....Acceptor [ARU] D - H H...A D...A D - H...A A..H..A* A'..H..A" Sum(XY,YZ) Sum(XZ)

---

1 Intra 1 N(2) --H(2A) ..O(5) [ ] 0.87(3) 2.18(3) 2.988(4) 156(3)

2 Intra 1 N(2) --H(2A) ..N(1) [ ] 0.87(3) 2.36(3) 2.706(4) 104(2)' 91.9(11)' 352(4)

3 Intra 1 N(3) --H(3A) ..O(5) [ ] 0.87(3) 2.17(3) 2.997(4) 158(4)

4 Intra 1 N(3) --H(3A) ..N(1) [ ] 0.87(3) 2.38(4) 2.713(4) 103(3)' 91.4(10)' 352(5)

5 Intra 1 C(7) --H(7A) ..O(1) [ ] 0.97 2.52 2.852(5) 100

6 Intra 1 C(7) --H(7A) ..O(2) [2556.01] 0.97 2.41 3.252(5) 145' 85' 330

7 Intra 1 C(15) --H(15) ..O(4) [ ] 0.93 2.39 3.306(5) 167

Translation of ARU-Code to CIF and Equivalent Position Code

==========

[2556.] = [2_556] =1/2-x,1/2+y,3/2-z

For C--H...Acceptor Interactions See: Th. Steiner, Cryst. Rev, (1996), 6, 1-57

H-Bond classification [G.A.Jeffrey, H.Maluszynska & J.Mitra., Int.J.Biol.Macromol.(1985),7,336-348]

2-Centre (linear) D-H...X most prob. angle 160 deg - also: G.A.Jeffrey & W.Saenger, Hydrogen Bonding in Biological Structures

3-Centre (bifurcated) SUM of 3 angl. about H = 360 deg Springer-Verlag, Berlin, 1991, pp 20.

4-Centre (trifurcated)

8 Literature References

S1. Fulmer, G. R.; Miller, A. J. M.; Sherden, N. H.; Gottlieb, H. E.; Nudelman, A.; Stoltz, B. M.; Bercaw, J. E.; Goldberg, K. I., *Organometallics* **2010**, 29, 2176–2179.

S2. CrysAlis CCD and CrysAlis RED, Oxford Diffraction, Oxford Diffraction Ltd: Yarnton, 2008.

S3. Clark, R. C.; Reid, J. S.; *Acta Cryst. Sect. A* **1994**, 51, 887–897

S4. Sheldrick, G. M.; *Acta Cryst. Sect. A* **2008**, 64, 112–122.

S5. Dierck, I.; Herman, G. G.; Goeminne, A. M.; Van der Kelen, G. P., *Bull. Chem. Soc. Belg.* **1993**, *102*, 63–66.

S6. Ong, W. Q.; Zhao, H.; Fang, X.; Woen, S.; Zhou, F.; Yap, W.; Su, H.; Li, S. F. Y.; Zeng, H., *Org. Lett.* **2011**, *13*, 3194–3197.

S7. (a) Fennel Evans, D.; Zawoyski, C.; Kay, R. L., *J. Phys. Chem.* **1965**, 69, 3878–3885; (b) Kay, R. L.; Hales, B. J.; Cunningham G. P., *J. Phys. Chem.* **1967**, 71, 3925–3930.

S8. Hopkins, Jr., H. P.; Jahagirdar, D. V.; Norman A. B., *J. Solution Chem.*, **1979**, 8, 147–155.

S9. Glugla, P. G.; Byon, J. H.; Eckert, C. A., *J. Chem. Eng. Data* **1981**, 26, 80–84.

S10. (a) M. Montalti, A. Credi, L. Prodi, M. T. Gandolfi, *Handbook of Photochemistry*, Third Edition, (CRC Press, 2006); (b) M. Wegener, M. J. Hansen, A. J. M. Driessen, W. Szymanski, and B. L. Feringa, *J. Am. Chem. Soc.* **2017**, 139, 17979-17986.

S11. J. Bernstein, R. E. Davis, L. Shimoni and H.-L. Chang, *Angew. Chem. Int. Ed.*, **1995**, 34, 1555–1573.

S12. A. L. Spek, *Acta Cryst. Sect. D*, **2009**, 65, 148.